1987

Synthesis and characterization of zirconium-antimony binary and interstitial ternary intermetallic compounds

Eduardo Garcia
Iowa State University

INFORMATION TO USERS

While the most advanced technology has been used to photograph and reproduce this manuscript, the quality of the reproduction is heavily dependent upon the quality of the material submitted. For example:

- Manuscript pages may have indistinct print. In such cases, the best available copy has been filmed.
- Manuscripts may not always be complete. In such cases, a note will indicate that it is not possible to obtain missing pages.
- Copyrighted material may have been removed from the manuscript. In such cases, a note will indicate the deletion.

Oversize materials (e.g., maps, drawings, and charts) are photographed by sectioning the original, beginning at the upper left-hand corner and continuing from left to right in equal sections with small overlaps. Each oversize page is also filmed as one exposure and is available, for an additional charge, as a standard 35mm slide or as a 17"x 23" black and white photographic print.

Most photographs reproduce acceptably on positive microfilm or microfiche but lack the clarity on xerographic copies made from the microfilm. For an additional charge, 35mm slides of 6"x 9" black and white photographic prints are available for any photographs or illustrations that cannot be reproduced satisfactorily by xerography.

Order Number 8721885

Synthesis and characterization of zirconium-antimony binary and interstitial ternary intermetallic compounds

Garcia, Eduardo, Ph.D.

Iowa State University, 1987

U·M·I
300 N. Zeeb Rd.
Ann Arbor, MI 48106

PLEASE NOTE:

In all cases this material has been filmed in the best possible way from the available copy. Problems encountered with this document have been identified here with a check mark __✓__.

1. Glossy photographs or pages _____
2. Colored illustrations, paper or print _____
3. Photographs with dark background _____
4. Illustrations are poor copy _____
5. Pages with black marks, not original copy _____
6. Print shows through as there is text on both sides of page _____
7. Indistinct, broken or small print on several pages ✓
8. Print exceeds margin requirements _____
9. Tightly bound copy with print lost in spine _____
10. Computer printout pages with indistinct print _____
11. Page(s) _____ lacking when material received, and not available from school or author.
12. Page(s) _____ seem to be missing in numbering only as text follows.
13. Two pages numbered _____. Text follows.
14. Curling and wrinkled pages _____
15. Dissertation contains pages with print at a slant, filmed as received _____
16. Other _____

_____

_____

Synthesis and characterization of zirconium-antimony binary and interstitial ternary intermetallic compounds

by

Eduardo Garcia

A Dissertation Submitted to the
Graduate Faculty in Partial Fulfillment of the
Requirements for the Degree of
DOCTOR OF PHILOSOPHY

Department: Chemistry
Major: Inorganic Chemistry

Approved:

Signature was redacted for privacy.
In Charge of Major Work

Signature was redacted for privacy.
For the Major Department

Signature was redacted for privacy.
For the Graduate College

Iowa State University
Ames, Iowa

1987

TABLE OF CONTENTS

INTRODUCTION

Interest in Zr_5Sb_3Z compounds was sparked by reports that revealed an extensive interstitial chemistry for M_5X_3 phases with the Mn_5Si_3 structure.[1-9] Much of the work on Mn_5Si_3-type compounds was done in the late 50s or early 60s, and often only qualitative information was reported. It is unclear whether many compounds described as binary phases, are in fact ternary compounds.

Recent experience has demonstrated that materials previously formulated as binary compounds, had actually been interstitial stabilized ternary phases.[10-12] It seemed possible that many Mn_5Si_3-type compounds would prove to be interstitial stabilized as well, but had gone undetected as such.

Initial attention was drawn to Zr_5Sb_3 because of this possibility, but Zr_5Sb_3Z compounds were investigated for additional reasons outlined in the introduction to Part II. This work is divided into two parts because, as experiments with the ternary interstitial compounds Zr_5Sb_3Z and the binary compound Zr_5Sb_3 progressed, it became clear that published reports of the zirconium-antimony binary system were incomplete or inaccurate. In order to provide a firm basis for investigating the ternary systems, the zirconium-antimony binary system was re-examined, and the results described and discussed in Part I.

EXPERIMENTAL

Materials

Most reaction starting materials consisted of the elements themselves or binary compounds which had been synthesized from the elemental components. A list of these elements, which were used as received is given in Table 1. Reactor-grade zirconium metal was obtained at the Ames Laboratory from F. Schmidt in the form of a crystal bar that had been cold-rolled to a thickness of about 20 mil. The metal was cleaned in a solution of 45% HNO_3, 10% Hf, and 45% H_2O, rinsed in water, dried, cut into pieces of suitable size for use in the arc-melter, and finally given a last rinse with acetone to remove any residue left from handling. When Zr powder was required, it was synthesized by placing Zr strips in a molybdenum boat which was subsequently put in a fused silica tube equipped with a stopcock, and attached to a hydrogen line. The temperature of the metal was raised under an atmosphere of H_2 until no further hydrogen uptake was observed (~650°C). The ZrH_x so formed was ground with a mortar and pestle in a dry box, and passed through a 100 mesh sieve. This powder was replaced in the molybdenum boat, and reattached to a vacuum line. The temperature was raised slowly, maintaining a 10^{-5} torr vacuum, to 700°C. This decomposes ZrH_x to Zr metal, and the evolved hydrogen is pumped away. The temperature must be raised slowly to prevent a vigorous evolution of H_2 that blows the powder out of the boat. This procedure results in lattice parameters for the Zr powder which are within 3σ of literature values.[13]

Table 1. Ternary components

Element	Source	Purity
Na	J. T. Baker Chem.	Purified
K	J. T. Baker Chem.	Purified
Mg	J. T. Baker Chem.	Purified
Ca	Ames Lab	Distilled
B	Robert Shelton, Physics	99.9+%
C	Union Carbide	Spectroscopic Grade
Al	United Mineral & Chemical	High Purity
Si	Ames Lab	Zone refined
P	J. T. Baker Chem.	Technical Grade
S	Alfa Products	99.999%
Cr	A. D. MacKay	
Mn	A. D. MacKay	99.9%
Fe	Plastic Metals	99.9%
Co	Alfa Products	99.5%
Ni	J. T. Baker Chem.	99.9%
Cu	J. T. Baker Chem.	99.99%
Zn[a]	Fisher Scientific	99.99%
Ge	Johnson Mathey	99.999%
Ge	Ames Lab	Zone refined
As	Alfa Products	99.9999%
Se	American Smelting & Refining Co.	99.999%
Ag	G. Frederick Smith Chem.	Reagent
Cd	Cominco Products	99.999%
In	Cominco Products	
Ru	Engelhard	99.5%
Bi[a]	Oak Ridge National Lab.	Reactor Grade

[a]Filtered through a glass frit.

Most reactions used reagent grade antimony from Allied Chemical and Dye Corporation, which produced no dross upon fusion. A few reactions used 99.999% Sb from Johnson Matthey, Inc., and no difference in reaction products was observed. Comminution of antimony is easily achieved by direct grinding of the element. The powders of both Sb and Zr were only handled under dry box or vacuum conditions.

The binary compounds ZrC and ZrN were obtained from Cerac and used as received. Zirconium dioxide was graciously donated by Steve Chen. It had been made by precipitating the hydrous oxide from an aqueous solution of $ZrOCl_2 \cdot 8H_2O$ through the addition of aqueous ammonia. The $ZrO_2 \cdot 2H_2O$ was washed with water to remove any residual chloride material and dehydrated at 400°C.

Synthesis Techniques

A variety of synthetic techniques were employed, each with certain advantages and disadvantages vis-a-vis the others. The preparation method selected must be based on a knowledge of the limitations of each technique, and how they will influence the experimental objectives of the preparatory reactions. The methods used fall under four general headings: arc-melting, chemical vapor transport, metal flux, and powder sintering.

Arc-melting

The highest reaction temperatures were obtained in arc-melting reactions. These were carried out in a Centorr 55A single arc furnace,

starting with pieces of the elements which were melted on a water-cooled copper hearth. The reaction proceeded under argon that had been gettered by previously melting zirconium, and the pressure maintained slightly greater than atmospheric. The advantage of this technique derives from the very high temperatures that can be achieved, ~3000°C, which tend to overcome kinetic barriers endemic in solid state experiments, and lead to complete reaction in very short reaction times of less than one minute. The importance of single crystals suitable for X-ray structure determination in exploratory solid state synthesis must be emphasized, and it is often possible to obtain such, from the products of arc-melted reactions. This is another important advantage to this technique.

Just as the advantages of arc-melting arise from the high reaction temperature, paradoxically, the disadvantages are derived from the same source. The water-cooled copper hearth prevents any reaction between the sample and the container, but it also results in a sharp temperature gradient, which may lead to compositional gradients between the top of the molten reaction mixture at 3000°C and the bottom at < 100°C. This problem was minimized by turning over the button and remelting it at least three times. Further homogenization can be achieved by annealing the products. This was accomplished by placing the solidified ingots in open Ta crucibles which were then sealed in fused silica containers under an atmosphere of Ar and heated in a vacuum induction or resistance furnace depending on the temperature. Annealing is important for a second reason; it is possible that peritectic compounds may not have time to form when samples are quenched by turning off the arc. The annealing

periods were on the order of several days and obviously nullified the advantage gained by the rapid initial reaction.

A further more serious complicating factor results from the high arc temperature. Many of the elements which were used as reactants, have high vapor pressures at the reaction temperature in the arc furnace. Although the suitability of this technique is actually determined by the equilibrium vapor pressure of the species above the product compound, not the reactants, some mass loss is inevitably incurred during initial heating. Furthermore, mass loss may still occur at a much reduced but still significant rate even after the initial 2-3 seconds. If only one component is volatile then the problem can be overcome by employing an excess of that species, and a product composition can be easily determined from the final weight. When two or more components are vaporized, then all synthetic control is lost.

Chemical vapor transport

Chemical vapor transport should allow for a more controlled synthesis since it can occur in a closed system. One would also expect to obtain better quality single crystals than by arc-melting. These reactions were carried out by allowing iodine, added as a binary iodide, to react with either a mixture of elemental powders, or a ground arc-melted pellet to give gaseous iodide species which under the proper thermodynamic conditions will undergo a reverse reaction to yield the desired intermetallic product, and regenerate the iodine or iodide. This is usually accomplished through a temperature gradient such that the forward reaction is favored at T_1, and the reverse reaction is favored at T_2, but

transport may still occur at a single temperature where the rates of the two reactions are comparable. Isothermal reactions were carried out in welded Ta tubes which were either sealed in evacuated silica containers and heated in air, or heated in vacuum furnaces.

Single crystals are sometimes difficult to grow by vapor transport unless a temperature gradient is applied. Obtaining such a temperature gradient with the intermetallic systems of interest, is experimentally difficult. Gaseous iodide species can be easily produced at low temperature (300°C) for most reaction components, but this ease of formation is equally applicable to, and precluded the use of, metal containers. The formation of metal iodides is a very exothermic process so that the reverse reaction to produce the intermetallic compound will only occur at high temperature (1300°C), therefore precluding the use of a fused silica container. This dilemma can be resolved by using a hot wire apparatus in which a Ta wire is sealed in a Pyrex container via glass-to-metal seals that allow an electric current to be passed through the wire to heat it to ~1300°C. The starting material along with a small amount of a transporting agent is also sealed in the Pyrex container, which is maintained at 300°C in a furnace. Crystals of the product grow on the Ta wire. Unfortunately the composition of the product is very dependent on the wire temperature which is constantly changing as the material deposited on it changes the electrical resistance. This leads to an inhomogeneous product and the method is generally unacceptable, but does demonstrate the feasibility of transport reactions if the experimental difficulties can be overcome.

Metal flux

Good quality single crystals can often be grown by precipitation from a solution. In a manner analogous to dissolving salt-like materials in fused salts, intermetallic compounds may be dissolved by molten metals. Crystals of the product can be grown by causing superstaturation of the solution either through lowering the temperature, or evaporation of the solvent. Good control of nucleation and subsequent growth has produced crystals of some oxide materials on the centimeter scale.[14] It can be seen that this technique has the potential of producing crystals which could be used for physical property measurements. Problems arose in the systems of interest that prevented this.

If supersaturation is induced by a lowering of the temperature, then the product can only be recovered by dissolving the solidified metal matrix. This seemed a rather brutal procedure which had a good chance of dissolving any new interesting compounds as well. The problem can be circumvented if the solvent is a low boiling point metal, and it is allowed to evaporate. The only metals which meet this requirement and dissolve significant amounts of zirconium, are Zn and Bi. These were used in several reactions with either an alumina or molybdenum container to give X-ray sized single crystals in several systems, but it was found that the products were contaminated by the solvent. With a more inert solvent and more controlled experimental conditions, the potential of growing large single crystals may yet be realized.

Powder sintering

The final synthetic technique employed, utilized the sintering of powders. This method has the advantage of good control over the final composition and can then yield a correlation between lattice parameters and composition. The disadvantages are the inability to produce single crystals, and the need for frequent regrinding and pressing of a pellet. Depending on the scale of the reaction, equilibrium may be difficult to achieve. The sintering reactions were carried out in both open and sealed Ta containers and with powders simply ground together or ground and pelletized at 8 kbar. A high temperature furnace (>1100°C) became available in the latter stages of this investigation, and greatly facilitated sintering reactions.

Characterization Techniques

X-ray diffraction

Guinier powder diffraction was used as the primary method of characterization. The diffraction patterns were obtained with NBS Si as an internal standard and monochromatic Cu $K\alpha_1$, radiation. The 2θ values of the diffraction lines from the standard were fit to a quadratic in line position, and lattice constants of the sample were calculated by a least-squares fit to indexed 2θ values. Lattice parameters for NBS α-Al_2O_3 obtained by this method differed from the reference values by 0.8 and 2.5 parts in 10^4. The identification of structure type was accomplished by comparing line position and intensity in the experimental pattern with the distribution calculated for a known structure by the program

POWD 5.[15] Some unknown powder patterns were indexed by the program TREOR[16] as were several superstructures.

Single crystal X-ray work was carried out in all cases with the sample mounted in a sealed thin walled capillary of 0.2, 0.3 or 0.5 mm diameter. Some phases, especially antimony-rich compounds of the binary Zr-Sb system, were air stable and could be mounted in air, but in most cases the crystals were placed into the capillary within a dry box equipped with a microscope. The open end of these was temporarily closed with grease, removed from the dry box, and sealed by fusing the glass with a torch. Oscillation photographs were utilized to determine if a crystal was indeed single, and zero and first layer Weissenberg photographs were also obtained if the crystal was so found. These also allowed the determination of unknown unit cells and indicated the presence or absence of superstructures.

Two four-circle diffractometers were used to collect data for structure determination during the course of this investigation; a commercial SYNTEX $P2_1$ and an Ames Laboratory instrument (DATEX). Both diffractometers employed monochromatic Mo $K\alpha$ radiation, and checked standard reflections every 50-75 reflections to determine instrumental stability and extent of any crystal decay. No decay was ever observed. All data were collected by using a ω scan.

Absorption corrections for the data sets were calculated using a ω-scan and correction factors for a cylinder or sphere as applicable.[17,18] The absorption-corrected data were reduced by DATRD[19] using a 3σ criterion to determine observed reflections after correction

for Lorentz-polarization effects. The data were averaged with FDATA[20] and reflections with structure factors that differed by more than 6σ were eliminated. The program ALLS[21] was used for full-matrix least-squares refinement. Structure factor calculations used neutral atom scattering factors corrected for anomalous dispersion effects. All refinements included a secondary extinction correction. Fourier electron density and difference maps were calculated with FOUR.[22] All ORTEP[23] drawings have thermal ellipsoids at a 95% probability level. The crystallographic calculations and drawings were done with the aid of a VAX 11/780 computer.

Magnetic susceptibility

Magnetic susceptibility measurements were made in collaboration with Professor Robert Shelton of the Physics Department on a Superconducting Quantum Interference Device (SQUID) from Quantum Designs equipped with an HP85B computer. Most samples consisted of pieces, circa 20 mg in weight, from arc-melted ingots, and these were attached to a metal suspension rod outside the detection zone by a length of dental floss (unflavored) tied around the sample. The dental floss was found to give a negligible signal. Air-sensitive or powdered samples were placed in 3 mm diameter fused silica tubes which were glued to a plastic connector with GE 7030 glue. The connector was in turn attached to the metal suspension rod. The susceptibility was normally measured by lowering the temperature to the starting point, usually 2 K, with the magnetic field at zero. Once the temperature had stabilized, the field was turned on and also allowed to stabilize at the chosen strength before the temperature was raised and

the susceptibility measured at preselected temperatures. Data above 400 K were collected on a Faraday balance.

Photoelectron spectroscopy

UPS and XPS experiments were conducted on an AEI-200B spectrometer using He (I) (21.2 eV) and Al Kα (1486.6 eV) radiation, respectively. Samples were ground in an agate mortar and pestle in a dry box attached directly to the spectrometer, and mounted on an indium substrate. The binding energy of peaks in the XPS spectra was determined by using adventitious carbon as an internal standard (285.0 eV).

The spectra were obtained by multiple scans and signal averaging using a Nicolet 1180 computer system.

Extended-Hückel calculations

The programs used for the calculations have been previously described.[24,25] The atomic energy levels used were either included in the program, or obtained from the literature.[26,27] In the case of Zr_5Sb_3Fe this gave unreasonable results for iron, so a self-consistent charge calculation was carried out. Double zeta expansions were used for the radial distribution of transition metal d orbitals,[28] and single zeta functions used for all others.[29] The atomic orbital parameters are listed in Appendix A.

Resistivity

Single crystal resistivity measurements were made by a four-probe alternating current technique using Professor Shelton's equipment. The

crystal was mounted on a glass frit to which 2 mil Pt wires had been epoxied. Electrical contact between the crystal and the Pt wires was assured through silver epoxy. The four Pt wires were soldered to four posts on a copper plate, and electrical connection of the resistivity cryostat was made to the measuring equipment outside the helium dewar. The low frequency (22 Hz) ac resistivity measurements were made with the aid of a lock-in amplifier which determined the current through two end leads, and the resulting voltage across the other two. The data were taken as the cryostat in the vacuum can was allowed to cool slowly via a small pressure of helium exchange gas. The temperatures above 30K were measured by a Pt thermometer, and below by a carbon glass thermometer.

PART I. ZIRCONIUM-ANTIMONY BINARY SYSTEM

INTRODUCTION

In the course of investigation of Zr_5Sb_3Z systems it became obvious that published accounts of the Zr-Sb binary system were incomplete or erroneous. Early work on Zr-Sb alloys over the range 0-40 at.% antimony indicated that Zr_2Sb was the most zirconium-rich binary alloy and that its powder and single crystal diffraction photographs could be indexed on the basis of a hexagonal cell (a = 8.4, c = 5.6 Å).[30] The solubility of antimony in zirconium could not be determined in this study because of both the high oxygen and nitrogen content of the starting zirconium, and additional contamination by carbon that occurred during the alloying reactions in a graphite crucible. Results of this investigation were, therefore considered very suspect, and this led to a re-examination of the phase diagrams in the 0-5 at.% antimony region.[31] The purity of the zirconium metal used in this second study was 99.95%, and the reactions were carried out by arc-melting the elements and annealing the products, a process which eliminates any container contribution to contamination. These experiments revealed that the α-β transition of zirconium was raised by about 10°C at 0.5 at.% antimony, the limit of solubility in α-Zr.

In addition to these preliminary studies on the phase relationships in the system, there are several reports of the synthesis of binary compounds. The first well-identified phase was Zr_5Sb_3[32,33] with the hexagonal Mn_5Si_3 structure. From the reported lattice parameters (a = 8.46, c = 5.80 Å[32] and a = 8.53, c = 5.84 Å[33]) it seems likely that this was the actual composition of the "Zr_2Sb" phase previously postulated.

Notwithstanding the previous assertion that this "Zr_2Sb" compound was the most zirconium-rich phase, a Zr_3Sb compound with the Fe_3P structure ($a = 11.35$, $c = 5.67$ Å) was subsequently synthesized.[34] Unfortunately, the experimental details could not be ascertained since the results were presented simply as a list of compounds, structure types, and lattice parameter data.

A later, more thorough report confirmed the existence of Zr_3Sb and also described a Zr_2Sb phase with apparently two structural modifications.[35] An unidentified powder pattern was observed when a Zr_2Sb composition obtained by arc-melting was annealed at 1150°C, while the diffraction lines could be indexed on the basis of a primitive tetragonal cell if the sample was annealed at 1000°C. A slightly more antimony-rich composition ($Zr_{5.1}Sb_3$) resulted in a second unidentified phase as well as Zr_5Sb_3. Since the unit cell of Zr_5Sb_3 was about 4.5% larger than the value interpolated from then-assigned phases, the compound was postulated to be, not a true binary compound but rather an oxygen-stabilized ternary phase. The zirconium employed as a starting material was reactor grade, but the purity of the antimony was not described. One further compound was discovered in this work, and identified as $ZrSb_3$. Its powder pattern could be indexed on the basis of a primitive orthorhombic cell ($a = 14.98$, $b = 9.94$, $c = 3.86$ Å). The crystal structure of this phase was later twice determined by single crystal X-ray diffraction, and the actual composition was shown to be $ZrSb_2$.[36,37]

RESULTS

The binary compounds found in the Zr-Sb system are outlined in Table 2; a representative list of reaction methods, conditions and results is given in Table 3; structure-type information and lattice parameters for the phases so identified are listed in Table 4. The parenthetical numbers following alloy compositions discussed in the text identify the reaction numbers in Tables 3 and 4. The reader should note that three nominal compositions each yield a pair of structure types depending on composition or temperature, namely Zr_5Sb_3, ZrSb, and $ZrSb_2$.

Zr_3Sb

Zirconium-rich samples are easy to prepare by arc-melting the elements since very little antimony volatilization occurs at these compositions. Conversely reactions in which powders are sintered do not give good results presumably because of the lower diffusion rate of the higher melting Zr as compared with Sb; therefore, products near the Zr_3Sb stoichiometry were always prepared by arc-melting.

A sample of overall composition $Zr_{0.81}Sb_{0.19}$ (1) was annealed for 2 days at 1100°C, and an additional 2 days at 850°C subsequent to are-melting, and yielded a mixture of α-Zr and Zr_3Sb. It is evident from the position of the lines in the Guinier powder pattern that there is a very limited solubility of Sb in α-Zr at 850°C. An as-cast sample of a more antimony-rich composition $Zr_{2.13}Sb(Zr_{0.68}Sb_{0.32})$ (2-1) exhibits the pattern of Zr_3Sb plus a component with many weak lines. This second phase is presumably the one which had been previously

Table 2. Compounds in the zirconium-antimony system[a]

Phases		Structures		
Phase Composition	Reference	Structure Type	Space Group	Reference
Zr_3Sb	35	Ni_3P	$I\bar{4}$	35
Zr_2Sb	35	La_2Sb	I4/mmm	38
X ($\sim Zr_2Sb$)	35	unknown	primitive orthorhombic	38
Zr_5Sb_3	38	Y_5Bi_3	Pnma	38
Zr_5Sb_3	33,34	Mn_5Si_3	$P6_3/mcm$	33,34
ZrSb	38	FeSi	$P2_13$	38
ZrSb	38	ZrSb	Cmcm	38
Zr_2Sb_3	38	unknown	primitive tetragonal	38
$ZrSb_2$	38	$PbCl_2$	Pnma	38
$ZrSb_2$	36,37	$ZrSb_2$	Pnnm	36,37

[a]See text regarding stoichiometric differences between pairs of Zr_5Sb_3, ZrSb and $ZrSb_2$ types. The first listed in each is antimony poorer.

Table 3. Summary of zirconium-antimony reaction types and products

Reaction[a]	Product composition (atomic)	Synthesis method[b]	Synthesis conditions temp(°C)	Synthesis conditions time (d)	Products[c]
1	$Zr_{0.81}Sb_{0.19}$	AM	1000 850	2 2	Zr, Zr_3Sb
2-1	$Zr_{0.68}Sb_{0.32}$	AM	as-cast		Zr_3Sb, Zr_5Sb_3
2-2	$Zr_{0.68}Sb_{0.32}$	AM	950	2	Zr_2Sb (Zr_3Sb)
3	$Zr_{0.72}Sb_{0.28}$	AM	950	1	Zr_3Sb, Zr_2Sb
4	$Zr_{0.66}Sb_{0.34}$	AM	1200	0.6	X,[d] Zr_5Sb_3
5	$Zr_{0.65}Sb_{0.35}$	AM	950	2	Zr_2Sb, Zr_5Sb_{3+x}
6	$Zr_{0.626}Sb_{0.374}$	AM	as-cast		Zr_5Sb_3, Zr_5Sb_{3+x}
7	$Zr_{0.60}Sb_{0.40}$	AM	1100 750	4 1	Zr_5Sb_{3+x}
8	$Zr_{0.56}Sb_{0.44}$	AM	900	5	$Zr_5Sb_{3+\underline{x}}$, $ZrSb_{1-x}$
9-1	unknown	V	1000	1	ZrSb, Zr_2Sb_3
9-2	unknown	V	1000	2	$ZrSb_{1-x}$, ZrSb
10	$Zr_{0.50}Sb_{0.50}$	VT	950	21	ZrSb
11	$Zr_{0.400}Sb_{0.600}$	PP	900	6	Zr_2Sb_3
12	Zr + excess Sb	MF	1100	0.5	$ZrSb_2$, Sb
13	$Zr_{0.250}Sb_{0.750}$	P	850 550	1 1	$ZrSb_2$, Sb
14	$Zr_{0.25}Sb_{0.75}$	VT	700	7	$ZrSb_{2-x}$

[a]Referenced in text with parenthetical numbers.

[b]Abbreviations: AM - arc-melted, conditions refer to annealing; V - vaporization of Sb from $ZrSb_2$ in vacuum; VT - vapor transport; PP - pressed pellet of ground powders; MF - Sb metal flux; P - ground mixture of powders.

[c]The groups Zr_5Sb_3, Zr_5Sb_{3+x}; $ZrSb_{1-x}$, ZrSb; $ZrSb_{2-x}$ ($\underline{x} \sim 0.04$), $ZrSb_2$ each involved a pair of different structure types.

[d]See text.

Table 4. Structure types and lattice parameters for zirconium-antimony reactions, Table 2

Reaction	Product	Structure type[a] (space group)	Lattice parameters (Å)[b]
1	Zr_3Sb	Fe_3P ($I\bar{4}$)	a = 11.351(1) c = 5.671(1)
2-1	Zr_3Sb	Fe_3P	a = 11.337(3) b = 5.669(2)
2-1	Zr_5Sb_3	Y_5Bi_3 (Pnma)	a = 7.468(1) b = 8.787(3) c = 10.865(3)
2-2	Zr_2Sb	La_2Sb (I4/mmm)	a = 4.1154(5) c = 15.786(3)
3	Zr_3Sb	Fe_3P	a = 11.3386(6) c = 5.6692(3)
3	Zr_2Sb	La_2Sb	a = 4.1172(6) c = 15.771(3)
4	Zr_5Sb_3	Y_5Bi_3	a = 7.465(1) b= 8.801(1) c = 10.865(2)
4	X (~Zr_2Sb)	orthorhombic (P)	a = 14.652(5) b = 9.058(4) c = 7.756(3)
5	Zr_2Sb	La_2Sb	a = 4.1156(4) c = 15.774(3)
5	Zr_5Sb_{3+x}	Mn_5Si_3 ($P6_3/mcm$)	a = 8.4175(6) c = 5.7678(6)
6	Zr_5Sb_3	Y_5Bi_3	a = 7.467(1) b = 8.797(1) c = 10.872(2)

[a]Reference 39.
[b]Based on indexed lines in Guinier pattern.

Reaction	Product	Structure type[a] (space group)	Lattice parameters (Å)[b]
6	Zr_5Sb_{3+x}	Mn_5Si_3	a = 8.468(1) c = 5.800(1)
7	Zr_5Sb_{3+x}	Mn_5Si_3	a = 8.518(1) c = 5.844(1)
8	Zr_5Sb_{3+x}	Mn_5Si_3	a = 8.573(1) c = 5.872(1)
8	$ZrSb_{1-x}$	FeSi ($P2_13$)	a = 5.6358(4)
9-1	$ZrSb_{1-x}$	FeSi	a = 5.6355(3)
9-1	ZrSb	ZrSb (Cmcm)	a = 3.809(1) b = 10.421(1) c = 14.045(2)
9-2	ZrSb	ZrSb	a = 3.808(4) b = 10.410(8) c = 14.059(6)
9-2	Zr_2Sb_3	tetragonal (P)	a = 9.567(2) c = 5.294(1)
11	Zr_2Sb_3	tetragonal	a = 9.565(1) c = 5.288(1)
14	$ZrSb_{2-x}$	$PbCl_2$ (Pnma)	a = 7.393(1) b = 3.9870(7) c = 9.581(1)
13	$ZrSb_2$	$ZrSb_2$ (Pnnm)	a = 14.963(3) b = 9.963(2) c = 3.8779(7)

observed but remained unidentified,[35] and it will be shown (below) to be a new structure for Zr_5Sb_3. A powder pattern of a third sample, $Zr_{0.72}Sb_{0.28}$ (3), that was annealed at 950°C for one day revealed a mixture of Zr_3Sb and Zr_2Sb appropriate to the composition.

The Fe_3P structure for Zr_3Sb was confirmed by powder patterns. The essential invariance of the lattice parameters over a wide composition range and thermal treatment conditions (see Tables 2 and 3) implies a small range of nonstoichiometry as a function of these thermodynamic parameters. The formation of Zr_3Sb is not dependent on post-casting thermal treatment, but the thermal history is important in determining the adjacent phase. On the zirconium rich side of Zr_3Sb, Zr is always found as the second product but on the antimony-richer side, either Zr_2Sb, HT-Zr_2Sb, or Zr_5Sb_3 will form in the two phase region depending on the material's thermal history (discussed below).

Zr_2Sb

This compound had been obtained in two structural modifications.[35] The transition temperature reportedly lay between 1000°C and 1150°C. In order to verify this, a sample of composition $Zr_{0.68}Sb_{0.32}$ (2-2) was prepared by arc-melting and annealed at 950°C for 2 days. A trace of Zr_3Sb could be detected in the powder pattern of the product. The remainder was presumably the low temperature modification of Zr_2Sb previously indexed on the basis of a primitive tetragonal cell (a = 6.52, c = 7.90 Å) but for an unidentified structure.[35] Although the observed powder pattern can be poorly described with this previous cell, the diffraction pattern is more properly indexed[16] on the basis of a body-

centered tetragonal cell (a = 4.1154(5), c = 15.786(3) Å). More importantly, the observed intensity distribution demonstrates that the compound in question possesses the La_2Sb[39] structure type. A comparison of observed and calculated intensities is given in Table 5. In this structure the positional parameters of one zirconium atom are fixed by symmetry, but those of a second zirconium and the antimony atoms have variable z values. The calculated powder pattern was based on the positional parameters of these atoms in La_2Sb and is, therefore, only an approximation.

This structure of Zr_2Sb contains an empty site, at the center of a zirconium octahedron, which in other compounds thought to be binary phases has later proved to contain an impurity atom, e.g., Ca_2Sb was determined to actually to Ca_4Sb_2O.[40] This type of impurity stabilization can be ruled out by reproducible quantitative yields of Zr_2Sb in a number of reactions which included preparation by both arc-melting and powder sintering. The lattice parameters of Zr_2Sb in equilibrium with Zr_3Sb or Zr_5Sb_3 are experimentally identical (see reactions 3 and 5, Table 4), indicating that Zr_2Sb is a line compound.

In an attempt to produce the higher temperature modification of Zr_2Sb, a product of composition $Zr_{0.66}Sb_{0.34}$ ($Zr_{1.94}Sb$) (4) was prepared by arc-melting, and was annealed at 1200°C for 15 hours in an induction furnace. The power to the induction coil was turned off and the sample cooled to 700°C within one minute. The powder pattern of this alloy contained lines which could be attributed to Zr_5Sb_3 (Y_5Bi_3-type) and a second phase x which is assumed to be the high temperature form of

Table 5. Observed and calculated powder patterns for Zr_2Sb (La_2Sb-type)

d(obs), Å	d(calc), Å	h k ℓ	I(obs)[a]	I(calc)[a]
7.94	7.89	0 0 2	2	2
3.985	3.982	1 0 1	5	12
3.952	3.947	0 0 4	3	3
2.912	2.910	1 1 0	25	26
2.729	2.730	1 1 2	80	90
2.630	2.631	0 0 6	50	37
2.504	2.505	1 0 5	20	34
2.340	2.342	1 1 4	100	100
1.9744	1.9777	0 0 8	15	20
1.6210	1.6209	2 0 6	20	37
1.5903	1.5900	2 1 5	10	19
1.4554	1.4550	2 2 0	15	25
1.4253	1.4259	2 1 7	10	16
1.3877	1.3876	1 1 10	7	11
1.3551	1.3551	1 0 11	9	20
1.2846	1.2841	3 1 2	10	23
1.2734	1.2733	2 2 6	12	20
1.2353	1.2359	3 1 4	20	37

[a]Cu $K\alpha_1$ radiation.

Zr_2Sb. The formulation of this compound as HT-Zr_2Sb is simply a matter of convenience for lack of a better label. The actual composition of this phase is, of course, dependent on the yield of Zr_5Sb_3, which is difficult to estimate accurately from the powder pattern. The limits of the Zr_5Sb_3 yield can be placed between 10% and 20% to give limits for the composition of the unknown phase as $Zr_{2.06}Sb$ and $Zr_{2.35}Sb$.

An attempt was made to index the powder pattern of "HT-Zr_2Sb" on the structural basis of other known compounds near the 2:1 stoichiometry in the twelve binary systems of transition metal group IV and main group V elements (excluding nitrogen). Some of these compounds included Hf_2As, Zr_8As_5, Ti_7P_4 and $Zr_{14}P_9$, but the attempt was unsuccessful. These lines instead were indexed[16] (Table 6) on the basis of the primitive orthorhombic cell listed in Table 4.

The number of atoms in this unit cell ($V = 1029$ Å^3) can be estimated from the average atomic volume found for other binary Zr-Sb compounds (Table 7). The most likely value would be 46 atoms/unit cell to give 22.4 Å^3/atom. The range of reasonable limits would span 44 to 48 atoms/cell where the atomic volumes would range from 23.4 to 21.4 Å^3/atom. These data were used to search Pearson's Handbook[39] which lists structure types according to Laue symmetry, whether the cell is centered or primitive, and finally the number of atoms per unit cell. Orthorhombic structures, both primitive and C-centered with from 44 to 48 atoms/unit cell were checked, but not found compatible with the unknown Zr_2Sb based on chemical grounds, or lattice parameters.

Table 6. Indexed Powder Data for Structurally Undetermined Zr–Sb Phases[a]

X (~Zr_2Sb)			Zr_2Sb_3		
d (Å)	h k ℓ	I_{obs}	d (Å)	h k ℓ	I_{obs}
3.877	0 0 2	10	3.380	2 2 0	2
3.850	2 2 0	5	2.849	2 2 1	100
3.779	1 2 1	5	2.727	3 0 1	100
3.393	4 1 0	10	2.647	0 0 2	100
2.741	5 0 1	20	2.392	4 0 0	50
2.731	2 2 2	20	2.371	2 3 1	50
2.554	4 1 2	20	2.248	2 1 2	10
2.543	1 0 3	20	2.118	1 4 1	10
2.521	3 2 2	50	2.084	2 2 2	75
2.484	0 1 3	100	1.9089	3 4 0	5
2.436	2 0 3	10	1.8718	3 2 2	2
2.382	0 3 2	5	1.7054	1 1 3	50
2.363	6 1 0	5	1.6109	4 4 1	10
2.335	5 0 2	20	1.5685	3 5 1	10
2.280	3 0 3	2	1.5125	6 2 0	35
2.264	2 3 2	2	1.5049	1 6 1	10
2.245	0 2 3	75	1.4739	5 2 2	10
2.231	4 3 1	75	1.4373	4 5 1	5
2.174	0 4 1	50	1.4238	4 4 2	2
2.156	1 4 1	5	1.3768	3 6 1	50
2.013	6 1 2	10	1.3214	0 0 4	10
1.9342	5 0 3	75	1.3131	2 6 2	10
1.8366	2 1 4	10	1.2846	5 1 3	15
1.8159	3 4 2	2	1.2508	2 5 3	5
1.7709	1 2 4	5	1.2322	2 2 4	10
1.5934	9 0 1	10	1.2243	6 5 0	10
1.4402	6 2 4	5			
1.3312	8 0 4	2			
1.3056	0 6 3	10			
1.2437	0 2 6	2			

[a]Guinier data, Cu $K\alpha_1$ radiation; cell constants in Table 4.

Table 7. Atomic volume in Zr-Sb binary compounds

Compound	Unit Cell Volume (A^3)	Z	A^3/Atom[a]
Zr_3Sb	728.85	8	22.8
Zr_2Sb (LT)	267.36	4	22.3
Zr_5Sb_3 (Y_5Bi_3)	713.82	4	22.3
Zr_5Sb_3 (Mn_5Si_3)	360.18	2	22.5
ZrSb (ZrSb)	557.32	12	23.2
$ZrSb_2$ ($ZrSb_2$)	578.10	8	24.1
$ZrSb_{1.96}$ ($PbCl_2$)	282.41	4	23.9

[a]Average volume per Zr atom = 21.1 A^3, average volume per Sb atom = 25.0 A^3.

Experience has shown that unit cells determined solely on the basis of indexed d-spacings without corroboration from single crystal data or by identification of the structure type, as in this instance, must be regarded as only tentative. There is also no conclusive evidence for describing this compound as Zr_2Sb but the composition must be near this stoichiometry. It can, however, be stated with certainty that this phase has a thermal stability range bounded by ~1000 – 1100°C and the effective quenching temperature of an arc-melted preparation (~1400°C).

Zr_5Sb_3

The first reports of a binary Zr-Sb phase[30] and first structure type identified[32,33] were of Zr_5Sb_3 and as such one would suppose it to be the best characterized compound of the system. But at the start of this work it was not even clear whether this was a true binary or an impurity stabilized ternary phase.[35] This question was addressed by a series of reactions near the ideal 5:3 stoichiometric ratio. The results from these reactions indicated that the question cannot be cast so simply, for there are actually two Zr_5Sb_3 phases. One, which is better formulated as Zr_5Sb_{3+x}, does indeed have a Mn_5Si_3-type structure and will be referred to as Zr_5Sb_3-M. The second compound is a stoichiometric Zr_5Sb_3 with the Y_5Bi_3-type structure, denoted as Zr_5Sb_3-Y.

Zr_5Sb_3-Y

When samples of composition Zr_5Sb_3 were prepared by arc-melting, the powder patterns of as-cast samples always contained a two-phase mixture. One phase could be identified as Zr_5Sb_3 with the Mn_5Si_3 structure, but

exhibiting significantly larger lattice parameters than obtained after some annealing reactions (5 and 6, Table 4). The second phase was also observed in a 50:50 mixture with Zr_3Sb in the powder pattern of an as-cast sample with an overall composition of Zr_2Sb. The assumption was, therefore made that this unknown phase was antimony poorer than Zr_5Sb_3. A single crystal of the material (from reaction 4) was indexed on the diffractometer, and refined lattice parameters were then obtained from powder data. The unit cell information allowed the structure of the unknown phase to be identified as either of the Y_5Bi_3[41] or the Yb_5Sb_3[42] type. These two structures are very similar.

In order to determine which structural modification was actually adopted, and because it was thought that this phase was antimony deficient Zr_5Sb_{3-x}, a single crystal structural investigation was carried out. The experimental details of data collection are listed in Table 8. Both Y_5Bi_3 and Yb_5Sb_3 occur in the space group Pnma, but the a and c axes are interchanged.

If Zr_5Sb_3-Y possessed the Yb_5Sb_3 structure then the unit cell parameters in the standard setting would have been a = 10.865, b = 8.801, c = 7.465 Å. This setting was used to collect the data, but after averaging, the systematic extinctions were found to place it in a nonstandard setting, space group Pcmn. The a and c axes were interchanged, and the h and ℓ parameters adjusted accordingly to give the standard space group Pnma. This indicated that the structural modification of Zr_5Sb_3-Y was of the Y_5Bi_3-type.

Table 8. Crystallographic data for single crystals

Compound	Zr_5Sb_3-Y	Zr_5Sb_3-M	ZrSb	$ZrSb_{1.96}$
Space group	Pnma	$P6_3/mcm$	Cmcm	Pnma
Lattice Parameters[a] (A)				
a	7.465(1)	8.4267(5)	3.827(1)	7.393(1)
b	8.801(1)	8.4267(5)	10.426(3)	3.9870(7)
c	10.865(2)	5.7856(6)	14.007(5)	9.581(1)
V, A^3	713.9(2)	355.79(6)	558.9(4)	282.42(7)
Crystal size (mm)	0.22	0.25	0.27	0.30
	0.07	0.04	0.18	0.08
	0.05	0.04	0.05	0.05
2θ(max), deg	55	55	55	55
Reflections				
checked	1892	2057	762	775
observed[b]	1179	1312	644	664
independent	657	144	327	345
R(ave)	0.022	0.047	0.015	0.039
R[c]	0.028	0.027	0.037	0.032
R_w[d]	0.029	0.034	0.045	0.039
Secondary ext. coeff.	0.018	0.030	0.018	0.055
Absorption coeff. (cm^{-1})	180	181	196	223
No. of variables	50	17	22	22

[a]From refined Guinier powder data.

[b]Reflections with $F_{obs} > 3\sigma_F$ and $I_{obs} > 3\sigma_I$ were considered observed.

[c]$R = \sum||F_o| - |F_c||/\sum|F_o|$.

[d]$R_w = [w(|F_o| - |F_c|)^2/\sum w|F_o|^2]^{1/2}$.

The structure refinement was initiated using parameters from Y_5Bi_3 and proceeded smoothly. In the final three cycles all variables except the Zr(1) multiplicity were simultaneously refined. The resulting site occupancy yielded the formula unit as $Zr_{4.99(1)}Sb_{3.02(3)}$, so that the compound was not substoichiometric in antimony as initially assumed. The possibility that the Y_5Bi_3 structure of Zr_5Sb_3-Y was stabilized by an impurity was eliminated by a final Fourier map which contained no residual electron density greater than 0.5 e/Å^3.

The refined variables and resulting interatomic distances are listed in Table 9. A projection of the structure onto (010) is shown in Figure 1, where shadings of the atoms represent the fractional y coordinate such that an atom at $y = 1/4$ is one-fourth shaded. The atoms that are half filled are near $y = 1/2$ and at $y = 0$ but these atoms, Zr(3) and Sb(1), do not have y parameters fixed by symmetry, and are actually displaced from the planes by 0.44 and 0.07 Å, respectively. These displacements are the features that distinguished the Y_5Bi_3 and Yb_5Sb_3 structures.

The Zr atoms at $y = 3/4$ have been connected in such a way as to help visualization of the structure, but these lines do not represent actual bonds. The net formed by the Zr atoms is composed of triangles and distorted hexagons. This same net, slightly displaced, is repeated by the Zr atoms at $y = 1/4$. The Sb(2) atoms at $y = 1/4$ and 3/4 are slightly displaced from the centers of the hexagons towards opposite edges. The Zr triangles compose opposite faces of trigonal prisms which are centered by the Sb(1) atoms at $y \approx 0, 1/2$. These prisms are stacked end-to-end to form an infinite chain of confacial prisms along the b axis, these chains

Table 9. Refined parameters and interatomic distances Zr_5Sb_3-Y

Atom	Site	x	y	z	B_{11}
Sb(1)	8(d)	0.0709(1)	-0.0078(1)	0.1756(1)	0.85(3)
Sb(2)	4(c)	0.0779(1)	1/4	0.4566(1)	0.72(4)
Zr(1)	4(c)	0.4699(2)	1/4	0.4898(1)	0.72(6)
Zr(2)	4(c)	0.3075(2)	1/4	0.2249(1)	0.90(6)
Zr(3)	8(d)	0.1998(1)	0.5543(1)	0.4425(1)	0.86(4)
Zr(4)	4(c)	0.1475(2)	1/4	0.7130(1)	0.86(6)

Interatomic Distances (Å)[a]

Sb(1) - Zr(2)	2.927(1)		Sb(2) - Zr(2)	2.824(2)
Sb(1) - Zr(4)	2.945(1)		Sb(2) - 2Zr(3)	2.833(1)
Sb(1) - Zr(1)	2.951(1)		Sb(2) - Zr(4)	2.835(2)
Sb(1) - Zr(1)	2.992(1)		Sb(2) - 2Zr(3)	2.912(1)
Sb(1) - Zr(4)	3.023(1)		Sb(2) - Zr(1)	2.951(2)
Sb(1) - Zr(3)	3.083(1)		Sb(2) - Zr(2)	3.048(2)
Sb(1) - Zr(3)	3.085(1)		Sb(2) - 2Zr(1)	3.806(1)
Sb(1) - Zr(3)	3.106(1)			
Sb(1) - Zr(2)	3.193(1)		Zr(1) - 2Sb(1)	2.951(1)
Sb(1) - Sb(2)	3.806(1)		Zr(1) - Sb(2)	2.951(2)
Sb(1) - Sb(1)	3.963(1)		Zr(1) - 2Sb(1)	2.992(1)
			Zr(1) - 2Zr(3)	3.099(2)
			Zr(1) - Zr(2)	3.125(2)
			Zr(1) - 2Zr(3)	3.393(1)
			Zr(1) - Zr(4)	3.419(2)
			Zr(1) - Zr(2)	3.437(2)
			Zr(1) - Zr(4)	3.491(2)

[a]Distances less than 4 Å.

B_{22}	B_{33}	B_{12}	B_{13}	B_{23}
0.53(3)	0.70(3)	0.02(2)	-0.04(2)	-0.02(2)
0.65(4)	0.66(4)	0	-0.02(3)	0
0.69(5)	0.65(6)	0	0.03(4)	0
1.13(6)	0.64(6)	0	0.03(5)	0
0.63(4)	0.85(4)	-0.02(3)	0.12(3)	0.00(3)
0.78(6)	0.61(6)	0	0.02(4)	0

Zr(2) - Sb(2)	2.824(2)	Zr(3) - Zr(3)	3.375(2)
Zr(2) - 2Sb(1)	2.927(1)	Zr(3) - Zr(1)	3.393(1)
Zr(2) - Sb(2)	3.048(2)	Zr(3) - Zr(3)	3.445(2)
Zr(2) - Zr(1)	3.125(2)	Zr(3) - Zr(2)	3.519(2)
Zr(2) - 2Sb(1)	3.193(1)	Zr(3) - Zr(4)	3.544(2)
Zr(2) - Zr(1)	3.437(2)	Zr(3) - Zr(2)	3.663(1)
Zr(2) - 2Zr(3)	3.519(2)	Zr(3) - Zr(4)	3.996(1)
Zr(2) - 2Zr(3)	3.663(1)		
Zr(2) - 2Zr(2)	3.777(1)	Zr(4) - Sb(2)	2.835(2)
		Zr(4) - 2Sb(1)	2.945(1)
Zr(3) - Sb(2)	2.833(1)	Zr(4) - 2Sb(1)	3.023(1)
Zr(3) - Sb(2)	2.912(1)	Zr(4) - Zr(3)	3.239(2)
Zr(3) - Sb(1)	3.083(2)	Zr(4) - Zr(1)	3.419(2)
Zr(3) - Sb(1)	3.085(1)	Zr(4) - Zr(1)	3.491(2)
Zr(3) - Zr(1)	3.099(2)	Zr(4) - 2Zr(3)	3.544(2)
Zr(3) - Sb(1)	3.106(1)	Zr(4) - 2Zr(4)	3.822(1)
Zr(3) - Zr(4)	3.239(2)	Zr(4) - 2Zr(3)	3.996(1)

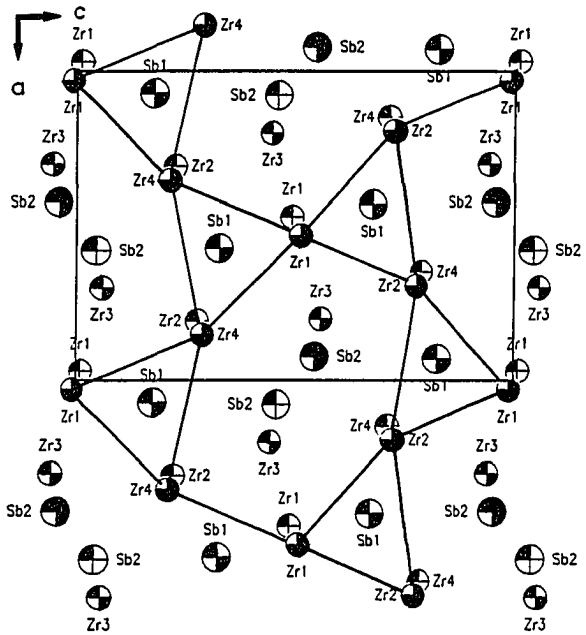

Figure 1. Projection of Zr_5Sb_3-Y onto (010). The shadings of the atom indicate their y coordinate. Half-filled atoms are at y ≈ 1/2. The ellipsoids are arbitrary. The triangular-hexagonal net of zirconium atoms at z = 3/4 has been emphasized

share edges to form hexagonal channels. The channels in addition to Sb(2) atoms, also contain Zr(3) atoms at $y \sim 0, 1/2$ which serve to cap the three rectangular faces of the trigonal prisms.

The nets at $y = 1/4, 3/4$ are almost identical in the Yb_5Sb_3 structure but the layers at $y = 0, 1/2$ are buckled differently. The difference can be seen in Figures 2a and 2b where only Sb(1) and Zr(3) from the Y_5Bi_3 structure and the equivalent atoms from Yb_5Sb_3 are projected onto the planes indicated. This slight perturbation of the two structures is not easily distinguished in a powder pattern.

The single crystal refinement of Zr_5Sb_3-Y resulted in a stoichiometry of 5:3 within experimental error, and powder diffraction data indicated that the composition does not vary significantly from this ratio. The lattice parameters of Zr_5Sb_3-Y in equilibrium with Zr_3Sb (2-1, Table 4) or with Zr_5Sb_3-M (6, Table 4) were essentially identical. Likewise, as-cast or annealed samples did not show any variations in lattice parameters.

There is a definite temperature dependence, however, in the formation of Zr_5Sb_3-Y. It is only observed in reactions that have been prepared by arc-melting. When stoichiometric amounts of Zr and Sb powders are sintered ($T \leq 1100°C$) only Zr_5Sb_3-M is formed. The Zr_5Sb_3-Y phase is, therefore, presumed to be a high temperature modification but the transformation temperature is not known since annealing reactions have yielded inconsistent results. As an example, a sample of $Zr_5Sb_{3.0}$ composition obtained by arc-melting was annealed at 1100°C for 1 week with no change in the observed Zr_5Sb_3-Y and Zr_5Sb_3-M proportions, but a

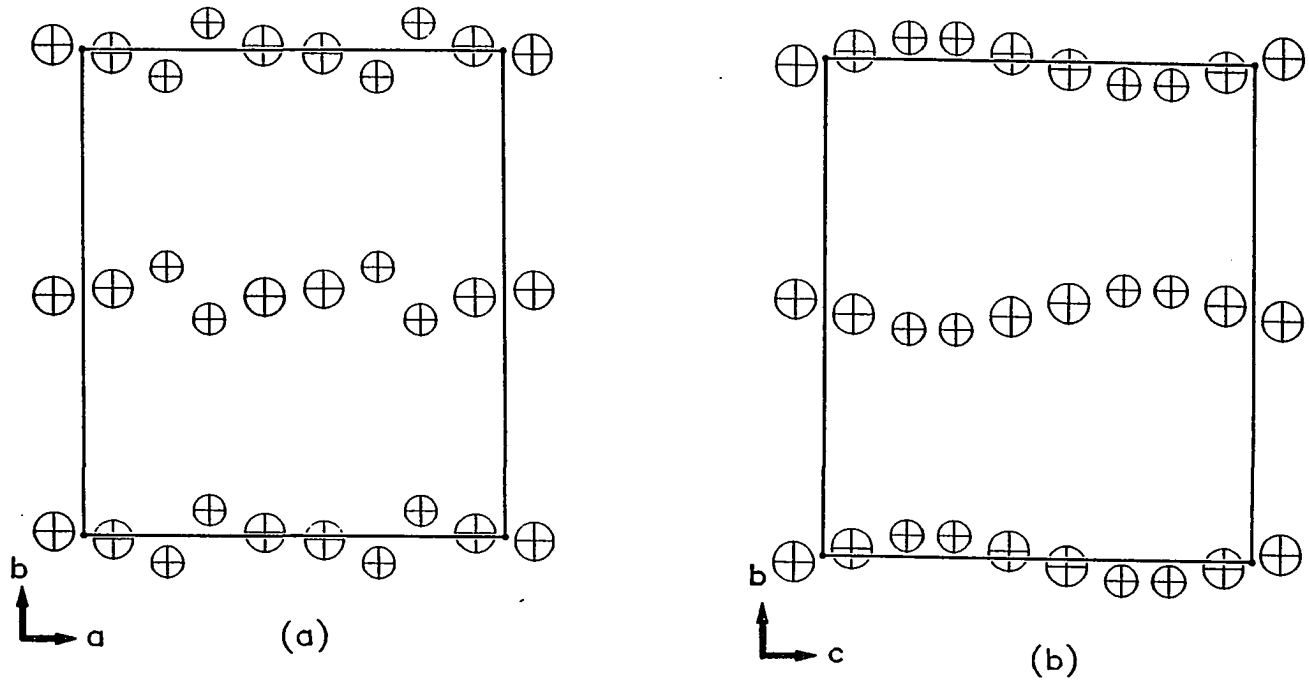

Figure 2. Projection of the Y_5Bi_3(a), and Yb_5Sb_3(b) structures onto (001) and (100), respectively. The difference between the structures can be seen in the buckled layers at y = 0, 1/2. In the interest of clarity, only the atoms on these planes are drawn. Smaller circles are the rare earth metals

sample of composition $Zr_5Sb_{2.7}$ annealed at 950°C for 2 days yielded only Zr_5Sb_3-M along with Zr_2Sb. It is possible that the transformation rate is very dependent on the size, and amount of contact between the grains of the different phase in the solidified button. These factors depend on the cooling rate of the sample after the arc is extinguished, which in turn is affected by the amount of material and phases present in the sample. The transformation is sluggish and must apparently overcome high kinetic barriers. The reverse reaction, Zr_5Sb_3-M to Zr_5Sb_3-Y, must take place above 1100°C.

Zr_5Sb_3-M

The Mn_5Si_3-type Zr_5Sb_3 can be synthesized by sintering powders, vapor phase transport or arc-melting. The vapor transport reactions are difficult experiments because of the high temperature required to form Zr_5Sb_3 from the gaseous iodide species. Hot wire reactions were only partially successful. They were carried out by sealing a stoichiometric amount of Zr and Sb powder and a small quantity (~25 mg) of iodide added in the form of SbI_3 in a Pyrex tube. The Pyrex vessel contained a Ta wire with external connections through which a current could be passed. The entire apparatus was placed in a furnace at 300°C and the wire heated to ~1300°C. This succeeded in producing Zr_5Sb_3, unfortunately the composition of the material deposited on the hot wire is very dependent on temperature and is independent of the starting composition. The wire temperature, is constantly varying as material, and hence electrical resistance, is deposited on it. If the wire temperature dropped too low, then $ZrSb_{1-x}$ or even ZrSb also formed.

Isothermal iodide transport reactions at 1300°C were also investigated. Stoichiometric amounts of Zr and Sb, and a small quantity of SbI_3 (~5 mg) were sealed in Ta tubes, and heated in an evacuated mullite tube. Unfortunately, the vacuum (10^{-5} torr) was not adequate to maintain compositional integrity during the two-week reaction time span. Some zirconium oxide, with consistent lattice parameters, was always observed (~10%). No X-ray size single crystals of Zr_5Sb_3 were obtained.

Preparations by arc-melting were generally satisfactory for compositions between $Zr_5Sb_{3.2}$ and Zr_5Sb_4, with sharp diffraction lines seen for both as-cast and annealed (1000-1100°C, 3 days) products. When the composition of the product was closer to Zr_5Sb_3, then Zr_5Sb_3-Y was also observed in as-cast samples. Annealing the multi-phase products yielded inconsistent results (discussed above). In preparations of Zr_5Sb_3 by sintering ($T \leq 1100°C$) or vapor transport, Zr_5Sb_3-Y is never seen.

It was difficult to achieve equilibrium in sintered powder reactions, and the samples had to be reground and pressed into a pellet two or three times and maintained at temperature (1000-1100°C) a total of one to two weeks. Most samples were, therefore, prepared by arc-melting and annealing (1000°C, 3 days).

The Zr_5Sb_3-M phase was once thought to be an impurity-stabilized compound on the basis of an observed atomic volume that was about 4.5% larger than the value interpolated between phases as then assigned. The fact that Zr_5Sb_3-M is a true binary compound can be established from the observation of reproducible and quantitative yields in many different reactions using different synthetic techniques. This investigation has

led to the determination that Zr_5Sb_3-M exhibits a substantial homogeneity range which may account for the abnormally high atomic volume previously observed.

The homogeneity range is shown graphically in Figure 3 where the data are plotted with a least-squares linear fit. The data points were obtained from products of annealed arc-melted reactions in which the final compositions Zr_5Sb_{3+x} were estimated by attributing all weight loss to antimony volatilization. The single phase data can be seen to intersect the antimony-poor, two-phase limit at a Zr_5Sb_x composition where x = 2.97. It seems likely that the substoichiometric limit is not real but an artifact of the small systematic error introduced by attributing all weight loss to antimony. This consideration is presumed to apply to the other phase limit as well. The uncorrected linear least-squares fit of lattice parameters yielded the following equations.

$$a = 0.31455(x) + 7.4864 \text{ (correlation factor 0.9998)}$$

$$c = 0.24465(x) + 5.04131 \text{ (correlation factor 0.9998)}$$

The equations were then used to calculate x values from measured lattice parameters of products in which the precise composition was not known. These were transport reactions employing either hot wire or isothermal conditions. Using the linear equation for the a-axis, a composition x was calculated, paired with the c-axis value of the same sample, and plotted. The data points for the a-axis were arrived at in the same manner by employing the c-axis fit. The scatter of the data points is a measure of the internal consistency of the two least-squares fits. The plotted points, Figure 4, can be seen to deviate from the previously

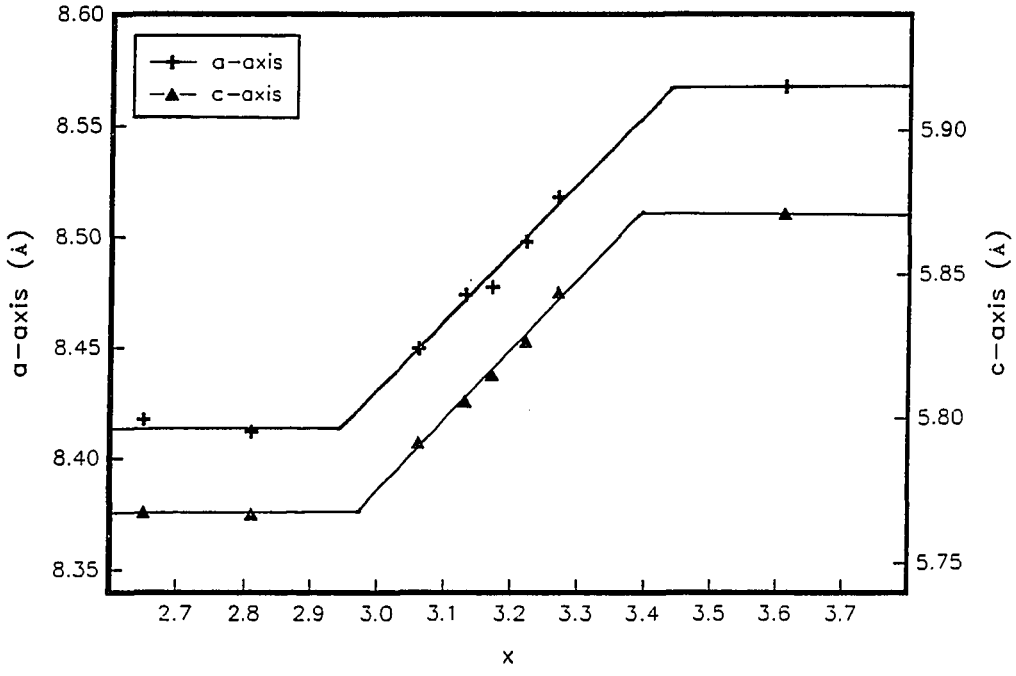

Figure 3. Lattice parameters vs composition plot for Zr_5Sb_x. There are additional data points in the two-phase regions that are outside the range plotted, but were used in fixing the horizonal lines

calculated least-squares line. This is especially true of the data plotted along the a-axis line, which implies that the c-axis equation used to calculate the composition of these points is not strictly applicable. Nevertheless, the deviations are small and the lattice parameters essentially show a linear dependence on composition.

Having established the existence of a homogeneity range for Zr_5Sb_3-M, from approximately $Zr_5Sb_{3.0}$ to $Zr_5Sb_{3.4}$, the question of composition formulation now arises. The composition may as easily be represented by $Zr_{5-y}Sb_3$, as by Zr_5Sb_{3+x}. The latter was chosen for compelling reasons.

The occupation by Sb of the interstitial site seems more likely than Zr vacancies. This supposition is based on the examples of Ti_5Ga_4[43] and Zr_5Sn_4[44] which have 'filled" Mn_5Si_3 structures, where the fourth main groups metal atom is found in the so-called interstitial site, viz., Zr_5Sb_3Ga and Zr_5Sn_3Sn. Similar behavior with antimony is reasonable and this circumstance was confirmed by a single crystal structural investigation.

The single crystal was obtained from an as-cast arc-melted preparation of overall composition $Zr_5Sb_{3.0}$, where the powder pattern contained a mixture of Zr_5Sb_3-Y and Zr_5Sb_3-M diffraction lines. The experimental details of data collection are outlined in Table 8. The data exhibited systematic absences consistent with the space group of the Mn_5Si_3 structure, $P6_3/mcm$. Initial least-squares refinement was carried out on approximate positional parameters based on Mn_5Si_3. The refinement proceeded in a well behaved manner, and after several cycles the

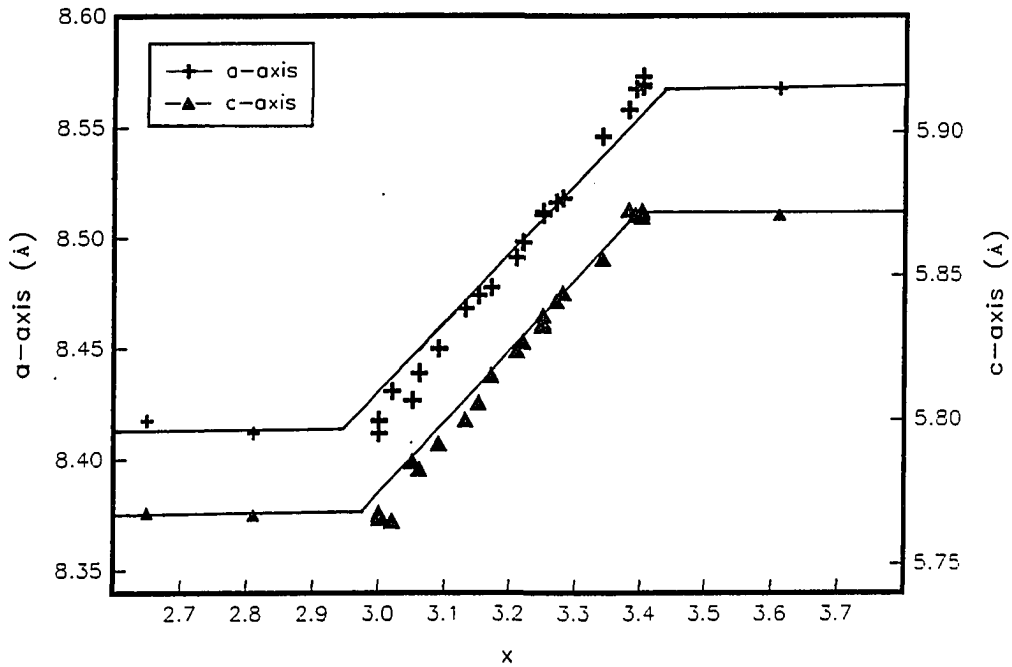

Figure 4. Plot of composition vs. lattice parameters for Zr_5Sb_x phases of unknown composition. The crosses indicate composition calculated from least-squares fit of c-axis data. The triangles indicate composition calculated from least-squares fit of a-axis data. The scatter of the data points is a measure of the internal consistency of the two least-squares fits

convergence of the variable positional parameters, anisotropic thermal parameters and secondary extinction correction factor yielded an R of 0.071. At this point a Fourier map revealed an electron density peak at the origin of the unit cell of approximately 7 e/Å^3. The electron density was assumed to be a random partial occupancy by antimony of the interstitial site and was refined as such. The distance of the surrounding Zr atoms to this site is 2.53 Å which excludes the possibility of occupancy by an oxygen atom. The final agreement factors converged at $R = 0.027$ and $R_w = 0.034$ with all variables except that for Zr(1) occupancy, varied simultaneously. The formula as determined by the refinement was $Zr_2Zr_{3.00(2)}Sb_{3.01(2)}Sb_{0.161(7)}$. A list of all refined parameters and resulting interatomic distances is given in Table 10.

The crystal structure confirms the supposition that the range of homogeneity observed by powder diffraction is due to insertion of antimony into the interstitial site. The refined antimony composition of 3.161(7) can be compared with the composition calculated from the previously derived linear least-squares fit, and the powder pattern lattice constants. The values calculated are $X_a = 3.14$ and $X_c = 3.13$ which are slightly lower than the single crystal result. This discrepancy can be accounted for if allowance is made for the systematic error introduced when deriving the equations (discussed above).

A projection of the Zr_5Sb_3-M structure down the c-axis is drawn in Figure 5. All atoms are located in special positions with fixed z parameters represented by the shading of the atoms. Filled circles are at z = 0 and 1/2, and z = 1/4 or z = 3/4 atoms are fractionally shaded

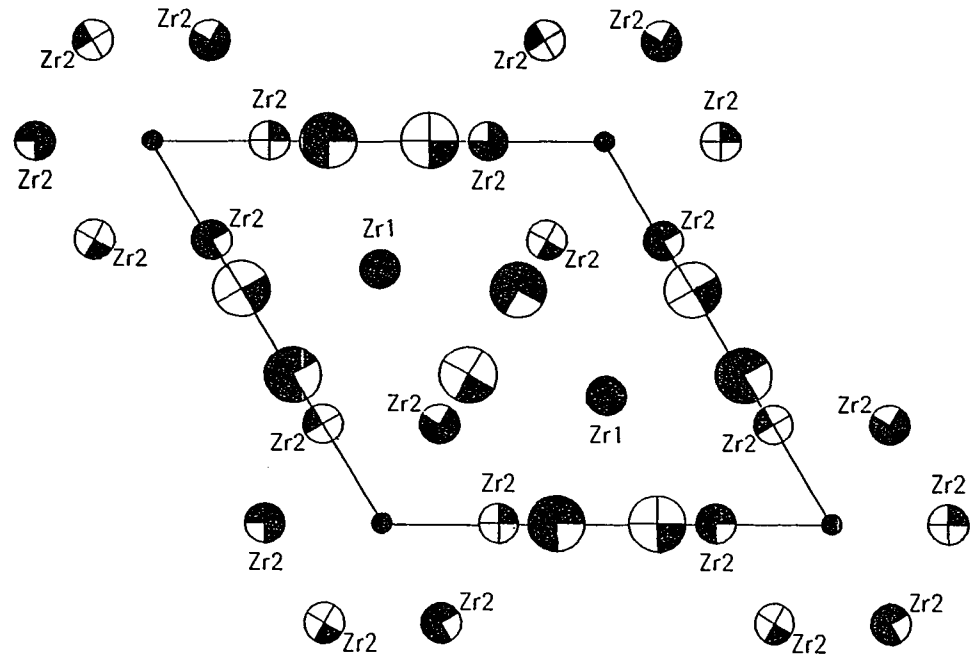

Figure 5. Projection of the Zr_5Sb_3-M structure onto (001). The thermal ellipsoid sizes are arbitrary; large circles are antimony, medium circles are zirconium, small circles mark the interstitial site at the unit cell origin. Fractionally shading of the atoms represents the height along the c-axis. Filled small circles are at both z = 0 and 1/2

Table 10. Refined parameters and interatomic distances for $Zr_5Sb_{3.16}$ (Mn_5Si_3)

Atom	Site	Occupancy	x	y	z
Sb(1)	6(g)	1.003(7)	0.6083(1)	0	1/4
Zr(1)	4(d)	1	1/3	2/3	0
Zr(2)	6(g)	1.000(7)	0.2466(3)	0	1/4
Sb(2)	2(b)	0.081(4)	0	0	0

Interatomic Distances (Å)

Sb(1) - 2Zr(2)	2.890(1)
Sb(1) - 4Zr(1)	2.974(1)
Sb(1) - Zr(2)	3.048(2)
Sb(1) - 2Zr(2)	3.141(1)
Sb(1) - 2Sb(1)	3.421(1)
Zr(1) - 2Zr(1)	2.893(1)
Zr(1) - 6Sb(1)	2.974(1)
Zr(1) - 6Zr(2)	3.545(1)
Zr(2) - 2Sb(2)	2.532(2)
Zr(2) - 2Sb(1)	2.890(1)
Zr(2) - Sb(1)	3.048(2)
Zr(2) - 2Sb(1)	3.141(1)
Zr(2) - 4Zr(1)	3.545(1)
Zr(2) - 4Zr(2)	3.562(1)
Zr(2) - 2Zr(2)	3.599(4)

B_{11}	B_{22}	B_{33}
1.82(4)	1.60(5)	1.66(5)
2.00(9)	B_{11}	1.40(8)
3.46(7)	1.79(7)	2.56(8)
2.5(6)	B_{11}	1.0(5)

accordingly. The structure can be described as being composed of two chains which extend along the c-axis (see Figure 6). The Zr(1) atoms form a linear chain with an extremely short Zr-Zr interatomic distance of 2.893(1) Å compared to 3.2 Å in hcp α-Zr.[13] This linear chain of very closely spaced transition metals is a notable feature of the Mn_5Si_3 structure type and is very similar to the linear transition metal chains found in the A15 compounds. A significant difference can be found in the fact that in Mn_5Si_3 the chains extend only in one direction, not the three found in the cubic A15 phases. The Zr(1) atoms of these chains are coordinated by six Sb(1) atoms at a distance of 2.974(1) Å, which is typical of Zr-Sb spacings in other binary compounds. The surrounding polyhedron is somewhat unusual in that the six-fold coordination cannot described as trigonal prismatic or trigonal antiprismatic but intermediate between these two extremes.

The second structural feature is formed by the Zr(2) atoms and can be viewed as an infinite stack of confacial octahedra, more properly trigonal antiprisms. The interstitial site is located at the center of these octahedra. In contrast to the Zr(1) atoms, the Zr(2)-Zr(2) interatomic distances are very long at 3.56 and 3.60 Å. In fact, the Zr(1)-Zr(2) distance of 3.55 Å is even shorter. The Sb(1) atoms are located above pairs of available faces of the shared octahedra in the manner of the well-known M_6X_8 clusters. Each of the Zr(2) atoms is shared between two octahedra, resulting in $Zr_{6/2}$. Two of the eight faces of the octahedron are unaccessible to Sb because of cluster condensation and the antimony bridging each of the remaining six faces is shared by

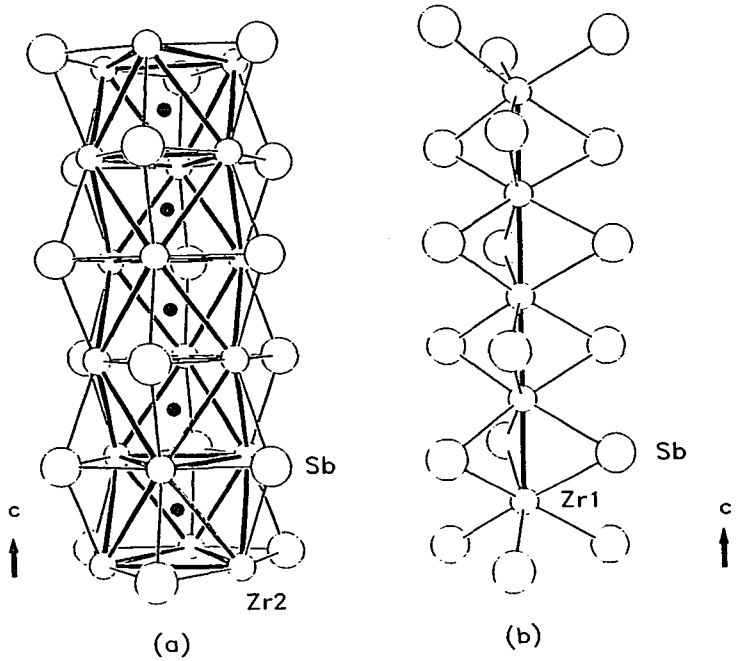

Figure 6. A view of the condensed octahedral Zr(2) chain (a), and the linear Zr(1) chain (b). The thermal ellipsoids are arbitrary. Filled circles denote the interstitial site. Note that Zr(1) and the interstitial site occur at the same height along c and have the same interatomic spacing

two octahedra resulting also in $Sb_{6/2}$. The stoichiometry of the chain is then Zr_3Sb_3. The same structural feature can be found in the condensed M_6X_8 cluster compound KMo_3S_3.[45] The two crystal structures are actually very similar; the difference comes about when each potassium is replaced by a pair of Zr atoms, forming the linear metal chain.

The Zr_5Sb_3-M structure is not as anisotropic as the above discussion of the structural features would seem to indicate. This is because each Zr atom in the two chains discussed is strongly bonded to the Sb(1) atoms which are shared between Zr(1) and Zr(2), and serve to couple the structure in three dimensions.

The ideal solid solution behavior of Zr_5Sb_{3+x} is manifested in the linear increase of lattice parameters with increasing Sb composition (Vegard's law). The possibility that some of these phases may have an ordered structure (superstructure) was considered. Superstructure formation with the Mn_5Si_3 structure has been observed with rare-earth metal silicides in which carbon is added as a ternary component and occupies the interstitial site.[46,47,48] Unlike Zr_5Sb_3-M, in $RE_5Si_3C_x$ (RE = Gd, Ho, Er) x could be varied from 0.0 to 1.0 and a superstructure of $a = \sqrt{3}a$ was observed at $x \simeq 0.5$ for all three metals, plus an additional tripling of the c-axis at $x = 1.0$ for Er and Ho. The plot of lattice parameters versus composition for $Gd_5Si_3C_x$ varied markedly from linearity.[48] Despite the obvious differences between Zr_5Sb_{3+x} and $RE_5Si_3C_x$, the possibility of superstructure formation was investigated.

The powder patterns of 23 reactions that yielded a single phase Zr_5Sb_3-M product were examined, and 17 showed no evidence of superstructure lines. These were prepared by a variety of techniques and included arc-melted, as-cast and annealed (T = 1000-1100°C) products, and sintered powders (T = 1000-1100°C) with and without a transport agent added. The remaining six reactions did exhibit weak diffraction lines indicative of a superstructure.

These six reactions were from a series designed to produce lattice parameter vs composition data. They had been loaded with a ground mixture of $Zr_5Sb_{3.0}$ prepared by arc-melting and Sb, and were sealed in Ta containers. The containers were placed in a vacuum furnace (10^{-6} torr) and the materials allowed to react at 1300°C for 3 days. The series of compounds Zr_5Sb_x, (x = 3.50, 3.40, 3.35, 3.30, 3.25, 3.20, 3.15) was supposed to have been produced by these reactions, but the lattice parameters for all the products were virtually identical, and within experimental error the same as the values for the antimony-rich limit $Zr_5Sb_{3.40}$ (Figure 3). The reactions originally loaded with the compositions $Zr_5Sb_{3.5}$ and $Zr_5Sb_{3.4}$ also contained in the powder patterns the strongest lines of $ZrSb_{1-x}$ (two and one lines, respectively). The other reactions may also have produced this phase, but below the detection limit of Guinier powder diffraction (~5%). In addition, most of the powder patterns contained the same 3 or 4 very weak extra lines that could be indexed on a larger hexagonal cell where a = $\sqrt{3}$a; the same one found for $RE_5Si_3C_{0.5}$. This does not constitute proof of a super

structure for Zr_5Sb_3-M because it is not certain that the powder patterns are of the binary compound.

The formation of products with identical lattice parameters from reactions loaded to yield different compositions can be explained by loss of Zr from the starting material to form ZrO_2. If enough oxygen were present, the Zr_5Sb_3-M product would shift to more and more antimony-rich compositions until the $Zr_5Sb_{3.4}$ limit was reached. In fact, the two or three most intense lines of monoclinic ZrO_2 can be seen as very weak lines in all of the powder patterns. The amount of oxygen required to shift the composition in the worst case, from $Zr_5Sb_{3.15}$ to $Zr_5Sb_{3.40}$, would be very small. Only 3 mg of Zr reacting to produce ZrO_2 would give this result. Such a small amount of oxygen could have easily come from the vacuum atmosphere and diffused through the Ta container, or been present in the zirconium powder starting material.

It is likely that the superstructure lines may indeed arise from an ordering of Sb in the interstitial site which occurs at 1300°C, but is not observed at lower temperatures because the kinetic barriers of Sb mobility have not been overcome. The great difficulty encountered in achieving equilibrium at 1000-1100°C with sintered powders is testimony to the fact that mobility of atoms is very low. No preparations of $Zr_5Sb_{3.4}$ by sintering of powders was attempted, and arc-melted samples were annealed for only 3 days. These factors may account for the absence of superstructure lines in all but the six reactions discussed. However, it is less likely, but also possible that the superstucture observed was caused by an ordering of antimony and oxygen atoms and that this accounts

for the absence of superstructure lines in reactions run under more inert conditions.

There is a temperature dependence to the formation of Zr_5Sb_3-Y or $Zr_5Sb_{3.0}$-M. The Y_5Bi_3 structure is found only as a metastable phase from high temperature preparations. The lattice constants of Zr_5Sb_3-M found with Zr_5Sb_3-Y in as-cast preparations are consistent with, and equal to those measured for $Zr_5Sb_{3.161(7)}$. This implies that the transformation from the Y_5Bi_3 structure to the Mn_5Si_3 modification is an incongruent process. There is also a compositional dependence since Zr_5Sb_3-Y has an extremely narrow homogeneity range and Zr_5Sb_3-M has an extensive one. An excess of antimony will thus favor the formation of the Mn_5Si_3 structure type.

The same two structural modifications have been observed for RE_5Bi_3 phases as well. The compounds Gd_5Bi_3 and Tb_5Bi_3 were found to be dimorphic.[49] The Y_5Bi_3 structure was observed from melted alloys (i.e., high temperature) with a more zirconium-rich composition. The phases were written as RE_5Bi_3 for the Mn_5Si_3 structure and $RE_{5+x}Bi_3$ for the Y_5Bi_3 modification. A subsequent crystal structure refinement of the compound Y_5Bi_3 established that it was a stoichiometric phase with no excess rare-earth metals, and so the Mn_5Si_3 polymorphs were now described as $RE_{5-x}Bi_3$.[41] The results of the present investigation of Zr_5Sb_3 seem to indicate that the Mn_5Si_3 structure for Gd_5Bi_3 and Tb_5Bi_3 should once again be rewritten, now as RE_5Bi_{3+x}.

The structural relationship between the Y_5Bi_3 and Mn_5Si_3 types described for the RE_5Bi_3 phases[41] is equally applicable to Zr_5Sb_3. A

structural feature common to both structure types is shown in Figures 1 and 7. A chain of opposite facing Zr trigonal prisms centered by Sb atoms runs parallel to the [101] direction in Zr_5Sb_3-Y (Fig. 1). Bisecting the trigonal prisms is a network of Zr and Sb atoms forming diamonds and pentagons. A similar chain of opposite facing Zr trigonal prisms can also be found in Zr_5Sb_3-M along the [001] direction, but it is now linear and not buckled as in Zr_5Sb_3-Y (Fig. 7). The network of Zr and Sb atoms bisecting the prisms forms a ribbon of triangles sharing edges. The distortion that resulted in the buckling of the prism chain also caused this regular network of triangles to form the pentagons and diamonds observed in the Y_5Bi_3 structure.

The differences between the two structures cannot be attributed solely to the simple distortion of the prism chains. In Zr_5Sb_3-Y the prisms share their trigonal faces to form planes composed of trigonal columns. These planes are connected by sharing the remaining edges to constitute the three dimensional structure and give the large hexagonal channels. The connectivity of the trigonal prisms in Zr_5Sb_3-M is very different. The prisms do not share either the trigonal faces or the remaining third edge (see Figure 7). A considerable rearrangement of the structure would be required to convert the Y_5Bi_3 into the Mn_5Si_3 structure, and could account for the large kinetic barriers found for the interconverion.

The interstitial site which is at the center of a Zr octahedron in Zr_5Sb_3-M can have a counterpart in Zr_5Sb_3-Y; it is, however, a tetrahedral site with a distance of ~2.1 Å to the neighboring Zr atoms. This

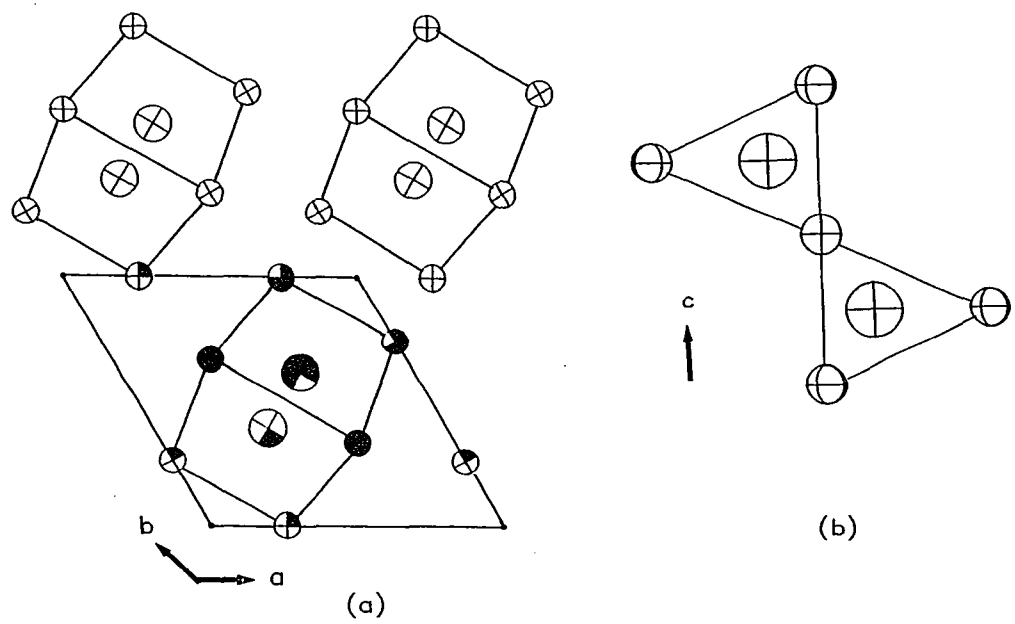

Figure 7. Trigonal prism chain of zirconium in Zr_5Sb_3 (Mn_5Si_3). In the interest of clarity only the atoms in the trigonal prism chain are drawn in the projection (a). The thermal ellipsoids are arbitrary; large circles are antimony, smaller circles are zirconium. One unit cell has been outlined. Fraction shading of the atoms represents the height along the c-axis. Filled circles are at both z = 0 and 1/2. Note that the antimony-centered trigonal prims face in alternate directions. This is better seen in (b)

is an extremely small hole for any excess Sb atoms, requiring a very large distortion. Extra Sb atoms can be much more easily accommodated in the interstitial site of Zr_5Sb_3-M and are likely to cause adoption of the Mn_5Si_3 structure for Zr_5Sb_{3+x} compositions.

A small nonmetal (B, C, N) atom would be more likely to fit in this site. Investigations of these Zr_5Sb_3Z systems (described in part II) showed that even the small nonmetal atoms prefer the octahedral hole in the Mn_5Si_3 modification.

ZrSb

There were no reports of a compound with an equiatomic composition in the Zr-Sb system but during the course of this investigation two phases with a stoichiometry near 1:1 were observed. One of these forms with the FeSi structure,[50] and the second is found in a unique structure type that will be denoted as ZrSb .

FeSi

When determining the antimony-rich limit of stoichiometry for Zr_5Sb_{3+x}, the second phase in the two phase mixture gave only a few lines in the powder pattern. These lines were not weak, and clearly not due to the expected $ZrSb_2$. The two-phase mixture was obtained reproducibly for arc-melted products, both annealed and as-cast, of many reactions. The diffraction pattern of the unknown phase was indexed[16] on the basis of a primitive cubic unit cell, a = 5.6358(4), from a sample of composition $Zr_{0.56}Sb_{0.44}$(8) prepared by arc-melting and annealed for 5 days at 900°C.

Once the unit cell was determined, an estimate of the number of atoms in the cell could be made from an estimate of the volume per atom (Table 7). The atomic volume, of the compound nearest in composition, used to make the calculation is 23.2 $Å^3$/atom which gives 7.7 atoms/unit cell. This number was rounded off to 8 atoms/unit cell and together with the symmetry information derived from the powder pattern, a search of known structure types in Pearson[39] was made. Calculated powder patterns for all cp8 (cubic, primitive, 8 atoms/unit cell) structure types were compared with the experimentally observed one, and the unknown compound was identified as ZrSb in the FeSi structure.[50] A comparison of observed and calculated intensities is given in Table 11.

An atomic volume of 22.4 $Å^3$/atom calculated on the basis of 8 atoms/unit cell is smaller than was expected for 4 Zr and 4 Sb atoms. This value is closer to those of the more zirconium-rich phases Zr_5Sb_3, Zr_2Sb, and Zr_3Sb. As the proportion of antimony with respect to zirconium increases, the average atomic volume of the compounds should increase because of the larger size of Sb. Two conclusions can be drawn from the anomalously low atomic volume of ZrSb in the FeSi structure; the compound has a very well-packed structure, or it contains less than 8 atoms/unit cell and is substoichiometric in Zr or Sb. A second ZrSb phase was found to be a stoichiometric compound with a composition $ZrSb_{1.96(1)}$ according to a single crystal structural refinement (see below). This second modification is never found in equilibrium with Zr_5Sb_{3+x} and is only found to coexist with the FeSi-type when the

Table 11. Observed and calculated powder patterns for $ZrSb_{1-x}$ (FeSi-type)

d(obs), Å	d(calc), Å	h k ℓ	I(obs)[a]	I(calc)[a]
3.983	3.985	1 1 0	1	0.1
3.253	3.254	1 1 1	15	13
2.818	2.818	0 0 2	10	9
2.520	2.521	0 2 1	100	100
2.300	2.301	1 1 2	50	56
1.992	1.993	2 2 0	1	0.8
1.879	1.879	0 0 3	7	7
1.782	1.782	3 1 0	4	2
1.700	1.699	1 1 3	9	13
1.5630	1.5630	2 0 3	5	5
1.5064	1.5063	3 1 2	35	40
1.4088	1.4091	0 0 4	6	11
1.3670	1.3670	4 0 1	6	8
1.3284	1.3285	1 1 4	5	5
1.2931	1.2930	3 1 3	8	15
1.2606	1.2603	2 0 4	4	2
1.2302	1.2299	4 2 1	17	22
1.2013	1.2016	3 3 2	4	4

[a]Cu $K\alpha_1$ radiation.

Zr_5Sb_{3+x} lines disappear from the powder pattern, which leads to the conclusion that the FeSi modification is substoichiometric in antimony.

Reactions of sintered powders were carried out with the same results as observed in arc-melting experiments, ruling out temperature as the driving force in structure determination. A further proof of this was obtained in an experiment where $ZrSb_2$ was heated in an alumina crucible in a dynamic vacuum of 10^{-5} torr. A powder pattern of the material was obtained after one day at 1000°C (9-1) which contained the lines of ZrSb (ZrSb-type) and a phase richer in antimony. After an additional day at 1000°C (9-2) and further antimony vaporization, the powder pattern showed the formation of ZrSb (FeSi) along with some remaining ZrSb (ZrSb). The FeSi modification is, therefore, better formulated as $ZrSb_{1-x}$.

A rough estimate of x can be obtained from the unit cell volume and an estimated atomic volume of 22.9 A^3/atom (the median of the Zr_5Sb_3-M and ZrSb values). This results in an x of 0.1 to give $ZrSb_{0.9}$.

The average atomic volume is, of course, dependent to a great extent on the packing efficiency of a particular structure type as well as relative sizes of the constituent atoms. In Figure 8 the average atom is volume is plotted as a function of antimony content and except for Zr_3Sb, the data points lie along a straight line. This demonstrates that the packing of the various structure type (excluding Zr_3Sb) has only a minimal effect on the average atomic volume.

The individual average atomic volume of zirconium and antimony can be calculated from the data in Table 7 (excluding Zr_3Sb) as $\bar{V}_{Zr}$ = 21.1 A^3 and $\bar{V}_{Sb}$ = 25.0 A^3. If these numbers are used to

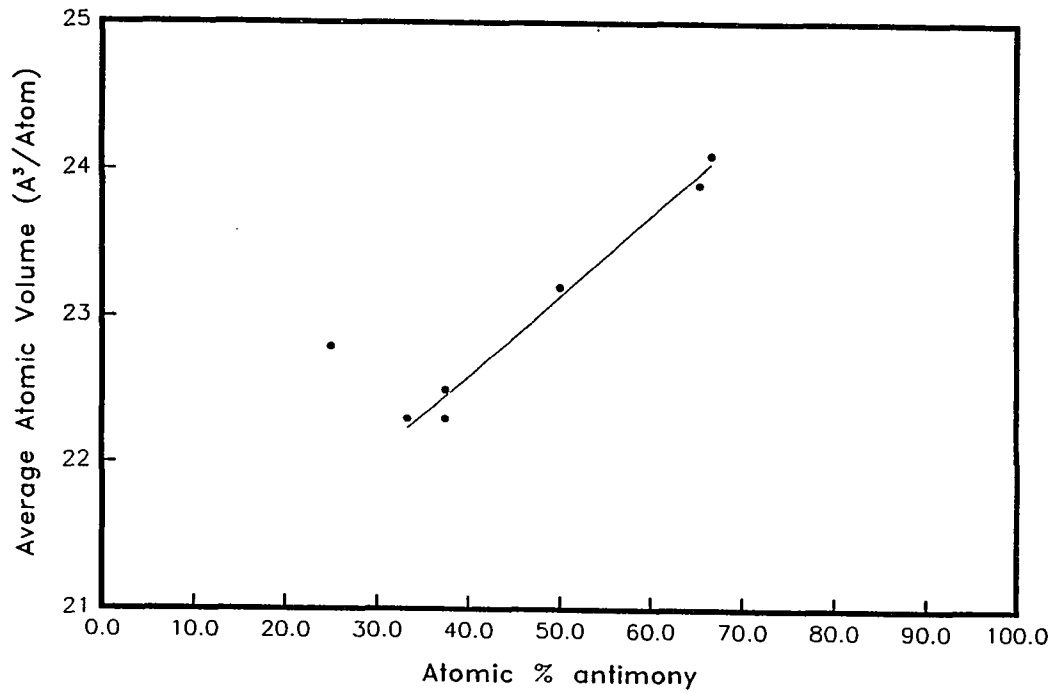

Figure 8. Plot of average atomic volume as a function of antimony content in the binary compounds, except for Zr_3Sb, a linear increase in average atomic volume with antimony content can be seen

estimate the composition of the FeSi phase then the formula is also calculated as $ZrSb_{0.9}$. This $ZrSb_{0.9}$ composition is only a very rough estimate and too much should not be made of it. It is interesting to note that at a slightly lower antimony composition, 0.8 Sb atoms would have 4 valence electrons and could satisfy the octet rule with the four valence electrons of Zr. This result in more intriguing when the range of homogeneity for $ZrSb_{1-x}$ is explored.

The $ZrSb_{1-x}$ phase exhibits line compound behavior as witnesses by the experimentally identical lattice parameters of the compound in equilibrium with Zr_5Sb_{3+x} or ZrSb (see Table 4 reactions 8 and 9). Such behavior is unusual for a nonstoichiometric compound. No superstructure lines were observed in the powder patterns indicating that the vacancies are not ordering.

A single crystal structural refinement was desirable in order to confirm the postulated antimony deficiency. Towards this end, crystals were grown by vapor transport in a hot wire apparatus and also in a flux of Bi which was slowly evaporated. These techniques yield large (0.2 = 0.5 mm) size gem-like crystals. Oscillation photographs of these indicated that they were single and crystals were mounted on the diffractometer. The expected cubic unit cell was obtained from BLIND[51] but, unfortunately, these crystals were always twinned. Repeated attempts resulted in data sets which could not be averaged with cubic symmetry.

ZrSb

This second ZrSb modification was first observed in a reaction designed to produce Zr_5Sb_4C. The elemental powders were sealed in a Ta

tube with a small amount of ZrI_4 as a transporting agent, and heated at 950°C for 2 weeks. The powder pattern of the products contained the lines of ZrC, and a second phase that could not be identified as any known Zr-Sb binary compound. It was, therefore, presumed to be a carbon-stabilized ternary compound and the structure determined.

Oscillation and Weissenberg photographs of a rectangular plate indicated that this compound crystallizes with C-centered orthorhombic symmetry. The approximate lattice parameters so obtained allowed the powder pattern to be indexed and provided the refined values listed in Table 4.

Experimental details of data collection are given in Table 8. The averaged data exhibited systematic absences consistent with the space group Cmcm. Initial determination of the positional parameters for two antimony atoms was accomplished by the use of MULTAN 80[52] and a Fourier map following refinement of these positions revealed the location of two zirconium atoms. Full-matrix, least-squares refinements with anisotropic thermal parameters proceeded smoothly. In the latter stages of the refinement, the multiplicity of three out of the four atoms was allowed to vary with the result that all positions were found to be fully occupied (refined formula $ZrSb_{0.96(1)}$). The final refinement cycle converged at R = 0.037 and R_w = 0.058. Because weaker reflections were observed to have larger values of $w\Delta^2$ ($\Delta = |F_o| - |F_c|$), the data set was reweighted in six overlapping groups sorted according to F_o so that $w\Delta^2$ values for all the groups were equal. The residuals were now R = 0.037, R_w = 0.045. A final electron density difference map revealed no residual peak greater than 1 e/Å^3 ruling out this compound as a carbon-

stabilized ternary phase. The refined positional and thermal parameters and important interatomic distances are listed in Table 12.

The principal bonding in ZrSb appears to be heteroatomic, although layers of antimony(2) are also present. The Zr-Sb distances range from 2.84 - 3.11 Å (Table 12) and as such probably represent strong bonding interactions when compared to 2.9 - 3.1 Å found in the other binary compounds. On the other hand, the Zr-Zr distances are fairly long at 3.40 Å, and only weak interactions between the transition metal atoms are expected. The Sb(2) - Sb(2) separations of 3.25 Å are intermediate both in distance and most likely in orbital overlap based on 2.91 Å and 3.36 Å found in the element.[53]

In order to simplify the conceptualization of the structure, the Sb(2) - Sb(2) and Zr-Zr interactions have been emphasized at the expense of the stronger Sb-Zr bonds in the projection shown in Figure 9. The antimony(2) atoms from a puckered layer centered about {002} that is actually a slightly distorted version of the layers found in elemental antimony, albeit with larger interatomic distances (3.25 Å vs 2.91 Å). A clearer view of this layer is given in Figure 10. Between these layers lie columns composed of confacial trigonal prisms of zirconium atoms with the pseudo three-fold axis parallel to [100], that are centered by antimony(1) atoms. Pairs of these columns displaced by a/2 are linked with 3.02 Å Zr(2) - Sb(1) contacts as well as more numerous Zr(1) - Zr(2) interactions at 3.40 Å. The shortest Zr-Zr separations of 3.39 Å are actually between the columns and across the antimony(2) layer. The

Table 12. Refined parameters for and distances in ZrSb

Atom	Site	x	y	z
Zr(1)	8(f)	0	0.0714 (1)	0.1088 (1)
Zr(2)	4(c)	0	0.3798 (2)	1/4
Sb(1)	4(c)	0	0.6694 (1)	1/4
Sb(2)	8(f)	0	0.6415 (1)	0.5477 (1)

Interatomic distances, (Å)[a]

Sb(1) – 2 Zr(2)	2.913(2)	Zr(1) – 2 Sb(1)	2.934(1)
Sb(1) – 4 Zr(1)	2.934(1)	Zr(1) – 2 Sb(2)	2.998(1)
Sb(1) – 1 Zr(2)	3.019(2)	Zr(1) – 2 Sb(2)	3.054(1)
		Zr(1) – 1 Sb(2)	3.113(2)
Sb(2) – 1 Zr(2)	2.835(1)		
		Zr(1) – 1 Zr(1)	3.385(2)
Sb(2) – 2 Zr(1)	2.998(1)		
		Zr(1) – 2 Zr(2)	3.399(1)
Sb(2) – 2 Zr(1)	3.054(1)		
Sb(2) – 1 Zr(1)	3.113(2)	Zr(2) – 2 Sb(2)	2.835(1)
Sb(2) – 1 Sb(2)	3.238(2)	Zr(2) – 2 Sb(1)	2.913(2)
Sb(2) – 2 Sb(2)	3.251(1)	Zr(2) – 1 Sb(1)	3.019(2)
		Zr(2) – 4 Zr(1)	3.399(1)

[a]Distances <3.5 Å.

B_{11}	B_{22}	B_{33}	B_{23}
1.03(5)	0.76(4)	0.67(5)	0.00(3)
1.13(7)	0.56(6)	0.40(6)	0
1.18(6)	1.41(5)	0.75(4)	0
1.22(5)	0.78(4)	0.72(3)	-0.03(2)

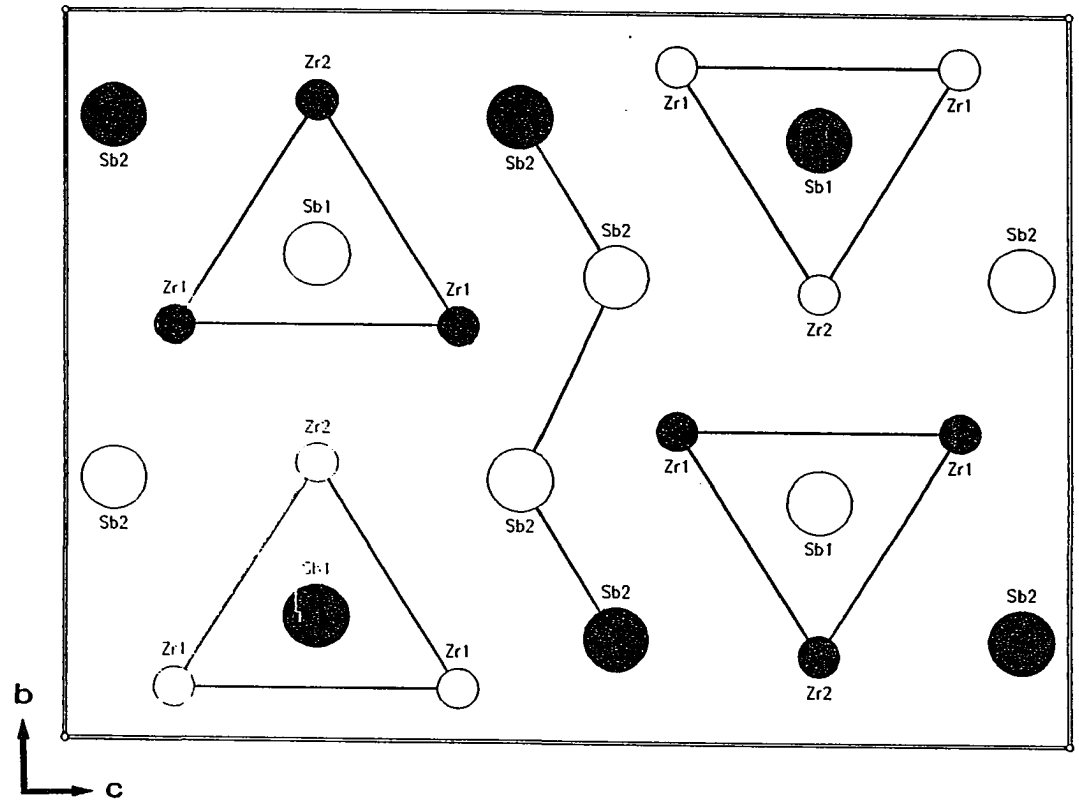

Figure 9. Projection of the orthorhombic crystal structure of ZrSb along the short a-axis emphasizing Zr—Zr and Sb—Sb relationships. Shaded atoms are at x = 1/2, open atoms are at x = 0. Many shorter Zr—Sb contacts have been omitted in the interest of clarity

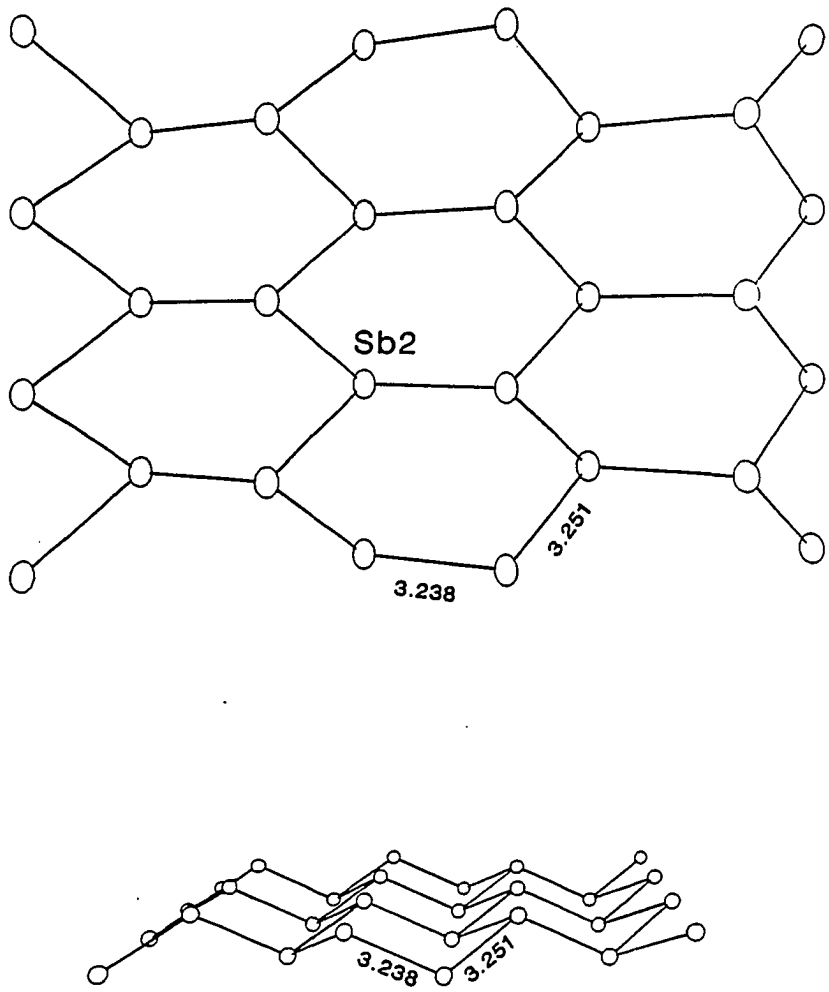

Figure 10. Antimony(2) atoms in ZrSb form a layer that is distorted but very reminiscent of that found in elemental antimony. (95% probability thermal ellipsoids)

resulting coordination involving only Zr-Sb bonding is shown in Figure 11 for all the atoms.

Once it was determined from the crystal structure that this new ZrSb binary compound was not stabilized by carbon, experimental verification was obtained by its synthesis in quantitative yields with vapor transport reactions in sealed Ta tubes at 950°C as well as by arc-melting or via pressed pellet reactions. Crystals of ZrSb can also be grown in a hot wire apparatus employing a Ta wire at 950°C and a Pyrex vessel at 300°C with I_2 as a transporting agent. Because the temperature of the wire is difficult to control $ZrSb_{1-x}$ often grows on the wire as well.

The ZrSb phase will lose antimony when heated to 1000°C under a dynamic vacuum of 10^{-5} torr to yield the substoichiometric $ZrSb_{1-x}$ which is accompanied by a structural transformation to the FeSi structure.

The structure type found for ZrSb has not been reported for any other compound, but HfSb gives a powder pattern that can be indexed on the basis of an orthorhombic unit cell (a = 3.78, b = 10.36, c = 13.87 Å)[35] very similar to that of the zirconium phase.

Zr_2Sb_3

In order to verify that there were no more phases between ZrSb and $ZrSb_2$, powders of Zr and Sb in the stoichiometric ratio of 2:3 were heated at 900°C for 6 days (11). This reaction failed to verify the lack of compounds between ZrSb and $ZrSb_2$ since it yielded yet another unknown phase. The powder pattern can be indexed[16] on the basis of a primitive tetragonal cell a = 9.565(1), c = 5.288(1) Å, indicating a single phase

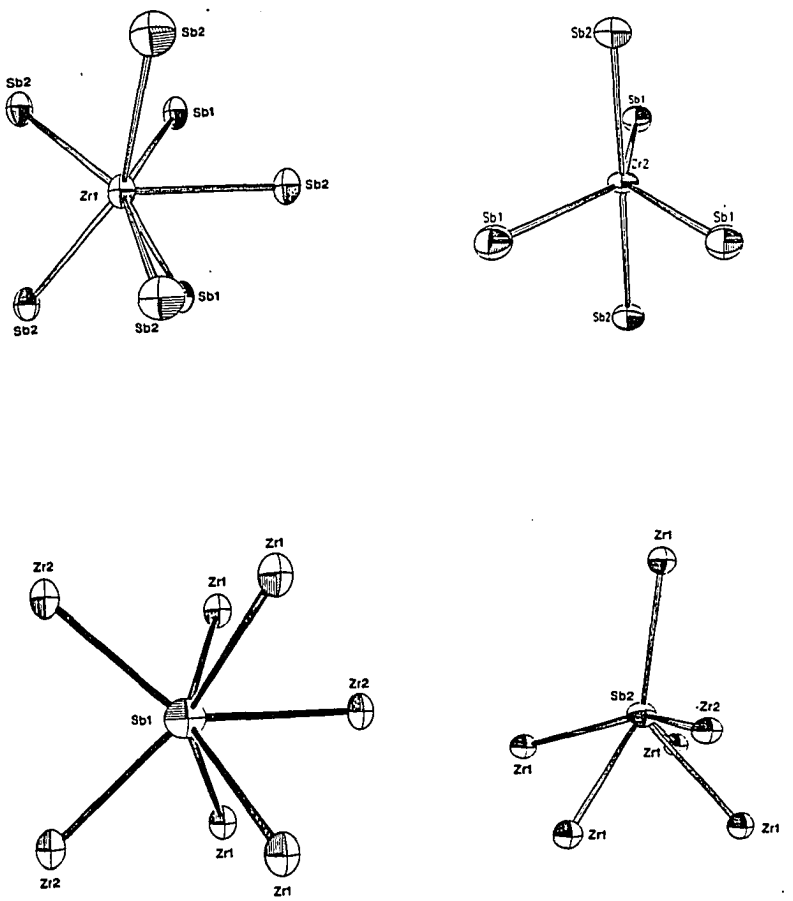

Figure 11. Primary heteroatom coordination spheres of the four independent atoms in the ZrSb structure. Atom ellipsoids are drawn at the 95% probability level

product with a composition at or very near Zr_2Sb_3. The compound can also be prepared by arc-melting, but the preparation is difficult due to copious amounts of antimony volatilization. In fact, Sb is lost from Zr_2Sb_3 even at 1000°C and a vacuum of 10^{-5} torr (see 9-1 and 9-2, Table 3).

The structure type of this compound could not be identified, in part because no reasonable value for the number of atoms per unit cell could be obtained. If there are four formula units per unit cell, the 20 atoms would have an average volume of 24.7 $Å^3$/atom. This number seems unreasonably large when compared to other values found in the binary system (Table 7). A more reasonable volume of 23.7 Å/atom would mandate an unlikely 20.8 atoms per unit cell.

Attempts to obtain single crystals of this compound by arc-melting to verify the unit cell failed. Experience has shown that unit cells determined solely on the basis of d-spacings and indexing without corroboration from single crystal data or by identification of the structure type must be regarded as only tentative. That is even truer in this case, and the tetragonal cell described above should be regarded with some suspicion.

$ZrSb_2$

The most antimony-rich compound reported and verified by this study is $ZrSb_2$, the structure of which has been previously described.[24,25] Large rod-crystals, about one centimeter in length, of this phase can be formed by dissolving zirconium powder in a large excess of antimony and allowing the solvent to evaporate slowly. This was accomplished at 1000°C in an Al_2O_3 crucible under 100 torr of argon. The compound can

also be synthesized by sintering. A reaction in which a 1-3 stoichiometric ratio of the elemental powders was allowed to react at 850°C for one day followed by one day at 550°C (13) confirmed that Sb is in equilibrium with $ZrSb_2$ in the two phase region.

The structure of this compound was verified in this work by powder diffraction but, as the case with Zr_5Sb_3 and ZrSb, a second structural modification has been observed.

β-$ZrSb_2$

In an attempt to grow single crystals of Zr_2Sb_3, a stoichiometric mixture of Zr and Sb powders was sealed in a silica container under vacuum, with CdI_2 as a transport agent. The reactants were heated at 700°C while the opposite end of the tube was maintained at 650°C for 9 days (14). It was evident upon removal of the reaction from the furnace that the fused silica had been attacked by zirconium and that an antimony-richer product should be expected. Some material had transported to the cool end of the reaction container but most (75%) remained in the hot end. The two products were visually identical and in the form of rod crystals about 1.0 mm x 0.1 mm x 0.1 mm. The powder patterns confirmed that the two products were identical, but different from the expected $ZrSb_2$.

A single crystal allowed the unit cell dimensions to be approximated by oscillation and Weissenberg techniques, and the precise lattice parameters given in Table 4 were then obtained by a least-squares fit to indexed Guinier powder diffraction data. The cell was found to be primitive orthorhombic. The small unit cell and especially the short b-axis

indicated that this was most likely a previously unreported Zr–Sb binary compound, and a structural determination was deemed appropriate.

The averaged diffraction data exhibited multiplicities and systematic extinctions consistent with the space group Pnma. Because of the synthetic route used, the composition of the sample was not known, but MULTAN 80[52] rendered atomic positions and relative electron densities, from which it became evident that the structure was composed of three independent atoms, each with a four-fold multiplicity, and that the stoichiometry was $ZrSb_2$. A shift of the origin revealed that the structure was actually the anti-Co_2Si[39] or $PbCl_2$ type which is also known for ZrP_2[54] and $ZrAs_2$.[55]

Full-matrix, least-squares refinement proceeded smoothly, and in the final cycle all positional, thermal and occupancy parameters except the Zr multiplicity were allowed to vary. This revealed a slight deficiency of Sb(1) and an overall composition of $ZrSb_{1.956(4)}$. Since there was attack of the glass during the synthesis of this compound, the possibility that it was interstitially stabilized by either silicon or oxygen was considered, but a final electron density difference map did not contain any residual peaks greater than 0.5 e/A^3.

The refined parameters are presented in Table 13. It should be noted that this phase appears to be substoichiometric in antimony, namely $ZrSb_{1.956(4)}$, as revealed by the nonunity value for the refined multiplicity of antimony(1). Such a property is also reminiscent of the pair of compounds at the equiatomic composition, viz., $ZrSb_{1-x}$ (FeSi) and ZrSb (ZrSb). Unfortunately, the compositional dependence of the free

Table 13. Refined parameters for and distances in $ZrSb_{1.956(4)}$ (β)

Atom	Site	Multipl.	x	y	z
Zr	4(c)	1.0	0.2606(1)	1/4	0.1622(1)
Sb(1)	4(c)	0.956(4)	0.8713(1)	1/4	0.04495(7)
Sb(2)	4(c)	1.0	0.9311(1)	1/4	0.64586(7)

Interatomic Distances, Å[a]

Zr – 1 Sb(1)	2.923(1)	Sb(1) – 2 Sb(1)	2.890(1)
Zr – 2 Sb(1)	2.976(1)	Sb(1) – 1 Zr	2.923(1)
Zr – 2 Sb(2)	3.032(1)	Sb(1) – 2 Zr	2.976(1)
Zr – 2 Sb(2)	3.060(1)	Sb(1) – 1 Zr	3.091(1)
Zr – 1 Sb(1)	3.091(1)	Sb(1) – 2 Sb(2)	3.146(1)
Zr – 1 Sb(2)	3.209(1)	Sb(1) – 1 Sb(2)	3.731(1)
Zr – 2 Zr	3.987(1)	Sb(1) – 1 Sb(2)	3.849(1)
Sb(2) – 2 Zr	3.032(1)	Sb(1) – 2 Sb(2)	3.859(1)
Sb(2) – 2 Zr	3.060(1)	Sb(1) – 2 Sb(1)	3.987(1)
Sb(2) – 2 Sb(1)	3.146(1)		
Sb(2) – 1 Zr	3.209(1)		
Sb(2) – 2 Sb(2)	3.581(1)		
Sb(2) – 1 Sb(1)	3.731(1)		
Sb(2) – 1 Sb(1)	3.849(1)		
Sb(2) – 2 Sb(1)	3.859(1)		
Sb(2) – 2 Sb(2)	3.989(1)		

[a]Distances < 4.0 Å.

B_{11}	B_{22}	B_{33}	B_{23}
1.05(4)	0.56(5)	1.06(5)	0.01(3)
1.13(3)	0.63(4)	1.05(4)	-0.02(2)
1.01(4)	0.55(4)	1.17(4)	0.07(2)

energy of formation is not as well established in the present case since attempts to synthesize $ZrSb_{1.96}$ by sintering powders have produced only $ZrSb_2$ with the previously reported structure.[36,37]

A projection of $ZrSb_{1.96}$ down the short b axis is shown in Figure 12 with the shorter Sb-Sb contacts emphasized. This structure allows close Sb(1) - Sb(1) contacts of 2.89 Å (Table 13) along an infinite zig-zag chain parallel to the b-axis, with each atom in this chain also coordinated further to two antimony(2) atoms at 3.15 Å, Figure 13. The antimony atoms also differ from above in their coordination to zirconium; antimony(1) is bonded to four zirconium atoms in a tetrahedral environment while antimony(2) is bonded to five zirconium atoms in a square pyramidal manner. The zirconium atom is nine-coordinate, as would be expected in this structure, but one Zr-Sb(2) distance at 3.21 Å is significantly longer than the average of the other eight, 3.02 Å. The implications of some of these distances will be discussed below as well as the simplistic view of the structure as $Zr^{4+}Sb^{3-}Sb^{-}$.

Comparable views of both the unit cell projection and ribbon of antimony atoms for the previously known $ZrSb_2$ structure[36,37] are shown in Figures 14 and 15 (space group Pnnm, a = 14.9684(8) Å, b = 9.9672(6) Å, c = 3.8813(3) Å). It should be noted that the α-type structure contains twice as many formula units per unit cell as the β ($PbCl_2$) form. Here there are isolated pairs of Sb(4) - Sb(4) atoms in addition to short (2.88 Å) Sb(1) - Sb(1) separations within the antimony ribbon. The zirconium atoms are coordinated by eight antimony atoms in a bicapped trigonal prism in much the same manner as found for $ZrSb_{1.96}$ with the

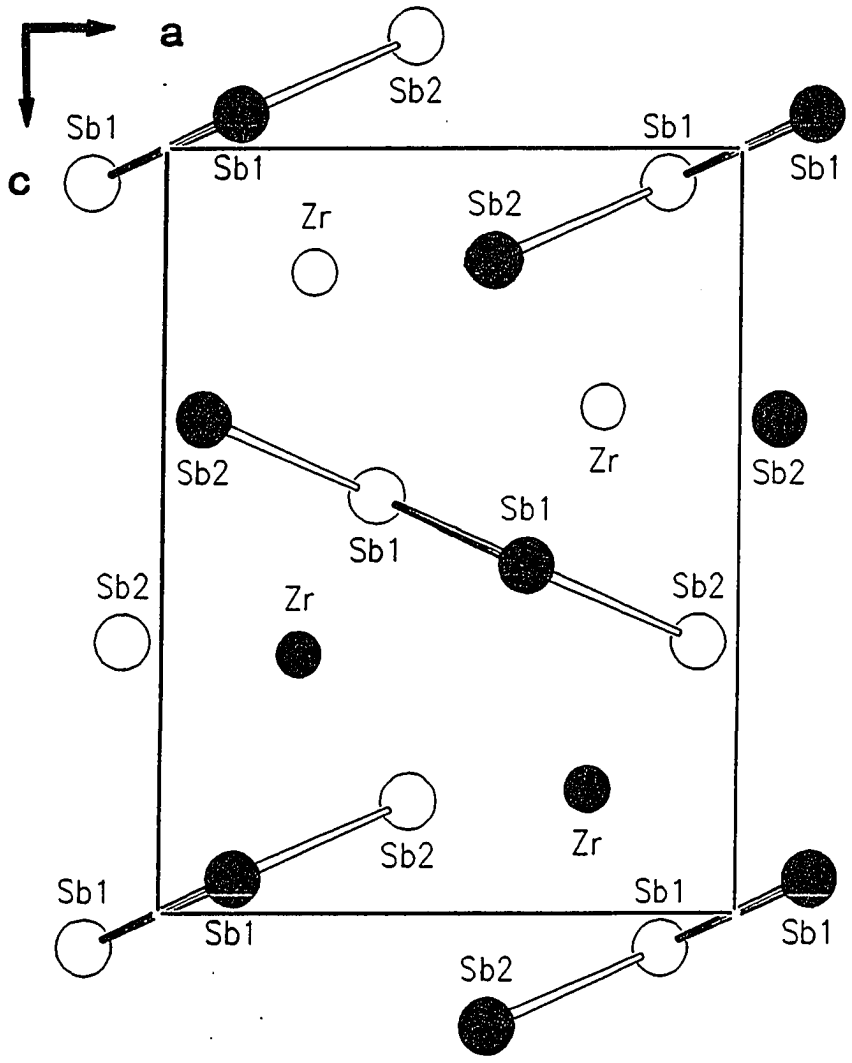

Figure 12. Projection of the β-$ZrSb_2$ ($PbCl_2$) structure along the short b-axis. All atoms are at y = 1/4 (open circles) or y = 3/4 (filled circles). Antimony—antimony contacts have been emphasized

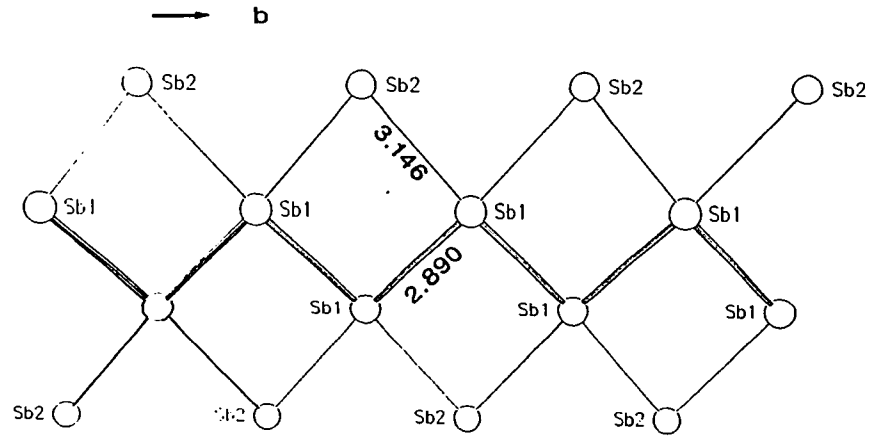

Figure 13. The ribbon of antimony atoms in β-$ZrSb_2$

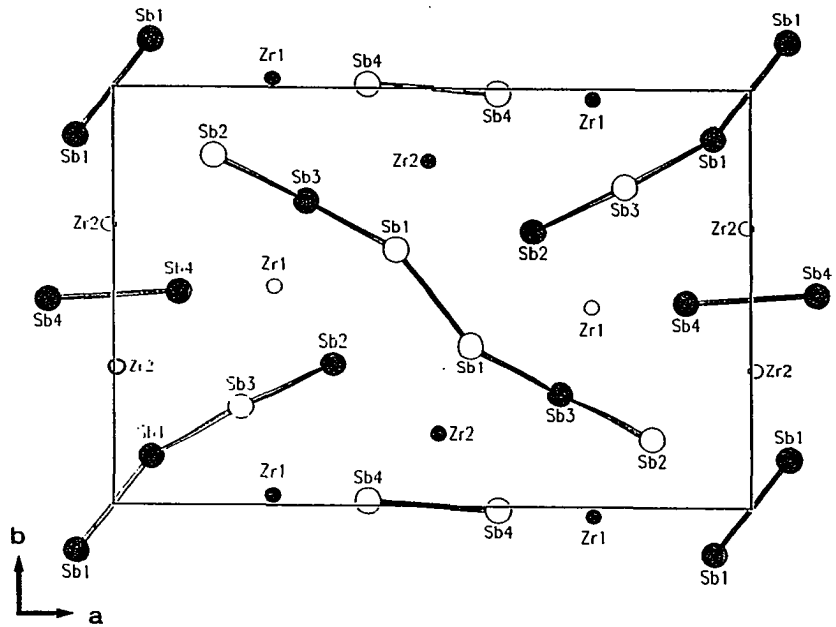

Figure 14. Projection of the α-$ZrSb_2$ structure along the short c axis. All atoms are at z = 0 (open circles) or z = 1/2 (filled circles). Antimony–antimony contacts have been emphasized

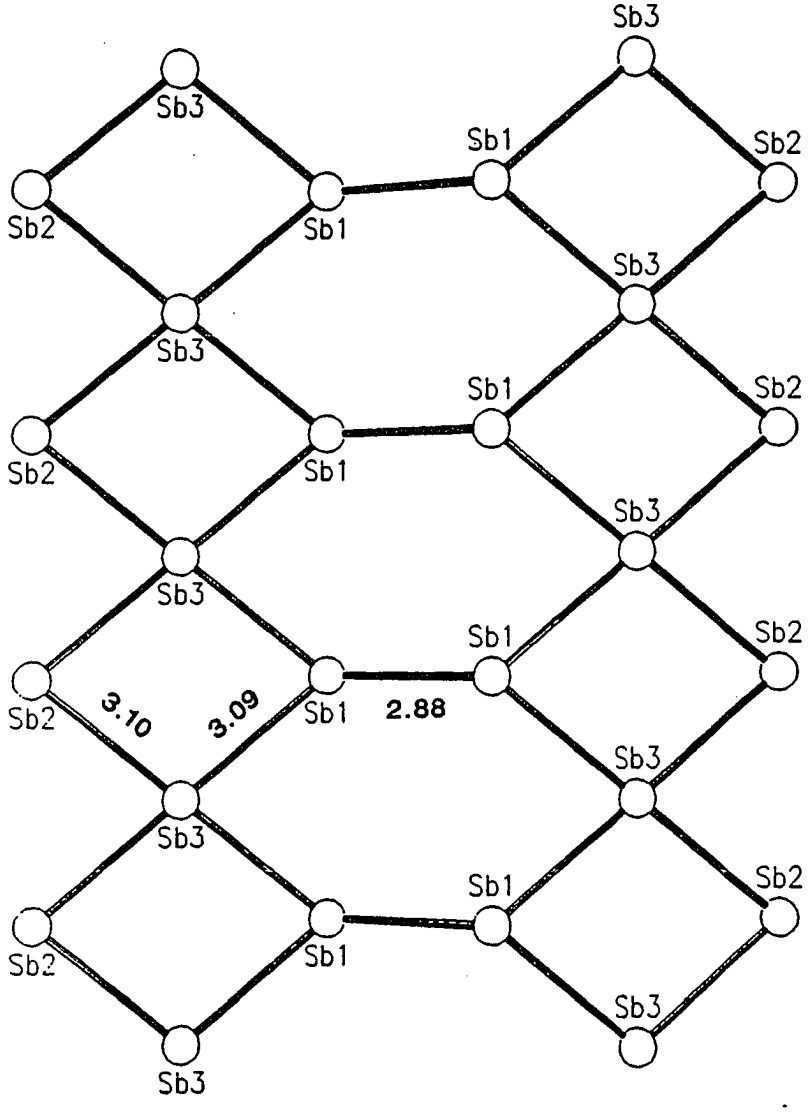

Figure 15. The ribbon formed by three of four antimony atoms in α-$ZrSb_2$

ninth atom now at a longer 3.4 Å. The coordination of the antimony atoms by zirconium and antimony near neighbors has also changed. With reference to Figure 14, Sb(1) and Sb(2) have three zirconium neighbors, Sb(3) four, and Sb(4) six, compared with four and five atom coordination spheres observed in $ZrSb_{1.96}$. The increased Sb-Zr interaction by antimony(4) is compensated by a drop in Sb-Sb bonding so that it has only one antimony near neighbor (Figure 14). The antimony atoms that are tetrahedrally bonded to four zirconium atoms are bonded to four Sb atoms in a square planar manner in both compounds (Sb(1) in $ZrSb_{1.96}$, Sb(3) in $ZrSb_2$). The remaining two antimony atoms in α-$ZrSb_2$ are both coordinated to three zirconium atoms but antimony(1) is bound to three antimony atoms while antimony(2) is bound to two.

The atomic numbering schemes used in the structural illustrations are also used in the presentation of the following calculational results.

Extended-Hückel calculations

Three-dimensional, extended-Hückel band calculations were carried out on the two $ZrSb_2$ structural modifications using the atom positional parameters derived from single crystal structural investigations.

The program utilized was developed and modified by Hoffmann and coworkers.[24,25] The parameters utilized are listed in Appendix A. The H_{ii} values for zirconium 4d, 5s and 5p orbitals were obtained by a linear interpolation between the parameters for Mo[56] and Y,[57] whereas the antimony 5s and 5p values were included in the program package. The exponents and coefficients of the double-zeta expansion for zirconium 4d and single-zeta expansion for all other orbitals used to calculate the

radial distribution function were as tabulated.[28,29] All overlap integrals were evaluated to a distance of 9.1 Å beyond which they were set equal to zero. The density-of-states (DOS) curves were calculated by using 125 and 27 evenly spaced, symmetry-weighted k points in the three-dimensional Brillioun zone for the $PbCl_2$-type and $ZrSb_2$ structures, respectively, and were smoothed with a Gaussian function of 0.1 eV half-width at half maximum.

The nonstoichiometry of $ZrSb_{1.96}$ cannot be explicitly addressed by these calculations but a rigid band approximation was applied in which the DOS curve calculated on the basis of $ZrSb_2$ was filled with 55 valence electrons for the $(ZrSb_{1.95})_4$ unit cell composition.

The density-of-states curve for $ZrSb_{1.96}$ is shown in Figure 16 with the shaded areas under the curve representing the individual atom contributions of the three independent atoms in the structure to the total. Two broad bands appear below the Fermi energy (-8.7 eV). The lower one from -23 to -16 eV is mainly antimony s orbital in character with a very small zirconium contribution. The second band from -16 to -8.7 eV has a significant contribution from all three atoms. The large degree of zirconium character in this band represents the extent of covalent interaction between antimony and zirconium since the Zr-Zr separations are all quite long. Located immediately above E_F is an empty band with a high density-of-states that is almost wholly zirconium in character. These three bands would be much narrower and have a great deal less mixing of the atomic states in any ionic description.

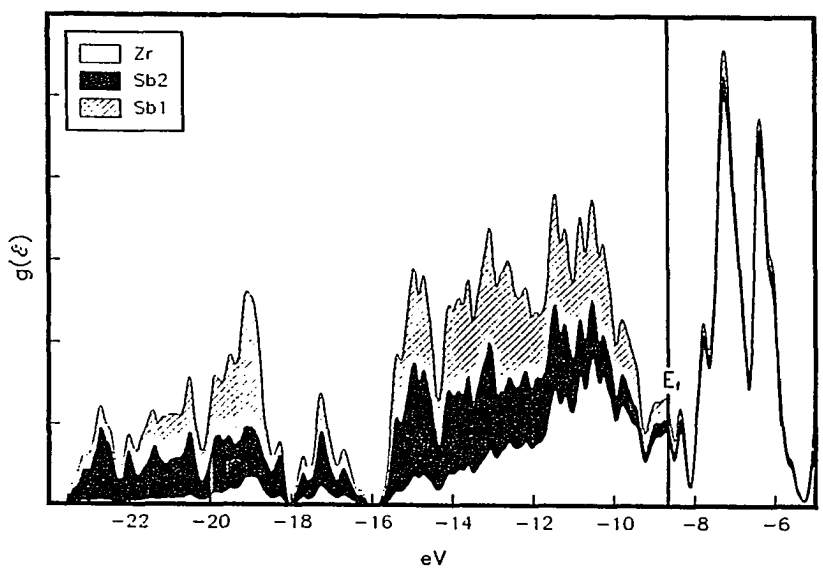

Figure 16. DOS curve for ß-$ZrSb_{1.96}$. The shaded areas under the curve represent the atomic orbital projections as indicated in the legend

More insight into the bonding in β-$ZrSb_2$ can be obtained from Figure 17 where the DOS curve has been overlap-weighted for various pairs of atoms such that a bonding interaction is positive and an antibonding one is negative. These crystal orbital overlap population (COOP) curves give a good representation of the bonding or antibonding effects for various atom pair interactions.[58] Thus the Zr-Sb(1) and Zr-Sb(2) interactions can be seen to be strongly bonding up to the Fermi energy with the largest bonding component located in the upper valence band where there is significant zirconium mixing. It is also evident that there is not much to differentiate the two types of Zr-Sb interactions, and that the two antimony atoms interact in energetically nearly equivalent ways with the metal atom. The COOP curves for the Sb-Sb interactions in Figure 14 show that here there is a clear difference in the two atoms. The short Sb(1) - Sb(1) separation corresponds to strongly bonding components in both occupied bands of the DOS, but these are limited to the lower part of the higher band, the remainder of the antimony orbitals being used for bonding to zirconium. The same can be said for Sb(1) — Sb(2) interactions in the energy regions where Sb(1) - Sb(1) is bonding but now at a somewhat reduced level. However, above -13 eV there is a large antibonding component in the Sb(1) - Sb(2) COOP curve that is not seen for Sb(1) - Sb(1). This means weaker Sb(1) - Sb(2) interaction although a significant net positive overlap remains.

The results of the calculations for the other (α) $ZrSb_2$ modification are plotted in Figures 18 and 19 in the same manner as above. In the interest of clarity, and because the projections of the atomic

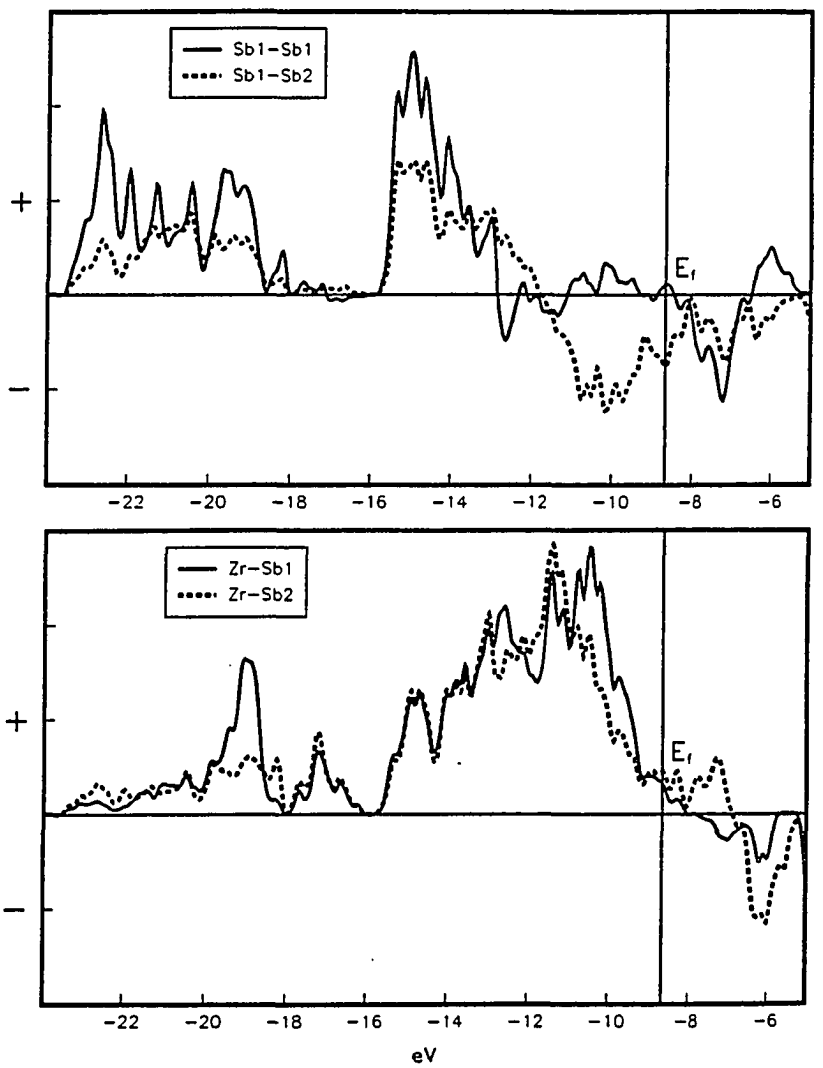

Figure 17. COOP curves for β-$ZrSb_{1.96}$. The positive values on the curves represent bonding interactions while negative values denote an antibonding character for the atom pairs as indicated

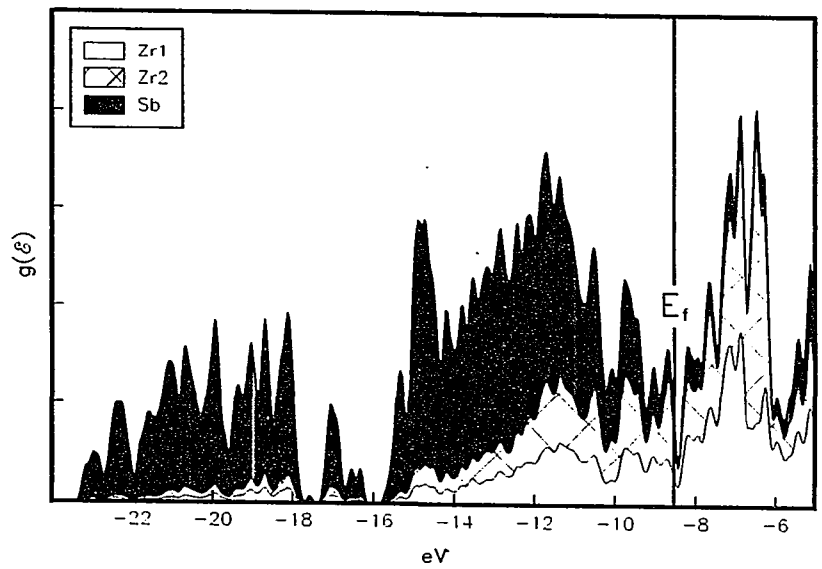

Figure 18. DOS curve for α-$ZrSb_2$. The shaded areas under the curve represent the atomic orbital projections as indicated in the legend. In the interest of clarity all the antimony projections have been summed and plotted as one

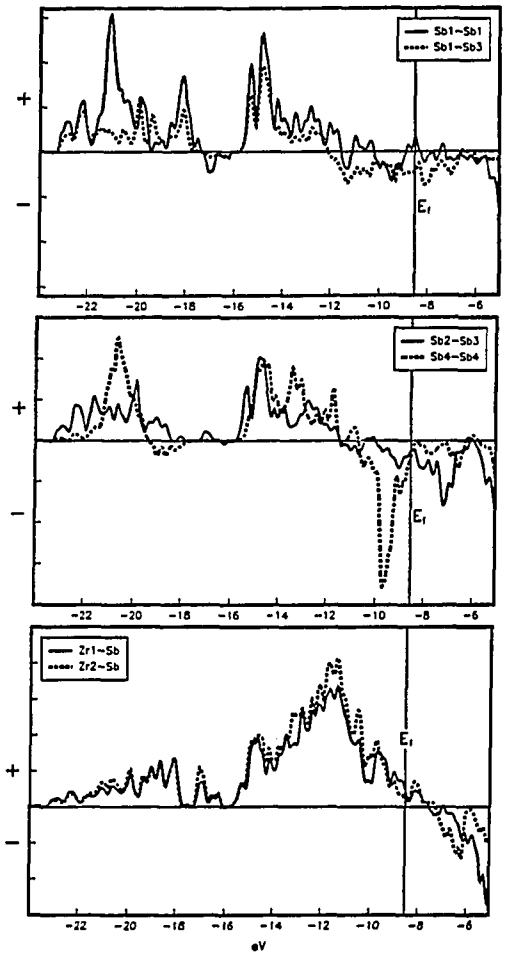

Figure 19. COOP curves for α-$ZrSb_2$. The positive values on the curves represent bonding interactions while negative values denote an antibonding character for the atom pairs as indicated. Because the curves for Zr–Sb are very similar only the sum is plotted

contributions to the DOS curve are essentially the same for the antimony atoms, only the total is plotted in Figure 18. Likewise, the sum of Zr(1) - Sb and Zr(2) - Sb interactions are plotted in Figure 19. A comparison of the DOS curves for $_{\alpha}$-$ZrSb_2$ (Figure 18) and $ZrSb_{1.96}$ (Figure 16) shows that they are very similar. An antimony s-band between -23 and -16 eV, the antimony p-band admixed with a large amount of zirconium states between -16 and -8.5 eV, and the empty zirconium-dominated band just above the Fermi energy are all reproduced. The fact that the two compounds do not differ in major detail is not unexpected since subtle energy differences often determine which of a pair of structure is adopted.

The DOS curves for both structures would indicate that each should exhibit metal-like behavior. This is more certain in $ZrSb_{1.96}$ but since the Fermi level for $ZrSb_2$ falls just short of what appears to be a nonzero minimum, this finite density-of-states could be either an artifact of the Gaussian smoothing or the result of small errors in the calculations. In order to confirm a metallic behavior, the resistivity of $ZrSb_2$ was measured by a single crystal four-probe technique along the antimony ribbon direction (c axis, Figure 15). The results are plotted in Figure 20. The compound is indeed metallic, confirming a qualitative conclusion published by Hulliger.[59] The room temperature resistivity of 1.2×10^{-4} ohm-cm is an order of magnitude greater than the metal zirconium or the semimetal antimony.

Comparison of the COOP curves for the two diantimony compounds (Figures 17 and 19) reveals that the Zr-Sb interactions are very similar,

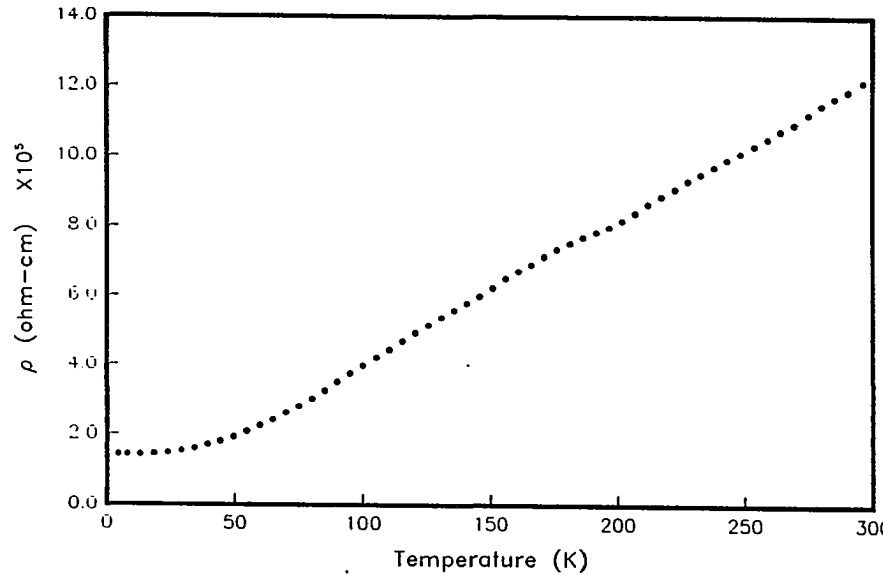

Figure 20. Plot of the resistivity of α-$ZrSb_2$ along the antimony sheet (c) direction as a function of temperature

as suggested by the DOS curves. The observation is not as valid when comparing the interantimony interactions. There is a large narrow antibonding component one eV below E_F in the result for the α-$ZrSb_2$ structure, from the more distant Sb(4) - Sb(4) pair, that has no counterpart in the $PbCl_2$-type structure. In addition, the character of the other antimony interactions are weakly antibonding in the two eV region below the E_F for α-$ZrSb_2$ structure but only the Sb(1) - Sb(2) curve of the β structure exhibits this behavior; the short and stronger Sb(1) - Sb(1) interaction in the latter is nonbonding in this region. The differences manifested in the Sb-Sb COOP curves are not surprising since the essential difference between the two structures involves Sb-Sb coordination.

DISCUSSION

The numerous compounds in the zirconium - antimony system can be categorized as intermetallic, but this classification does not provide much insight into the electronic nature of the phases since many intermetallic compounds have strong ionic and covalent contribution to the bonding energy. The Zintl valence compounds[60] provide good examples of the latter. A good understanding of the zirconium-antimony compounds will require further study since even such basic knowledge as the number and structure of the phases is not complete. Obviously, very little is known of the physical characteristics of these compounds. Some preliminary conclusions can be drawn from these synthetic and structural investigations, however.

Deducing the electronic nature of a compound solely from the crystal structure can be fraught with peril. The NaCl structure is found for such chemically diverse compounds as the alkali metal halides and transition metal carbides. This structure type is stable for different materials for different reasons. This is not always the case, however, since the diamond structure is found only for compounds with a strong covalent character to the interatomic bonding. In this manner, unique structure types found for Zr-Sb phases may provide insight beyond the "intermetallic" classification.

$ZrSb_2$ phases

The determination that a composition near $ZrSb_2$ can be found in the $PbCl_2$ structure is not in and of itself enlightening since $ZrSb_2$ and

$PbCl_2$ are sufficiently chemically dissimilar to surmise that diverse factors determine the adoption of this structure. An examination of the resulting interatomic distances does provide further insight.

It is possible as a very crude approximation to describe β-$ZrSb_2$ as $Zr^{4+}Sb^{3-}Sb^{1-}$. If the Zintl concept is then applied, Sb^{3-} would have a complete octet of electrons and not form any covalent bonds to other antimony atoms, while Sb^{1-} would only need to be bonded to two other Sb atoms in order to satisfy the octet rule. This behavior for the nominal Sb^{1-} is observed in $CaSb_2$ where a zig-zag chain analogous to that in elemental tellurium is formed.[61] This chain is very similar to that formed by antimony(1) in $ZrSb_{1.96}$ (d(Sb-Sb) = 2.915 Å in $CaSb_2$ vs 2.890 Å in $ZrSb_2$) with the important difference here that each antimony(1) atom is also a neighbor to two antimony(2) atoms at a longer but not insignificant 3.15 Å distance. The antimony(III) atoms which would be isolated from other antimony atoms in the $Zr^{+4}Sb^{3-}Sb^{1-}$ formulation are in fact not, and the simple strictly ionic view of the compound breaks down. Since zirconium is less electropositive than calcium, the extent of electron transfer or ionicity is also reduced. If there is incomplete transfer of electrons and a significant mixing of antimony p with zirconium d states, the antimony ions do not formally complete their octets and, as is the case when there is an electron deficiency, electron delocalization and metallic bonding also occur. Neglecting one long Zr-Sb contact at 3.21 Å, the bonding distances average at 3.02 Å, very typical of Zr—Sb interatomic separations in other binary compounds in this system. There are no significant Zr-Zr interactions, and so it can be stated that the

lattice energy of $ZrSb_2$ in the $PbCl_2$ structure is derived mainly from Zr-Sb bonding but that a quite significant portion can be attributed to Sb-Sb contacts and that these main group metal interactions are critical in the adoption of this structure.

The results of the extended-Huckel calculations for $ZrSb_{1.95}$ can be compared to the $Zr^{4+}Sb^{3-}Sb^{1-}$ formulation. The immediate breakdown of the ionic limit can be seen in the broad bands that contain significant amounts of Zr - Sb orbital mixing. A more quantitative measure of the extent of charge transfer is obtained by integrating under the atomic projections in the DOS up to the Fermi level for each element. This gives a rough indication of the amount of electrons "owned" by each element, although the method characteristically often overestimates the polarity developed. These numbers listed in Table 14 for both $ZrSb_{1.95}$ and $ZrSb_2$ verify the limited polarity of these compounds. Despite the large difference in the magnitude of the assigned charges, $Zr^{4+}Sb^{3-}Sb^{1-}$ vs $Zr^{0.4+}Sb^{0.4-}Sb^{0}$, the Zintl concept is still applicable in the very broad sense that the antimony atom with fewer valence electrons compensates with more and stronger covalent interactions, especially within the antimony(1) chain (Figure 13).

When the structure goes from $PbCl_2$ to $ZrSb_2$-type, Zr-Sb interactions remain virtually identical as far as the zirconium is concerned since an appropriate coordination sphere of bicapped trigonal prisms can be found in both cases. However, since the connectivity of these trigonal prisms is different, the coordination of antimony by zirconium does not remain the same. The Sb-Sb interactions are also different in the two

Table 14. Electron transfer as estimated by extended-Hückel means

	Atom	e/atom	Oxidation State
$ZrSb_{1.95}$	Zr	3.59	+0.41
	Sb(1)	4.77[a]	-0.02
	Sb(2)	5.39	-0.39
$ZrSb_2$	Zr(1)	3.59	+0.41
	Zr(2)	3.84	+0.16
	Sb(1)	5.05	-0.05
	Sb(2)	5.28	-0.28
	Sb(3)	4.76	+0.24
	Sb(4)	5.48	-0.48

[a]Sb(1) is substoichiometric and the calculations correspond to 95% occupancy (96% observed).

structures. When the β ($PbCl_2$) structure is compared with that of α-$ZrSb_2$, the average number of Zr-Sb bonds from each antimony changes from 4.5 to 4.0 with the average overlap population (integrated COOP curve) for each Zr-Sb bond increasing from 0.32 to 0.35 (Table 15). There are an average of three Sb-Sb interactions in the ribbon of antimony in both structures but the average overlap changes from 0.27 to 0.30. This increase of antimony bonding in the ribbon structure is compensated by the isolated Sb(4) - Sb(4) pair in the latter with an average overlap of only 0.18. In total, a small amount of Zr-Sb bonding is lost and a small amount of Sb-Sb bonding is gained when the structure type is changed from $PbCl_2$ to $ZrSb_2$ type.

With the exception of $TiAs_2$, the transition metal group IV diarsenides and diphosphides are found in the $PbCl_2$-type structure.[39] Since the orbitals of phosphorus and arsenic have a smaller radial distribution function compared with those for antimony and bismuth, the α-$ZrSb_2$ structure which sacrifices heteroatomic bonding in favor of homoatomic interactions would not be favored for the former. The exception occurs at $TiAs_2$ where the smaller sizes of both elements compensate. The larger and more metallic antimony and bismuth tend to favor the α-$ZrSb_2$ structure, and this is found for all zirconium and hafnium diantimonides and dibismuthides. The small size of Ti apparently renders both structures unstable, the compound $TiSb_2$ has the Al_2Cu[39] structure, and no $TiBi_2$ phase has been found.

The observed interatomic distances and the calculations based thereon lead to the conclusion that the upper valence bands of both $ZrSb_2$

Table 15. Average pair-wise overlap populations in $ZrSb_2$ phases

β-$ZrSb_2$		α-$ZrSb_2$	
Sb(1) – Sb(1)	0.43	Sb(1) – Sb(1)	0.51
Sb(1) – Sb(2)	0.17	Sb(1) – Sb(3)	0.21
Zr – Sb(1)	0.30	Sb(2) – Sb(3)	0.29
Zr – Sb(2)	0.33	Sb(4) – Sb(4)	0.18
		Zr(1) – Sb(2)	0.37
		Zr(1) – Sb(1), Sb(3)	0.37
		Zr(1) – Sb(3), Sb(4)	0.26
		Zr(2) – Sb(1)	0.41
		Zr(2) – Sb(2), Sb(3)	0.33
		Zr(2) – Sb(4)	0.40

phases contain a considerable contribution from the antimony atoms. There is some charge transfer from the zirconium to antimony but to a much smaller extent than occurs in alkali or alkaline earth metal — antimony compounds. The Zintl phase concept is applicable only in the broadest sense in that the more covalently bonded antimony atoms carry a lesser amount of charge.

ZrSb

The exclusive ZrSb structure type may also occur for one more example, HfSb. Unreported powder pattern data for the compound have been indexed on the basis of an orthorhombic unit cell (a = 3.78, b = 10.36, c = 13.87 Å)[35] which is dimensionally quite similar to that of ZrSb.

In ZrSb there are no longer any short Sb-Sb distances, but the Zr-Zr distances are not significantly shorter either. It can therefore be surmised that Sb-Sb orbital overlap provides much less of a contribution to the stability of this compound and that Zr-Zr interactions are not significantly increased when compared to $ZrSb_2$. The greatest part of the lattice energy must be provided by Zr-Sb bonding. It seems likely that the states near the Fermi energy are weakly bonding Zr-Zr or Sb-Sb states. Despite the small contribution of these interactions to the total lattice energy they must play a critical role in the formation of this unique structure.

The second phase near the equiatomic composition is evidently sub-stoichiometric and in the much more widely adopted FeSi structure-type.[39] This structural modification is not found exclusively for antimony compounds or even limited to those involving the phosphorus family. The

majority of the 45 phases known to have this structure are similar to FeSi, viz., compounds of 3d transition metals with Si, Ge, Sn, but compounds such as MgPt and AuBe also adopt this structure. This would indicate that formation of the FeSi structure is not determined exclusively by electronic factors. It is interesting to note that even though this form is substoichiometric, $ZrSb_{1-x}$, it exhibits characteristics of a line compound. A very narrow range of lattice constants and compositional stability implies an inability of a structure to tolerate a varying electron count, which would seem to contradict the previous assertion that the FeSi structure is not rigidly controlled by electronic factors. This raises the intriguing concidence for $ZrSb_{0.8}$ which is isoelectronic with HfSn,[62] a compound known to have the FeSi structure. A noteworthy feature is the determinative effect of a small compositional variation on the formation of the FeSi or ZrSb structural modification. The dependence of these two as a function of other thermodynamic variables should yield interesting results, and these together with further physical characterization will provide a more quantitative insight than simple structural comparisons.

Zr_5Sb_3

The neighboring Zr_5Sb_{3+x} phase is remarkable not for the unique nature of its structure, but rather for the widespread nature of its Mn_5Si_3-type structure. There are 294 phases, either binary or ternary, known to adopt it.[39] This situation is analogous to the NaCl structure in which categorically contrasting interatomic interactions are accommodated by a single structure. The interstitial site probably plays a

large role in the stability of this structure for many systems where a ternary (Z) atom may go undetected. The wide compositional stability range for Zr_5Sb_{3+x} implies that the electronic states near the Fermi level are nonbonding and in a wide band, and as such are able to tolerate a varying electron count. Such features are evident in the formation of a considerable variety of Zr_5Sb_3Z phases (discussed in Part II).

In contrast, a second Zr_5Sb_3 modification exhibits line compound behavior. This phase is found only in arc-melted samples and becomes metastable at low temperatures (<1100°C). Its Y_5Bi_3 structure-type is not distinguished in Pearson from the Yb_5Sb_3 structure but the differences, albeit subtle, have been discussed.[41] The number of compounds found with either of these structures is not large, 19, and they are so far exclusively adopted by compounds of the arsenic family with either the heavier rare earth metals or the early transition metals.[39] The structure type and small range of nonstoichiometry imply a strong electronic factor in the structure's stability.

Zr_2Sb

An empty octahedral site reminiscent of that in the Mn_5Si_3 structure can also be found in Zr_2Sb. The analogy can be extended further since some compounds with the La_2Sb structure which had been thought to be binary phases were later shown to be impurity-stabilized ternary compounds, e.g., Ca_2Sb[63] was determined to actually be Ca_4Sb_2O.[40] However, the reproducible quantitative synthesis of Zr_2Sb indicates that such a stabilization is not required in the zirconium-antimony system. It seems certain that Zr-Zr interactions play the critical role in the formation

of this structure that Sb-Sb interactions do in $ZrSb_2$. It also seems certain that the majority of the lattice energy arises from Zr-Sb bonding. These same considerations also apply to the most zirconium-rich phase, Zr_3Sb.

FUTURE WORK

The present study has revealed that a total of 10 compounds exist in the zirconium-antimony binary system. Two of these compounds, HT-Zr_2Sb and Zr_2Sb_3, have not had their structures elucidated and should be a focus of further investigations. Crystals of Zr_2Sb_3 can probably be grown from the melt under more propitious conditions than arc-melting. The melting point of Zr_2Sb_3 is most likely less than 1500°C. A stoichiometric mixture of the elements could be reacted at this temperature for a short length of time and the temperature lowered slowly to 1200°C to produce X-ray size crystals. The zirconium activity in the antimony-rich melt may be low enough to allow the use of alumina or graphite crucibles which would have to be sealed in Ta containers to prevent Sb loss.

The formation of HT-Zr_2Sb crystals will be a more formidable task because of the limited thermal stability range. The best route to growing these crystals is by repeating the reaction conditions listed in Table 3, but maintaining the sample at 1200°C for a longer period of time to allow for solid diffusion and grain enlargement. It would be interesting to see whether this compound is in truth Zr_2Sb, thereby resulting in four nominal compositions of the system found in two structural modifications, or simply a compound near this stoichiometry.

The nonstoichiometry of $ZrSb_{1-x}$ should be further explored. The line compound property implies a rigid electronic control and a $ZrSb_{0.8}$ composition can be formulated as a valence compound. This could be explored through further attempts to obtain single crystals.

These crystals though possibly of use in a structural investigation would be more likely to yield fruitful results in resistivity measurements. The nonstoichiometry could be further explored by microprobe. Rietfeld refinement of powder diffraction data is an additional tool that can be applied to the nonstoichiometry problem. The Zr-Sb compounds are chemically intermediate between the Zintl phases and alloys of transition metals. It would be interesting to see how the physical properties varied from $ZrSb_2$, dominated at the Fermi energy by Sb-Sb interactions, to Zr_3Sb which would be expected to have extensive Zr-Zr interactions and a transition metal-like character.

The present investigation has also shown that a system that had been previously investigated may yet possess golden nuggets that wait to be unearthed. Many of the transition metal-main group metal systems were examined in the late 50s and early 60s, and impure starting materials or inadequate synthetic techniques may have led to erroneous conclusions as in the Zr-Sb system. Investigations of these other systems may yield as many fruitful results.

In addition to the structural work, the physical properties of the other compounds could be examined.

PART II. Zr_5Sb_3Z-TERNARY COMPOUNDS

INTRODUCTION

The first part of this work dealt with the zirconium-antimony system and the binary compounds found therein. The structure-type of one of those phase, Zr_5Sb_3 (Mn_5Si_3-type), is widely adopted in other systems with 294 compounds, either binary or ternary, reported.[39] The Mn_5Si_3 structure contains an octahedral (more correctly trigonal antiprismatic) hole and in many (approximately 60) cases,[1-9,39] a small nonmetal impurity is found or is thought to fill this site and stabilize the structure.

Interest in these interstitial systems was derived from previous work with zirconium halides, where compounds initially thought to be binary later proved to be ternary phases. These were compounds in which a small nonmetallic element that occupied an interstitial octahedral hole had gone undetected.[10-12] This circumstance is paralleled by compounds with the Mn_5Si_3 structure where much of the work, frequently very qualitative, characterizing these intermetallic phases was done in the late 50s or early 60s. It is entirely possible that compounds reported as binary are in fact ternary phases. The Zr_5Sb_3Z systems were investigated in part for the reason.

The stability of the Zr_5Sb_3 as a binary phase had been questioned, and it was not clear whether oxygen is a required interstitial component.[35] In addition to this point of contention, there was a report that three other ternary compounds Zr_5Sb_3Z (Z = Ni, Cu, Zn) could be synthesized.[64] The supposition that a 3d transition metal could be made to occupy the same interstitial site of a compound as oxygen, seemed

chemically counterinituitive. An environment that can be occupied by a small electronegative oxygen atom should not be favored by such an electropositive element as Zn. For all four reported ternary phases, the compounds had been prepared by sintering stoichiometric mixtures in evacuated silica tubes at 800°C. This seems an extraordinarily low temperature even if the eight week reaction time is taken into account. No mention of yield was made and the phases were identified by intensity comparison of calculated and observed powder patterns. The intensity differences between $Zr_5Sb_{3.0}$ and, e.g., Zr_5Sb_3Cu are slight, and are also mimicked by Zr_5Sb_{3+x}. No single crystal work was done to verify and provide quantitative data for the phases postulated.

The lattice parameters reported for the compounds were also a source of doubt (Table 16). The variation of the lattice parameters with different interstitial elements was much smaller than expected based on experience in the zirconium halide systems. The purported existence of these Zr_5Sb_3Z phases was very much open to question and was the impetus for investigation of these systems.

The matter of Zr_5Sb_3 forming as a true binary compound led to a re-examination of the entire Zr-Sb system which is described in detail in the first part of this work. The conclusion drawn there is that Zr_5Sb_3 is indeed a binary compound but one which exhibits a stoichiometric range encompassing $Zr_5Sb_{3.0}$ to $Zr_5Sb_{3.4}$. The additional antimony was found to occupy the interstitial site.

This second section deals with the Zr_5Sb_3Z systems. The synthesis of the previously reported ternary phases was contrary to expectations

Table 16. Lattice parameters of reported Zr_5Sb_3Z phases

Compound	a	c	Reference
Zr_5Sb_3O	8.53	5.85	35
Zr_5Sb_3Ni	8.530(5)	5.773(5)	66
Zr_5Sb_3Cu	8.526(7)	5.786(5)	64
Zr_5Sb_3Zn	8.555(7)	5.820(5)	64

reproduced, but more amazingly, an additional 14 elements were also successfully incorporated into the interstitial site. Single crystal studies on several compounds provided confirmation of their formulation and also quantitative interatomic distance data.

The results of the synthetic investigation, initially spurred by the dichotomous situation in which oxygen and zinc could occupy the same crystallographic site in Zr_5Sb_3, uncovered the fact that many different, and chemically very diverse elements (e.g., Z = O, Zn, Se, Ag, Fe, Al, etc.) could be accommodated as well. In an attempt to understand this unprecedented situation, extended Hückel calculations were made. The results of these calculations allowed the stability of the various Zr_5Sb_3Z phases to be rationalized in a meaningful manner.

The ability of Zr_5Sb_3Z to incorporate many different elements allows the systematic examination of physical properties of these compounds as

Z, and hence, the nature of the band structure near the Fermi level, is varied. The good possibility exists that this will not be limited to Zr_5Sb_3Z, but that other Mn_5Si_3-type phases will also exhibit such behavior. This raises almost unlimited possibilities for the synthetic chemist since one can envision not only substitution or mixing of the Z element, but also the replacement of antimony in various amounts with other main group metals or zirconium with other transition metals or even a combination of all of these. Some of these other systems were investigated as well.

RESULTS

The Zr_5Sb_3 structure was described in part 1 of this work, and reference can be made to the methods, discussion and figures presented there. The structural description is equally applicable to the ternary Zr_5Sb_3Z systems in which Z occupies the interstitial site. Experimental details of single crystal structural studies are listed in Table 17, and general crystallographic parameters for the Zr_5Sb_3Z structure in Table 18. Lattice parameters obtained from Guinier powder data are presented in Table 19.

Second Period Nonmetal Interstitial Compounds

Zr_5Sb_3O

Synthesis of Zr_5Sb_3O was attempted by sintering a stoichiometric mixture of ZrO_2, Zr, and Sb at 1300°C for 3 days. This resulted in an incomplete reaction; ZrO_2, $Zr_5Sb_{3.4}$ and $ZrSb_{1-x}$ all being observed in the powder pattern. However, the diffraction pattern of a Zr_5Sb_3Z phase with a small unit cell was also present. Because the indexed lines of this phase yielded lattice parameters which are smaller than those of $Zr_5Sb_{3.0}$ by a highly significant amount (8.3017(6) vs 8.4177(7) Å and 5.7126(7) vs 5.766(1) Å, Table 19) this phase is presumed to be $Zr_5Sb_3O_x$. As a result of the incomplete reaction it is not certain that x = 1, but the large decrease of the lattice parameters and comparison with the parameters of Zr_5Sb_3C (Table 19) imply the interstitial site is substantially filled. The sharp lines of the powder pattern indicate that the range of x in this phase is very narrow.

Table 17. Crystallographic data for Zr_5Sb_3Z single crystals

Z	Al	Si	S	Fe
Lattice Parameters[a] (Å)				
a,	8.522(3)	8.5686(7)	8.435(1)	8.580(1)
c	5.846(2)	5.7934(8)	5.859(3)	5.836(1)
Crystal size (mm)	0.06	0.13	0.07	0.13
	0.06	0.13	0.07	0.10
	0.10	0.33	0.33	0.14
2θ(max)[b], deg	55	55	55	55
Reflections				
checked	992	870	968	977
observed[b]	823	789	830	757
independent	176	176	185	162
R(ave)	0.023	0.045	0.035	0.040
R	0.017	0.021	0.040	0.021
R_w	0.025	0.030	0.043	0.037
Secondary ext. coeff.(σ)	0.0269(5)	0.050(1)	0.26(5)	0.022(3)
Absorption coeff. (cm^{-1}) (Mo Kα)	176	177	181	192
No. of variables	17	17	17	17

[a]From refined Guinier powder data.
[b]Octants checked in each case were $\pm h$, $+k$, $+\ell$.

Zn	$Fe_{2/3}In_{1/3}$
8.6074(7)	8.642(1)
5.8362(8)	5.872(1)
0.06	0.07
0.06	0.07
0.30	0.33
55	55
1022	1022
799	839
172	180
0.025	0.023
0.013	0.015
0.013	0.016
0.013(2)	0.23(1)
204	195
17	17

Table 18. Crystallographic parameters for Zr_5Sb_3Z (Mn_5Si_3) structure

Space Group $P6_3/mcm$

Atom	Site	Position			Thermal Parameters					
Sb	6(g)	x	0	1/4	B_{11}	B_{22}	B_{33}	$1/2B_{22}$	0	0
Zr(1)	4(d)	1/3	2/3	0	B_{11}	B_{11}	B_{33}	$1/2B_{11}$	0	0
Zr(2)	6(g)	x	0	1/4	B_{11}	B_{22}	B_{33}	$1/2B_{22}$	0	0
Z	2(b)	0	0	0	B_{11}	B_{11}	B_{33}	$1/2B_{11}$	0	0

Table 19. Lattice parameters[a] for Zr_5Sb_3Z phases[b]

Z	Synthetic technique[c]	a (Å)	c (Å)	V (Å^3)
C	S	8.3017(6)	5.7126(7)	340.95(7)
O	S	8.3146(6)	5.6954(4)	340.99(6)
Al	R	8.5802(6)	5.8465(8)	372.76(8)
Si	S	8.5409(5)	5.8248(7)	367.97(6)
P	S	8.462(1)	5.813(1)	360.4(1)
S	S	8.4265(4)	5.8999(6)	362.80(5)
Fe	VT	8.551(1)	5.853(1)	370.6(1)
Co	S	8.6138(8)	5.852(1)	376.0(1)
Ni	VT	8.6004(6)	5.828(7)	373.33(7)
Cu	S	8.5999(4)	5.8293(5)	373.36(5)
Zn	F	8.6074(7)	5.8362(8)	374.46(8)
Ga	S	8.6358(4)	5.8398(6)	377.15(5)
Ge	S	8.5593(5)	5.8286(6)	369.80(6)
As	S	8.5007(5)	5.8490(7)	366.03(6)
Se	S	8.4824(4)	5.9046(6)	368.08(5)
Ru	S	8.634(1)	5.855(2)	378.0(2)
Ag	VT	8.6235(3)	5.8808(5)	378.74(4)
$Fe_{2/3}In_{1/3}$	F	8.642(1)	5.872(1)	379.8(1)
$Zr_5Sb_{3.0}$	S	8.4177(7)	5.766(1)	353.81(9)
$Zr_5Sb_{3.4}$	AM	8.5694(6)	5.8727(7)	373.48(7)

[a]Space group $P6_3/mcm$.

[b]Least-squares fit to lines in Guinier powder diffraction data.

[c]Abbreviations: S - sintered powder; R - reduction of AlI_3 by lithium; VT - isothermal vapor transport; F - flux growth; AM - arc melting.

The lattice parameters for $Zr\ Sb_3O$ as previously reported (Table 16) are much larger than those observed in the present investigation and are actually within the range of Zr_5Sb_{3+x} parameters. The conclusion reached is that the compound reported as Zr_5Sb_3O[35] was in fact Zr_5Sb_{3+x} but that as demonstrated above, Zr_5Sb_3O can indeed be synthesized.

In an attempt to obtain complete reaction, the product from the reaction sintered at 1300°C was ground, pressed into a pellet and arc-melted. A 3% weight loss occurred, and the powder pattern of the as-cast material contained broad lines many of which were weak and unidentified. There was also a Zr_5Sb_3Z-type diffraction pattern but of a much larger cell than observed in the sintered product.

The poor quality of the pattern prevented a quantitative measure of the lattice dimensions but qualitatively it can be said that they are in the range of those for Zr_5Sb_{3+x}. Apparently Zr_5Sb_3O is not stable at the high temperature reached in the arc-furnace, and as-cast samples were cooled too rapidly to allow for its formation. Judging from the incomplete reaction at 1300°C, attempts to reach equilibrium by annealing arc-melted products will have to be at $T > 1300$°C in order to achieve the requisite mobility.

Zr_5Sb_3C

The phase Zr_5Sb_3C reportedly could not be synthesized,[6] but a reaction of a stoichiometric mixture of Zr, Sb and graphite sintered at 1300°C for 3 days yielded a single phase product with a characteristic Zr_5Sb_3Z diffraction pattern. The unit cell volume of this phase is almost identical to that of Zr_5Sb_3O but the axial lengths of the carbide

differ by -15σ and +21σ, respectively where the oxide has a longer a-axis but a smaller c parameter (see Table 19).

Preparation of the carbide by arc-melting gave ambiguous results. These reactions, which employed Zr, ZrC, and Sb as the starting materials, always contained ZrC as a product. They also produced a Zr_5Sb_3Z-type phase but with the lattice parameters larger (a = 8.3828(8), c = 5.7616(9) Å) than measured for Zr_5Sb_3C and approaching those of $Zr_5Sb_{3.0}$. This phase may or may not be a substoichiometric $Zr_5Sb_3C_x$ compound. When a sample of composition $Zr_5Sb_3C_{0.5}$ was arc-melted, the lines of ZrC in the powder pattern were proportionally much less intense, but the lattice parameters of the supposed $Zr_5Sb_3C_x$ phase remained the same as for x = 1 arc-melted sample. A reaction mixture designed to produce $Zr_5Sb_3C_{0.08}$ did not exhibit any lines of ZrC in the powder pattern but did give two Zr_5Sb_3Z type patterns of larger lattice dimensions than previously observed. These results imply that a $Zr_5Sb_3C_x$ phase, $0.08 < x < 0.5$, is formed in as-cast samples, but because of uncontrollable and differing amounts of antimony volatilization in the reactions, this conclusion must be regarded as only tentative.

The oxide phase is not stable at arc-furnace reaction conditions and apparently neither is $Zr_5Sb_3C_{1.0}$ but, despite previous assertions to the contrary, Zr_5Sb_3C can be synthesized at lower temperatures.

Zr_5Sb_3B

Reactions designed to produce Zr_5Sb_3B were not extensively pursued. A stoichiometric mixture of the elements that were arc-melted produced ZrB_2 and a Mn_5Si_3-type compound. The lattice parameters of the latter

phase are a = 8.4045(6) and c = 5.7768(7) A, much larger than either the oxide or carbide but arguably different than the values for $Zr_5Sb_{3.0}$ (14σ and 9σ, see Table 19). The compound may be a $Zr_5Sb_3B_X$ phase analogous to the postulated $Zr_5Sb_3C_X$. It is clear that Zr_5Sb_3B is not stable at high temperature (~>1400°C) but by analogy with Zr_5Sb_3C and Zr_5Sb_3O, it may be possible to synthesize it by sintering powders at 1300°C. Results for Zr_5Sb_3N were analogous to the boride.

Third Period Interstitial Compounds

Zr_5Sb_3Al

A stoichiometric amount of Zr and Al were arc-melted with a slight excess of Sb in order to produce Zr_5Sb_3Al. The final composition was $Zr_5Sb_{3.1}Al$ based on solely loss of Sb. This as-cast sample contained only one phase but the lines in the powder pattern were broader than normally encountered in Zr_5Sb_3Z systems. The high standard deviations of the measured lattice parameters (a = 8.563(2), c = 5.844(1) A) are a reflection of this fact.

A crystal of the material, obtained by crushing the solidified button, was mounted in an X-ray capillary for a structural investigation. The experimental details of data collection are listed in Table 17. The systematic absences in the data set were consistent with the space group $P6_3/mcm$ as expected. Initial least-squares refinement was carried out on approximate positional parameters based on Mn_5Si_3, but an aluminum atom at the interstitial site was also included. After convergence of all variable positional parameters, the residuals were R = 0.12 and R_W =

0.18. When next the thermal parameters were varied isotropically, the aluminum value repeatedly refined as less than zero. The thermal parameter, for Al was then held fixed at B = 1.0 while the other thermal parameters and Al multiplicity were varied. Convergence was attained, and the aluminum multiplier refined to almost double the value for full occupancy with the resulting agreement factors at R = 0.051, R_w = 0.077. The thermal parameters of the Zr and Sb atoms were then allowed to vary anisotropically, after which the Al multiplier was held constant while its thermal parameters was refined isotropically, yielding R = 0.029 and R_w = 0.053. At this point the Sb and Zr(2) multipliers were also allowed to vary with a result that indicated the Zr(2) position was fully occupied but that the Sb position was not. Lastly, the aluminum thermal parameters were allowed to vary anisotropically and the final residuals R = 0.017 and R_w = 0.025 were obtained. The refined positional and thermal parameters and resulting interatomic distances are given in Table 20. A final electron density difference map revealed no residual electron density greater than 0.5 e/A^3. It is of course physically impossible for 1.8 (see Table 20) aluminum atoms to occupy one site. Based on the observation in the binary system, that antimony may partially fill this position, the assumption was made that the 23.4 electron peak was a statistical result of occupation by 72% Al and 28% Sb. On the other hand, the partial occupancy of the antimony lattice site can be explained if some aluminum is substituted for antimony. The refined electron density is accounted for by 87% Sb and 13% Al filling the 6(g) crystallographic site.

Table 20. Parameters and interatomic distances for Zr_5Sb_3Al[a]

Atom	Site[b]	Occupancy	x	B_{11}	B_{22}	B_{33}
Sb	6(g)	0.900(4)	0.61194(7)	0.66(3)	0.47(3)	0.86(3)
Zr(1)	4(d)	1	1/3	0.56(3)	B_{11}	0.54(4)
Zr(2)	6(g)	0.984(8)	0.2664(1)	1.98(3)	0.64(4)	1.99(4)
Al	2(b)	1.82(1)	0	0.42(7)	B_{11}	0.65(9)

Interatomic Distances[c] (Å)

Sb	- 2Zr(2)	2.930(1)	Zr(2)	- 2Al	2.700(1)
Sb	- 1Zr(2)	2.944(2)	Zr(2)	- 2Sb	2.930(1)
Sb	- 4Zr(1)	3.016(1)	Zr(2)	- 1Sb	2.944(2)
Sb	- 2Zr(2)	3.101(1)	Zr(2)	- 2Sb	3.101(1)
Sb	- 2Sb	3.491(1)	Zr(2)	- 4Zr(1)	3.485(1)
Sb	- 2Al	3.616(1)	Zr(2)	- 4Zr(2)	3.701(1)
			Zr(2)	- 2Zr(2)	3.933(2)
Zr(1)	- 2Zr(1)	2.923(1)			
Zr(1)	- 6Sb	3.016(1)	Al	- 6Zr(2)	2.700(1)
Zr(1)	- 6Zr(2)	3.486(1)	Al	- 2Al	2.923(1)
			Al	- 6Sb	3.616(1)

[a]Refined formula = $Zr_5Sb_{2.6}Al_{0.4}$ $(Al_{0.7}Sb_{0.3})$.
[b]Space group $P6_3/mcm$.
[c]Distances less than 4 Å.

The partial replacement of Sb by Al is reasonable since the Mn_5Si_3-type compound Zr_5Al_3[65] exists. Solid solution behavior between Zr_5Sb_3 and Zr_5Al_3 at the high temperature encountered in the arc-furnace is not surprising. In fact, solid solution behavior between Zr_5Al_3 and Zr_5Sb_3 has been investigated,[66] but interstitial site occupancy was not taken into account. Additionally, the alloys were prepared by melting in boron nitride crucibles, and annealed in silica tubes at 1000°C, which likely resulted in contamination. In the present investigation the very good agreement factors obtained in the structural refinement imply that the crystal was of high quality. The broad lines in the powder pattern are, therefore, due not to poor crystallinity but to a range of compositions in the product as a result of solid solution behavior. Presumably, the rapid quenching of the sample did not allow for low temperature phase separation to occur.

An arc-melted sample of overall composition $Zr_5Sb_{2.98}Al$ was annealed at 1000°C for 3 days in an attempt to achieve equilibrium. The powder pattern was essentially the same as that observed for the as-cast product. A third reaction was designed to prevent the initial solid solution formation. The compound $Zr_5Sb_{3.0}$ was prepared by arc-melting, ground into a fine powder, and reacted with three equivalents of Li in a Ta tube. The material of overall composition $Zr_5Sb_3Li_3$ was then ground again and sealed in a Ta tube with one equivalent of AlI_3. The hope was that reduction of gaseous AlI_3 by lithium would produce finely divided aluminum which would react with the finely ground Zr_5Sb_3. The temperature of the reaction was slowly raised to 1100°C and maintained there for

six days after which the LiI was separated from Zr_5Sb_3Al by vacuum sublimation. The powder pattern again indicated only a single phase was present, but the lines were now sharp. The lattice parameters of Zr_5Sb_3Al produced by this method were larger than those of the arc-melted sample and are listed in Table 19. This increase in size was expected on the basis of the larger parameters seen for the Mn_5Si_3 framework of Zr_5Sb_3 compared to Zr_5Al_3[65] (8.4177 vs 8.184 Å, and 5.766 vs 5.702 Å, respectively). This implies that at lower temperature (1100°C) the solid solution composition range is very much smaller or nonexistent.

Zr_5Sb_3Si

The solid solution behavior evidenced by the broad powder pattern lines of arc-melted Zr_5Sb_3Al preparations was also observed in Zr_5Sb_3Si syntheses. If the Sb to Zr ratio dropped below 3:5, the lines were especially broad. A Mn_5Si_3-type Zr_5Si_3 phase has been reported as impurity stabilized with B, C, N or O[67-69] and solid solutions characteristics are not unexpected. Attempts to improve the situation by annealing at 950-1000°C were not successful. A better approach was to sinter (1300°C, 3 days) an appropriate mixture of $Zr_5Sb_{3.0}$ and Si powders. This produced a single phase product with very sharp lines and the lattice parameters listed in Table 19.

In addition to the powder information, single crystal data was sought in order to provide a quantitative basis for comparison to Zr_5Sb_3Al. Crystals of Zr_5Sb_3Si were obtained through the use of a flux reaction in which a stoichiometric mixture of Zr, Sb, and Si was dissolved in a Zn solvent at 900°C using an Al_2O_3 crucible. The crucible

had been sealed in a silica tube under an atmosphere of argon. After seven days all the Zn had evaporated from the crucible and condensed in a cooler part of the glass tube. A 100% yield of single phase rod crystals were obtained. The lattice parameters of this product (a = 8.5686(7), c = 5.7934(6) Å), were larger than those measured for the sintered Zr_5Sb_3Si sample but smaller than Zr_5Sb_3Zn (Table 19). One of these crystals was employed for the structural refinement.

Experimental details of data collection are outlined in Table 17. The systematic absences in the data set were consistent with the space group $P6_3/mcm$ as expected. Initial least-squares refinement was carried out on approximate positional parameters based on Mn_5Si_3 with the inclusion of a Si atom at the interstitial site. The refinement proceeded smoothly and final parameters and interatomic distances are listed in Table 21.

The calculated occupancy of the interstitial atom again appears to be greater than unity but much less significantly so than in Zr_5Sb_3Al. In this case it is presumably due to partial substitution of Si by Zn. The refined occupancy of 15.8 can be accounted for by a statistical distribution of 89% Si and 11% Zn. The deviation from unity is only 6.5σ so too much cannot be made of this observation, but the comparison of lattice parameters as discussed above is consistent with this supposition. The Sb position is also only partially occupied as it was in the Zr_5Sb_3Al refinement but again the deviation from unity is only 7σ and this site may or may not be partially filled with Si.

Table 21. Parameters and interatomic distances for Zr_5Sb_3Si[a]

Atom	Site[b]	Occupancy	x	B_{11}	B_{22}	B_{33}
Sb	6(g)	0.972(4)	0.60630(8)	1.01(1)	0.87(3)	1.56(3)
Zr(1)	4(d)	0.976(6)	1/3	0.90(5)	B_{11}	1.42(5)
Zr(2)	6(g)	1	0.2619(1)	1.00(3)	0.99(4)	1.53(5)
Si	2(b)	1.13(2)	0	1.3(2)	B_{11}	1.7(2)

Interatomic Distances[c] (Å)

Sb	- 1Zr(2)	2.951(1)	Zr(2)	- 2Si	2.671(1)
Sb	- 2Zr(2)	2.974(1)	Zr(2)	- 1Sb	2.951(1)
Sb	- 4Zr(1)	3.008(1)	Zr(2)	- 2Sb	2.974(1)
Sb	- 2Zr(2)	3.109(1)	Zr(2)	- 2Sb	3.109(1)
Sb	- 2Sb	3.422(1)	Zr(2)	- 4Zr(1)	3.518(1)
Sb	- 2Si	3.671(1)	Zr(2)	- 4Zr(2)	3.664(1)
			Zr(2)	- 2Zr(2)	3.887(2)
Zr(1)	- 2Zr(1)	2.897(1)			
Zr(1)	- 6Sb	3.008(1)	Si	- 6Zr(2)	2.671(1)
Zr(1)	- 6Zr(2)	3.519(1)	Si	- 2Si	2.897(1)
			Si	- 6Sb	3.671(1)

[a]Refined formula = $Zr_5Sb_{2.9}Si_{0.1}$ $(Si_{0.9}Zn_{0.1})$ (see text).
[b]Space group $P6_3/mcm$.
[c]Distances less than 4 Å.

Zr_5Sb_3P

Arc-melting was not considered a good method of preparing Zr_5Sb_3P since concomitant vaporization of P along with Sb renders synthetic control inadequate. This problem is somewhat reduced, but not eliminated, by pre-reacting Zr and P at a lower temperature. An alternative to preparation by arc-melting was utilized in which the vapor pressure of phosphorus was used to advantage. A sample of $Zr_5Sb_{3.0}$ was prepared by arc-melting and ground into a powder which was reacted with a suitable amount of red phosphorus in a sealed fused silica tube at 650°C for 1 day. The mixture was reground and pressed into a pellet, sealed in a Ta tube and heated at 1000°C for 3 days. These conditions proved inadequate for complete reaction. The preparation was repeated, but the pellet was maintained at 1300°C for 3 days in an evacuated (10^{-6} torr) recrystallized alumina muffle tube. This yielded in addition to a trace of ZrO_2 a single phase product with very sharp diffraction lines. The lattice parameters are listed in Table 19.

Zr_5Sb_3S

The same considerations apply to the synthesis of Zr_5Sb_3S by arc-melting as were discussed for Zr_5Sb_3P. The sulfide was, therefore, synthesized by sintering stoichiometric amounts of $Zr_5Sb_{3.0}$ and S in a sealed Ta tube. The temperature was slowly raised to 1300°C (room temperature to 1300°C in 18 hours) and maintained for 3 days. The product was single phase with sharp diffraction lines. The Ta container was nonbrittle indicating no dissolved sulfur. The lattice parameters are presented in Table 19 where it should be noted that the a-axis is smaller

and consistent with the trend observed with Z = Al, Si, P but that the c-parameter did not decrease and is, in fact, quite a bit larger than even in the aluminide phase.

No sulfur interstitial Zr compounds were known previous to this work and because of the anomalous c-axis length, a single crystal structural investigation was desirable. Sintering of powders does not generally lead to suitable crystals, and attempts to grow them with a Zn flux as done for Zr_5Sb_3Si were unsuccessful. A final recourse was to attempt the preparation by arc-melting despite the loss of synthetic control this entailed.

The reaction was carried out by pre-reacting Zr and S in a 5:1 molar ratio using a sealed silica tube at 900°C. The mixed zirconium sulfides were arc-melted with a slight (10%) excess of Sb, and the final weight of the product was 5% less than calculated for Zr_5Sb_3S. This is a somewhat larger weight loss than usually incurred for Zr_5Sb_3Z systems. The sample was annealed at 950°C for 1 day. The diffraction lines in the powder pattern were much broader than for the sintered powder reactions. The lattice parameters a = 8.435(1), c = 5.859(3) gave a unit cell size intermediate between $Zr_5Sb_{3.0}$ and the sintered Zr_5Sb_3S (see Table 19).

A crystal was obtained by breaking up the ingot and a structural investigation was undertaken. The experimental details of data collection are outlined in Table 16. The data set exhibited systematic absences consistent with the space group $P6_3/mcm$. Initial least-squares

refinement was carried out with the usual approximate positional parameters and inclusion of sulfur at the origin.

The refinement proceeded smoothly and in the final cycle all variables except Zr(2) multiplier were allowed to vary, with the results presented in Table 22. The sulfur position was found to be only 70 ± 2% occupied.

The substoichiometry of sulfur is undoubtedly due to losses incurred during arc-melting. The repeat distance along the c-axis is intermediate between those of Zr_5Sb_3S (by sintered powders) and $Zr_5Sb_{3.0}$. In fact, 70% of the difference between the c-parameter of $Zr_5Sb_{3.0}$ and Zr_5Sb_3S gives a value of c = 5.86 Å, identical to c = 5859(3) Å measured for the arc-melted sample. Unfortunately, the behavior of the a-axis is not so straightforward.

Fourth Period Main Group Metal Interstitial Compounds

Zr_5Sb_3Ga

The problem of solid solution formation was anticipated for gallium samples. The binary compound Zr_5Ga_3[70] is a known phase and some substitution of gallium in the antimony sites in Zr_5Sb_3Ga in a manner analogous to Zr_5Sb_3Al was expected. A preparation of Zr_5Sb_3Ga by arc-melting confirmed such behavior.

A stoichiometric amount of zirconium and gallium were arc-melted with a slight (10%) excess of antimony. Assuming only antimony volatilization, the final composition was $Zr_5Sb_{3.09}Ga$. This sample was annealed for three days at 1000°C, after which the powder pattern exhibited broad lines such as those observed for Zr_5Sb_3Al. The range of

Table 22. Parameters and interatomic distances for $Zr_5Sb_3S_{0.7}$[a]

Atom	Site[b]	Occupancy	x	B_{11}	B_{22}	B_{33}
Sb	6(g)	1.020(8)	0.6050(1)	0.48(3)	0.43(5)	0.94(5)
Zr(1)	4(d)	0.93(1)	1/3	0.29(8)	B_{11}	0.74(7)
Zr(2)	6(g)	1	0.2515(1)	0.69(4)	0.39(6)	1.48(7)
S	2(b)	0.70(2)	0	0.4(3)	B_{11}	2.0(3)

Interatomic Distances[c] (Å)

Sb	- 2Zr(2)	2.921(1)	Zr(2)	- 2S	2.578(1)
Sb	- 4Zr(1)	2.976(1)	Zr(2)	- 2Sb	2.921(1)
Sb	- 1Zr(2)	2.982(1)	Zr(2)	- 1Sb	2.982(1)
Sb	- 2Zr(2)	3.170(1)	Zr(2)	- 2Sb	3.170(1)
Sb	- 2Sb	3.423(1)	Zr(2)	- 4Zr(1)	3.532(1)
Sb	- 2S	3.640(1)	Zr(2)	- 4Zr(2)	3.617(1)
			Zr(2)	- 2Zr(2)	3.674(2)
Zr(1)	- 2Zr(1)	2.930(2)			
Zr(1)	- 6Sb	2.976(1)	S	- 6Zr(2)	2.578(1)
Zr(1)	- 6Zr(2)	3.532(1)	S	- 2S	2.930(2)
			S	- 6Sb	3.640(1)

[a]Refined formula = $Zr_{4.9}Sb_{3.0}S_{0.7}$
[b]Space group $P6_3/mcm$.
[c]Distances less than 4 Å.

compositions produced was not evenly distributed as the lines were markedly more intense on the low angle side, but phase separation did not occur.

The sintering of powders at high temperature (1300°C) which had proven successful in synthesizing other Zr_5Sb_3Z systems was also attempted for Zr_5Sb_3Ga. Because gallium cannot be ground into a powder, a gallium antimony stoichiometric mixture in the ratio 1:3 was melted in an alumina crucible. The reaction was carried out in an atmosphere of Ar within a sealed silica tube at 800°C. A stoichiometric amount of the solidified $GaSb_3$ (GaSb + 2Sb)[71] and zirconium powders were ground together and sealed in a Ta tube. This was placed in a recrystallized alumina tube which was evacuated to 10^{-6} torr and heated at 1300°C for three days.

The powder pattern of the product contained the four strongest lines of ZrO_2 and five weak unidentified lines, as well as a strong sharp Zr_5Sb_3Z-type pattern. The lattice constants of this phase, presumably Zr_5Sb_3Ga are listed in Table 19 and can be compared to those of Zr_5Ga_3[70] (a = 8.020, c = 5.678 Å) and Zr_5Ga_4[72] (a = 8.350, c = 5.757 Å).

Zr_5Sb_3Ge

Since Zr_5Ge_3 is a known compound,[73] Zr_5Sb_3Ge was not prepared by arc-melting. Solid solution behavior was observed in other Zr_5Sb_3Z systems where a Zr_5M_3 binary phase also exists (e.g., see Zr_5Sb_3Al). The compound was prepared by more controlled vapor transport and sintering techniques.

Stoichiometric amounts of Zr, $ZrSb_2$ and Ge were ground together and sealed in a tantalum tube with a small amount of ZrI_4 (5 mg) as a transport agent. This was allowed to react at 1300°C for one week in an evacuated (10^{-5} torr) mullite tube. Mullite is more porous than recrystallized alumina and a small amount of ZrO_2 (10%) was observed in the powder pattern in addition to a Zr_5Sb_3Z diffraction pattern. The product was microcrystalline with many reflective faces but all too small for single crystal X-ray work. The diffraction lines of this Zr_5Sb_3Z phase were very sharp and gave lattice parameters of a = 8.5284(6) and c = 5.8186(7) A.

The synthesis was repeated but $Zr_5Sb_{3.0}$ (prepared by arc-melting) was reacted with powdered germanium and no transport agent was used. The reaction was allowed to proceed in a Ta tube at 1300°C for three days. The tantalum container was heated in an evacuated recrystallized alumina muffle tube (10^{-6} torr). Only a trace of ZrO_2 (strongest line) was detected in the powder pattern. The rest of the diffraction lines were very sharp and could be indexed on the basis of a Zr_5Sb_3Z-type cell. The lattice parameters (Table 19) for this Zr_5Sb_3Ge compound are significantly larger than the previously observed phase.

In fact, the lattice parameters of the germanium compound that was produced along with 10% ZrO_2 are smaller than those measured for Zr_5Sb_3Si (see Table 19). This could be explained by a mixture Ge and O in the interstitial site. The larger cell listed in Table 19 is more representative of a true Zr_5Sb_3Ge composition.

Zr_5Sb_3As

The volatility of arsenic made sintering, the technique of choice for the preparation of Zr_5Sb_3As. A ground mixture of $Zr_5Sb_{3.0}$ (prepared by arc-melting) and arsenic was ground and sealed in a tantalum tube. The temperature was raised over a period of 18 hours to 1300°C in an evacuated (10^{-6} torr) recrystallized alumina muffle tube. The temperature was maintained for three days.

The Ta tube was still malleable after removal from the furnace, indicating no significant reaction of the arsenic with the tantalum container. The powder pattern contained the strongest line of ZrO_2 at a very weak intensity, otherwise, the pattern could be indexed on the basis of a Zr_5Sb_3 Z-type cell. The diffraction lines were very sharp and the refined lattice constants of this presumed Zr_5Sb_3As phase are listed in Table 19.

Zr_5Sb_3Se

No attempt was made to synthesize the selenide phase by arc-melting. A stoichiometric amount of $Zr_5Sb_{3.0}$ previously prepared by arc-melting, and selenium were ground together and placed in an alumina crucible. The crucible was sealed in a fused silica jacket under an argon pressure of 250 torr. The reaction was maintained at 400°C for two days after which the temperature was raised to 1050°C where it remained for 5 days. These conditions were not sufficient to achieve equilibrium.

A second attempt to synthesize Zr_5Sb_3Se was made by grinding $Zr_5Sb_{3.0}$ and Se, but the reactants were now sealed in a Ta tube. The container was placed in an evacuated recrystallized alumina tube. The

reaction temperature was raised to 1300°C over a span of 18 hours and allowed to remain there for three days. The tantalum container did not react with the selenium as evidenced by its malleability after the reaction.

The powder pattern contained only Zr_5Sb_3Se diffraction lines, and no evidence of ZrO_2 was observed. The lattice parameters of the selenide phase are listed in Table 19. The anomalously large repeat distance along the c-axis observed for the sulfide is also observed with Zr_5Sb_3Se.

Transition Metal (3d) Interstitial Compounds

Zr_5Sb_3Fe

Synthesis of the iron interstitial compound was initially carried out by arc-melting. A stoichiometric amount of zirconium and iron were reacted with a slight excess (5%) of antimony. The volatilization of antimony from Zr_5Sb_3Fe (and other transition metal) melts was observed to be much less than for main group interstitial compounds. The final composition based on only antimony loss was $Zr_5Sb_{2.9}Fe$.

The powder pattern of this as-cast material, with the exception of one weak inidentified line, could be indexed on the basis of a Zr_5Sb_3Z-type cell. The sharp lines observed implied a well-ordered homogeneous product. Lattice constants were refined as a = 8.580(1), c = 5.836(1) A. In the course of grinding this sample for a powder pattern, a roughly spherical crystal was found among the ground material and mounted in an X-ray capillary. An oscillation photograph verified the singular nature of the crystal, and it was used for a structural refinement.

Experimental details of data collection are outlined in Table 17. The systematic extinctions in the data were consistent with the space group $P6_3/mcm$. Initial refinement was based on a Zr_5Sb_3 composition using approximate positional parameters from Mn_5Si_3. After convergence of the positional parameters the agreement factors were R = 0.199 and R_W = 0.289. An iron atom was then included at the interstitial site and the positional parameters further refined. The residuals now dropped to R = 0.051 and R_W = 0.064. Least-squares calculations proceeded smoothly from this point and in the final cycle, all variable parameters except the Zr(1) multiplier were allowed to vary simultaneously. The final residuals were R = 0.021 and R_W = 0.037, and refined parameters are listed in Table 23. A final Fourier difference map revealed no residual electron density greater than 0.5 e/Å^3.

The structure refinement unambiguously confirmed the existence of Zr_5Sb_3Fe with iron in the interstitial site. The ease in which the compound was initially obtained is ironic in light of later difficulties. The phase was also found to be magnetically ordered at room temperature by using a sophisticated instrument, the horseshoe magnet. The magnetic properties are more fully discussed below.

The refinement yielding a $Zr_5Sb_{3.05(2)}Fe_{1.00(1)}$ composition may have been serendipitous. When the preparation of the iron compound was repeated, the lattice parameters were found to vary considerably. Arc-melted samples both annealed and as-cast always gave sharp diffraction lines indicative of a single phase homogeneous product, but the unit cell size was found to vary (see Table 24).

Table 23. Parameters and interatomic distances for Zr_5Sb_3Fe[a]

Atom	Site[b]	Occupancy	x	B_{11}	B_{22}	B_{33}
Sb	6(g)	1.016(8)	0.6122(1)	0.59(3)	0.37(5)	0.76(5)
Zr(1)	4(d)	1	1/3	0.37(9)	B_{11}	0.57(9)
Zr(2)	6(g)	1.00(1)	0.2583(2)	0.89(6)	0.59(8)	0.82(7)
Fe	2(b)	1.00(1)	0	0.2(2)	B_{11}	1.1(2)

Interatomic Distances (Å)[c]

Sb - 2Zr(2)	2.934(1)	Zr(2) - 2Fe	2.653(2)
Sb - 4Zr(1)	3.031(1)	Zr(2) - 2Sb	2.934(1)
Sb - 1Zr(2)	3.036(2)	Zr(2) - 1Sb	3.036(2)
Sb - 2Zr(2)	3.122(1)	Zr(2) - 2Sb	3.122(1)
Sb - 2Sb	3.496(1)	Zr(2) - 4Zr(1)	3.545(1)
Sb - 2Fe	3.633(1)	Zr(2) - 4Zr(2)	3.664(1)
Zr(1) - 2Zr(1)	2.918(1)	Fe - 6Zr(2)	2.653(2)
Zr(1) - 6Sb	3.031(1)	Fe - 2Fe	2.918(1)
Zr(1) - 6Zr(2)	3.545(1)	Fe - 6Sb	3.633(1)

[a]Refined formula = $Zr_{5.00(3)}Sb_{3.05(2)}Fe_{1.00(1)}$.
[b]Space group $P6_3/mcm$.
[c]Distances less than 3.8 Å.

Table 24. Zr_5Sb_3Fe preparations and lattice parameters

Preparation Method	Nominal Composition	c/a	Lattice Parameters a (Å)	c (Å)
arc-melting, as-cast	$Zr_5Sb_{2.9}Fe$	0.6802	8.580(1)	5.836(1)
arc-melting, as-cast	$Zr_5Sb_{3.2}Fe$	0.6818	8.533(2)	5.818(2)
arc-melting, as-cast	$Zr_5Sb_{3.0}Fe$	0.6813	8.528(1)	5.810(1)
arc-melting, annealed (1000°C)	$Zr_5Sb_{3.1}Fe$	0.6803	8.585(1)	5.840(1)
arc-melting, as-cast	$Zr_5Sb_{3.1}Fe$	0.6801	8.555(1)	5.818(1)
$Zr_5Sb_3Li_2$+FeI_2, 1100°C	$Zr_5Sb_{3.0}Fe$	0.6838	8.557(1)	5.851(1)
$Zr_5Sb_3Li_2$+FeI_2, 1100°C	$Zr_5Sb_{3.0}Fe$	0.6833	8.5495(7)	5.842(1)
Vapor transport, 1300°C	$Zr_5Sb_{3.0}Fe$	0.6833	8.5880(5)	5.8679(7)
Vapor transport, 1150°C	$Zr_5Sb_{3.0}Fe$	0.6845	8.551(1)	5.853(1)

For comparison purposes the compound was also prepared by reaction of $Zr_5Sb_3Li_2$ and FeI_2. Stoichiometric amounts of zirconium and antimony powder were sintered to form $Zr_5Sb_{3.0}$, and then reacted with two equivalents of lithium in a Ta tube. This is the most likely source of error in this procedure as the 17 ± 2 mg of lithium used had a 10% margin of error. The product of overall composition $Zr_5Sb_3Li_2$ was ground into a fine powder and allowed to react with a stoichiometric amount of FeI_2 in a Ta tube at 1100°C for six days. This method was used because great difficulty was encountered in achieving equilibrium by sintering of elemental powders. The reduction of FeI_2 by lithium should produce a much more finely divided iron powder. Accordingly, a single phase Zr_5Sb_3 Z-type material was produced, but the iodide salt sublimed from the product exhibited a slight yellow color. Lithium iodide is of course white, so the color was due to another metal iodide. Zirconium, antimony or iron iodides all could have produced this color (and most likely formed because of an insufficient amount of lithium caused by weighing errors).

Some isothermal vapor transport reactions were also carried out. These involved stoichiometric mixtures of zirconium, antimony, and iron powders sealed in a tantalum tube with a small quantity of SbI_3. One reaction was loaded with powdered $ZrFe_2$ rather than elemental iron, and heated at 1300°C for seven days in an evacuated (10^{-5} torr) mullite tube. The lattice parameters of this product along with a second transport reaction protected by a fused silica jacket and heated for 19 days at 1150°C are listed in Table 24.

Lattice constants from other reactions are also listed in this Table. There is a very large difference in the measured parameters of what was hoped would be Zr_5Sb_3Fe preparations. The arc-melted examples show the greatest variation, with the vapor transport and lithium reduction reactions much more consistent. Since these latter reactions are more controlled and consistent they are more likely to have produced a stoichiometric Zr_5Sb_3Fe.

The single crystal refinement showed unambiguously that a stoichiometric Zr_5Sb_3Fe can exist. The powder data imply that this compound may also exist off-stoichiometry. A second factor encountered in other systems may also come into play. Solid solutions formation at high temperature (see Zr_5Sb_3Al) can be a problem in this system as well. Certainly one may imagine partial replacement of the iron interstitial with antimony to yield larger lattice parameters. Iron is known to be partially replaced by indium in another Zr_5Sb_3Z phase (see $Zr_5Sb_3Fe_{2/3}In_{1/3}$). Perhaps some of the zirconium is being substituted by iron, in which case a smaller unit cell would be expected. A Mn_5Si_3-type Fe_5Si_3 compound is known,[74] and a small amount of zirconium substitution by iron in Zr_5Sb_3Fe would not be unreasonable. These are all open questions which would benefit from further investigation.

In order to probe the nonstoichiometry of iron it was necessary to prepare samples by sintering powders. Confidence in a fixed zirconium and antimony composition while varying the iron content is best achieved in such a controlled experiment. Even in transport reactions there is always a metal iodide product which slightly changes the composition.

Two reactions designed to produce $Zr_5Sb_3Fe_{1.0}$ and $Zr_5Sb_3Fe_{0.5}$ used a ground mixture of Zr, $ZrSb_3$ and FeSb. The powder was pressed into a pellet and heated at 1100°C for 18 hours. This reaction time is much too short. The main phase in both reactions was a Zr_5Sb_3Z-type phase and, despite the different iron content, the same lattice parameters were observed. Additional unidentified lines in the powder pattern indicated that the reaction had not gone to completion. The synthesis of $Zr_5Sb_3Fe_{1.0}$ was repeated and the temperature maintained at 1000°C for three days. The powder pattern was almost identical to that of the sample heated for 18 hours. Apparently, initial formation of a Zr_5Sb_3Z-type phase off stoichiometry is facile, but the atomic mobility is very low at 1000°C making it difficult to obtain complete reaction at this temperature. Further experiments need to be performed at higher temperature. Arc-melting of products obtained by sintering at 1000°C should result in only a minimal loss of antimony, but it would be best to attempt sintering at 1300° - 1400°C first. Along with the apparent non-stoichiometry and or solid-solution of the Zr_5Sb_3Fe phase, an additional question arose in connection with magnetic susceptibility measurements of arc-melted samples. Were single phase products being obtained? Arc-melted, as-cast and annealed (1350°C, three days) samples always contained one extra line in the powder pattern. This extra line was observed in the same $2\theta = 42°$ (Cu K_{α_1}) region, but was found to vary with the lattice parameters of the majority Zr_5Sb_3Fe phase. There was some speculation as to whether the extra line was due to a small amount of $ZrFe_2$.

This iron-zirconium binary compound is a Laves phase[72-78] with a face-centered cubic unit cell and a lattice constant a = 7.074.[79] The high symmetry and small cell result in few diffraction lines for this compound. There are only five diffraction lines between 2θ = 0 to 80° (Cu $K\alpha_1$) one of which falls on a silicon line. Three other lines would be masked by Zr_5Sb_3Fe diffraction lines. The compound $ZrFe_2$ is a ferromagnetically-ordered material below 650 K[80] and would have a large effect on the measured magnetic properties. Preliminary neutron diffraction results have eliminated this possibility.[81]

Difficulties have been encountered in synthetic control during Zr_5Sb_3Fe preparation but the single crystal structural refinement has shown that the stoichiometric phase can be made.

Zr_5Sb_3Co

Arc-melting was initially used to prepare the cobalt phase. A stoichiometric mixture of zirconium and cobalt was melted with a slight (10%) excess of antimony. Final composition was estimated as $Zr_5Sb_{2.98}Co$. The powder pattern of this as-cast sample had very sharp diffraction lines. With one exception they could be indexed on the basis of a Zr_5Sb_3Z cell with dimensions a = 8.5637(7), c = 5.8029(8) Å. The unindexed line was too weak to measure accurately but occurs at $2\theta \approx 42°$.

A second sample of Zr_5Sb_3Co was prepared by sintering. A stoichiometric amount of Zr and $CoSb_3$ were ground together and sealed in a tantalum tube. The $CoSb_3$ had been synthesized by heating the appropriate mixture of Co and Sb powders in an alumina crucible. The cobalt and antimony mixture was heated to 1000°C in an atmosphere of argon to

produce a melt. The solidified binary compound is very brittle and can be ground much finer than cobalt metal. It was chosen for this reason.

Because of the poor results of Zr_5Sb_3Fe preparation at 1000°C, the mixture of Zr and $CoSb_3$ was heated at 1300°C for three days. An evacuated (10^{-6} torr) recrystallized alumina muffle tube was used to protect the tantalum container from oxidation. Only a trace of ZrO_2 was observed in the product. The powder pattern indicated that 1300°C was sufficient to drive the reaction to completion. Only the diffraction lines of a Zr_5Sb_3Z phase were observed but the unit cell (Table 19) is significantly (0.05 Å each) larger than obtained after arc-melting.

Since the sintered powder reaction was a more controlled experiment, the lattice parameters identified with a Zr_5Sb_3Co composition were those obtained by this technique. The sharp lines of as-cast samples indicate that there is no problem achieving equilibrium under quenching conditions, and Zr_5Sb_3Co is probably a congruently melting compound. Unfortunately, the composition cannot be carefully controlled, and the lattice constants suggest that the compound has a homogeneity range and the considerations enumerated for Zr_5Sb_3Fe also apply here.

Zr_5Sb_3Ni

The variability of lattice parameters with preparation method that was noted for Zr_5Sb_3Fe and Zr_5Sb_3Co was also found with Zr_5Sb_3Ni. An as-cast sample with a 100% yield of a Zr_5Sb_3Z-type phase produced a powder pattern with sharp lines. They were indexed to give lattice parameters of a = 8.547(1), c = 5.7731(2) Å.

In a more controlled experiment stoichiometric amounts of Zr, Sb and Ni were sealed in a tantalum tube with a small amount of (10 mg) of SbI_3 to act as a transporting agent. The metal container was sealed in an evacuated fused silica jacket and heated at 1150°C for 18 days. The isothermal transport conditions did not produce any X-ray size single crystals, but the constituents were mobile enough to yield a single phase product. The lattice parameters of this phase were again much larger (0.05 Å) than those of the arc-melted sample and are identified as constants for Zr_5Sb_3Ni in Table 19.

This system is chemically very similar to Zr_5Sb_3Fe and Zr_5Sb_3Co and postulates put forth to explain varying lattice parameters in those systems can also be applied here.

Zr_5Sb_3Cu

The nonstoichiometry involved to explain variable lattice parameters for other Zr_5Sb_3Z (Z = Fe, Co, Ni) phases must also be postulated for Zr_5Sb_3Cu. An as-cast mixture of zirconium, antimony and copper with an estimated final composition of $Zr_5Sb_{3.3}Cu$ yielded a single phase Zr_5Sb_3Z-type product with again very sharp diffraction lines. The refined lattice constants of this phase are a = 8.578(1), c = 5.830(1) Å.

The compound was also prepared by sintering powders. A binary mixture of composition $CuSb_3$ (Cu_2Sb + 5 Sb)[71] was prepared by melting copper and antimony in an alumina crucible under an atmosphere of argon at 750°C. This $CuSb_3$ was easily ground into a fine powder and mixed with an appropriate amount of zirconium powder. The reactants were sealed in a Ta tube which was placed in a recrystallized alumina muffle tube. The

muffle tube was evacuated (10^{-6} torr), and the temperature raised to 1350°C over a span of twelve hours. The temperature was maintained at 1350°C for three days.

Only a trace of ZrO_2 (strongest line was observed at very weak intensity) was seen in the powder pattern. The remaining lines were very sharp and typical of a Zr_5Sb_3Z-type phase. The lattice constants of this Zr_5Sb_3Cu compound are given in Table 19 and it should be noted that the the constant only is 0.02 Å larger than those of the arc-melted sample.

Zr_5Sb_3Zn

The high volatility of zinc makes arc-melting a poor technique for synthesizing Zr_5Sb_3Zn. Vaporization of antimony and zinc renders the composition uncertain, and the amounts of reactants cannot be accordingly adjusted. A good method of preparing the desired compound which has the added benefit of producing crystals is a flux technique.

Stoichiometric amounts of zirconium and antimony powders were placed in an alumina crucible with a large excess of zinc (Zr:Zn = 5:95). The crucible was sealed in a fused silica jacket under an atmosphere of argon. The reaction was heated to 1000°C and the silica tube placed such that, after six days all the molten zinc had evaporated from the crucible and condensed in a cooler part of the glass jacket. A quantitative yield of rod crystals (~0.1 x 0.1 x 1.0 mm) was obtained. The powder pattern indicated a single phase Zr_5Sb_3Z-type product, and the lattice parameters are listed in Table 19. A crystal was chosen for structural refinement and verification of the Zr_5Sb_3Zn interstitial formulation.

Experimental details of data collection are outlined in Table 17. Systematic absences in the data were consistent with the space group $P6_3/mcm$. Due to a malfunction by the DATEX diffractometer that was not detected until after the crystal was removed, the psi-scan data was unusable. Refinement of the structure proceeded without an absorption correction. Initial least-squares refinement was based on approximate positional parameters from Mn_5Si_3 and inclusion of a zinc atom at the origin. The refinement proceeded very smoothly and in the last cycle all variable parameters with the exception of the Zr(2) multiplier were allowed to vary simultaneously. Resulting refined variables and calculated interatomic distances are listed in Table 25. The agreement factors $R = 0.013$ and $R_w = 0.013$, were taken as indicative of an acceptable refinement and psi-scan data were not recollected.

The structural refinement is unambiguous about the Zr_5Sb_3Zn formulation for the compound obtained by use of the zinc flux method ($Zr_{5.01(1)}Sb_{3.02(1)}Zn_{0.999(6)}$). The excellent residuals attest to the fact that this method produces very high quality crystals. It seems likely that Zr_5Sb_3Zn can exist off-stoichiometry as many other Zr_5Sb_3Z systems do, but this was not investigated.

Magnetic susceptibility

Because of the magnetic ordering detected for Zr_5Sb_3Fe, magnetic properties of Zr_5Sb_3Z (Z = Fe, Co, Ni) were more extensively investigated. A plot of susceptibility vs temperature for Zr_5Sb_3Co and Zr_5Sb_3Ni prepared by arc-melting, along with $Zr_5Sb_{3.0}$ is shown in Figure 21. The susceptibilities are essentially temperature independent and weakly

Table 25. Parameters and interatomic distances for Zr_5Sb_3Zn[a]

Atom	Site[b]	Occupancy	x	B_{11}	B_{22}	B_{33}
Sb	6(g)	1.008(4)	0.61504(5)	0.57(1)	0.43(2)	0.68(2)
Zr(1)	4(d)	1.005(5)	1/3	0.49(2)	B_{11}	0.53(3)
Zr(2)	6(g)	1	0.27045(7)	0.60(2)	0.49(3)	0.79(3)
Zn	2(b)	0.999(6)	0	0.42(4)	B_{11}	0.67(6)

Interatomic Distances (Å)[c]

Sb - 2Zr(2)	2.947(1)	Zr(2) - 2Zn	2.747(1)
Sb - 1Zr(2)	2.966(1)	Zr(2) - 2Sb	2.947(1)
Sb - 4Zr(1)	3.046(1)	Zr(2) - 1Sb	2.966(1)
Sb - 2Zr(2)	3.080(1)	Zr(2) - 2Sb	3.080(1)
Sb - 2Sb	3.527(1)	Zr(2) - 4Zr(1)	3.494(1)
Sb - 2Zn	3.621(1)	Zr(2) - 4Zr(2)	3.733(1)
Zr(1) - 2Zr(1)	2.918(1)	Zn - 6Zr(2)	2.747(1)
Zr(1) - 6Sb	3.047(1)	Zn - 2Zn	2.918(1)
Zr(1) - 6Zr(2)	3.494(1)	Zn - 6Sb	3.621(1)

[a]Refined formula = $Zr_{5.01(1)}Sb_{3.02(1)}Zn_{0.999(6)}$.
[b]Space group $P6_3/mcm$.
[c]Distances less than 4 Å.

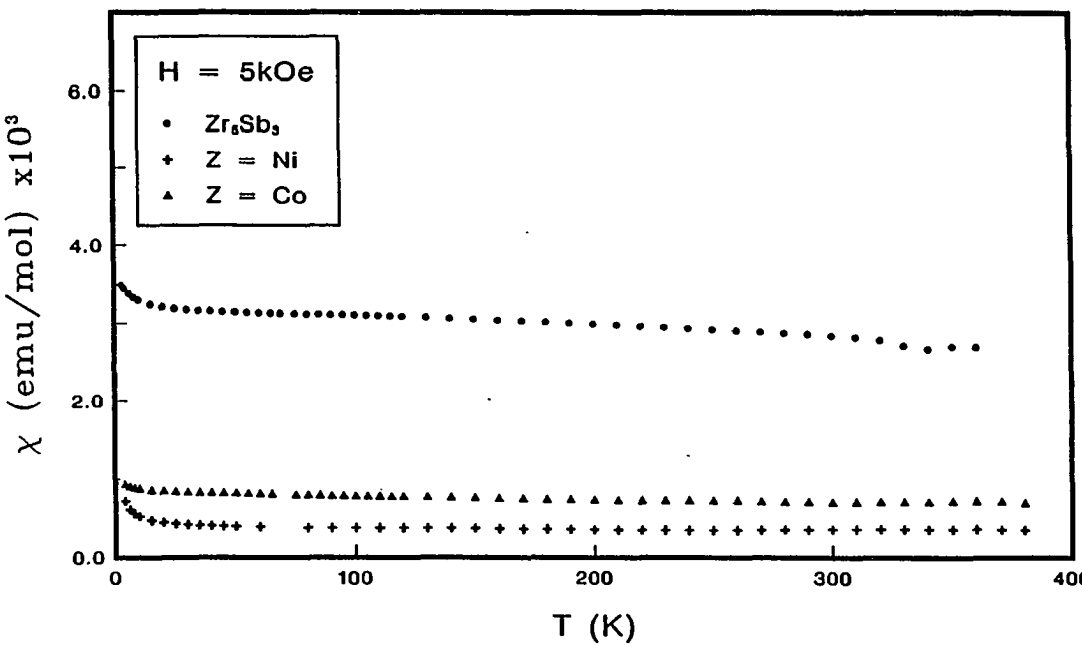

Figure 21. Plot of molar magnetic susceptibility as a function of temperature for Zr_5Sb_3, Zr_5Sb_3Ni, and Zr_5Sb_3Co. The temperature-independent weak paramagnetism is typical of metallic materials

paramagnetic. This type of magnetic behavior is typical of metals, and no evidence is found for any magnetic ordering down to 4.2 K. Small Curie tails due to magnetic impurities can be seen in all three curves, but the increase is very slight, indicating that these are very pure samples with respect to magnetic impurities.

The arc-melting method by which all three of these samples were prepared can lead to nonstoichiometric materials. The resulting susceptibilities cannot, therefore, be taken as an absolute number but the temperature independent weakly paramagnetic behavior is not likely to change with a small variation in composition.

The iron interstitial compound on the other hand is very strongly paramagnetic. The ordered magnetic behavior deduced from qualitative observations (horseshoe magnet) is confirmed by the more sophisticated SQUID susceptometer. Magnetization vs temperature data up to 300K were collected on a SQUID, and higher temperature data were obtained on a Faraday balance using the same sample. The combined data are plotted in Figure 22.

The measured sample was prepared by arc-melting (final composition $Zr_5Sb_{3.11}Fe$) and annealed at 1100°C for one day and at 750°C for an additional day. The lattice parameters of this product were calculated as a = 8.585(1), c = 5.840(1) Å. The diffraction lines in the powder pattern, with one exception, could be indexed on the basis of this cell.

Magnetic susceptibility is defined as $\chi = dM/dH$, and since in most materials M is linear in H this reduces to $\chi = M/H$. Such is not the case for ferromagnetic materials that have a spontaneous magnetization in

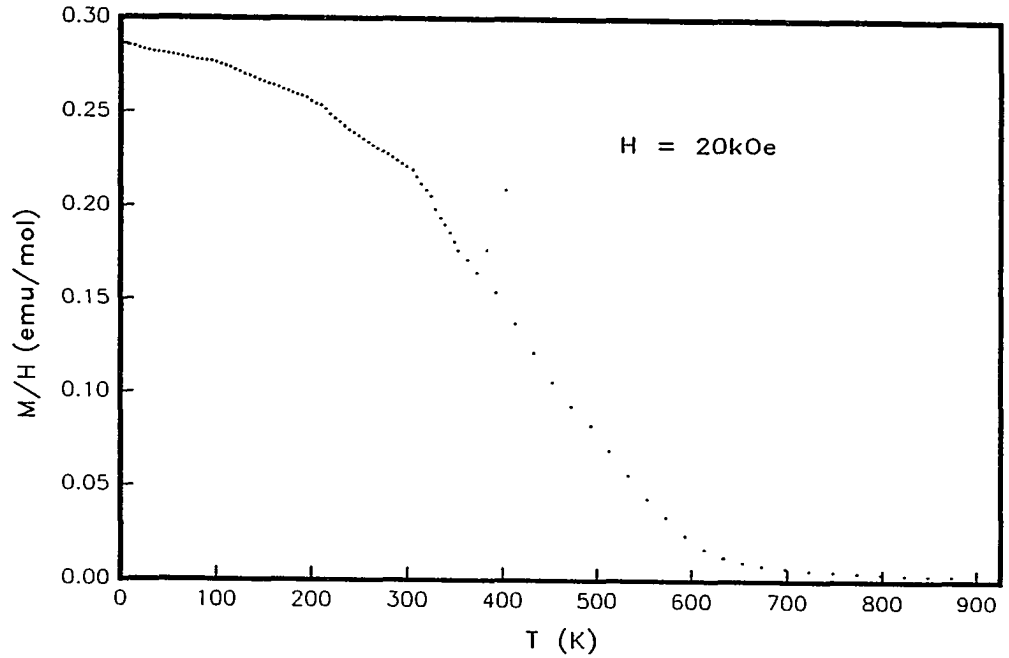

Figure 22. Plot of magneization divided by the applied field strength as a function of temperature for Zr_5Sb_3Fe. This is typical behavior of a ferromagnetic or ferromagnetic ordered material

zero applied field. For this reason the ordinate of Figure 22 is labeled as M/H not χ. It should be noted that in ferromagnetic materials the magnetization remains constant at constant temperature for different fields, assuming all domains are aligned. This means the magnetization of Zr_5Sb_3Fe is actually about three orders of magnitude greater than Zr_5Sb_3, Zr_5Sb_3Ni or Zr_5Sb_3Co as measured at 5 KOe.

The curve follows the expected behavior of a ferromagnetic or ferrimagnetic sample (Figure 22). The kinks observed between 100 - 300 K are not reproduced at different fields, although other anomalies occur in the curve at different temperatures. It is not certain whether these are real magnetic features or instrumental phenomena. This point should be further investigated.

At temperatures greater than 600 K the data are typical of Curie-Weiss behavior. This is more clearly seen in the inverse susceptibility plotted in Figure 23, where the data points above 600 K are observed to fall on a straight line. From this line a Weiss constant of 523 K is obtained. The effective magnetic moment can be estimated from the derived slope as 2.8 Bohr magneton. This indicates two unpaired spins above ~550 K per formula unit of Zr_5Sb_3Fe.

It would be of interest to determine the effect of a varying sample composition on the magnetic properties. In order to make a rigorous comparison, the different samples should have been measured at the same applied magnetic field, but unfortunately they were not. The magnetization at 8K of several samples is listed in Table 26. The samples that were prepared by sintering were allowed to react at 1000°C for three

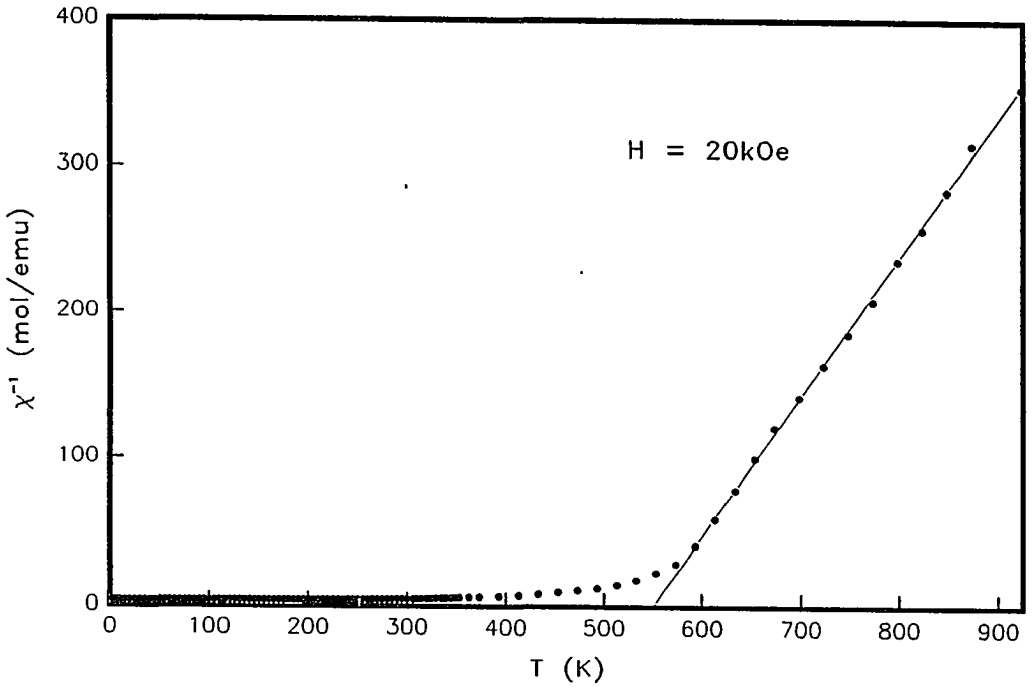

Figure 23. Plot of inverse susceptibility of Zr_5Sb_3Fe as a function of temperature. The Curie temperature is seen to be ~550 K. Curie-Weiss behavior is observed for data above 600 K

Table 26. Magnetization of Zr_5Sb_3Fe[a]

Nominal Sample Composition	Preparation Method	Applied Field (G)	$4\pi M(g)$
$Zr_5Sb_3Fe_{0.25}$	sintered, 1000°C 3 days	1000	87.0
$Zr_5Sb_3Fe_{0.50}$	sintered, 1000°C 3 days	1000	182
$Zr_5Sb_3Fe_{0.75}$	sintered, 1000°C 3 days	1000	374
$Zr_5Sb_3Fe_{1.0}$	sintered, 1000°C 3 days	1000	402
$Zr_5Sb_{3.16}Fe$	as-cast	200	197
$Zr_5Sb_{3.06}Fe$	as-cast	1000	510
$Zr_5Sb_{2.89}Fe$[b]	arc-melted annealed 1100°C, 1 day	20000	646
$Zr_5Sb_{2.89}Fe$[b]	arc-melted annealed 1100°C 1 day	50000	700

[a]Temperature = 8 K.
[b]Same sample measured at 20000 and 50000 Oe.

days. The diffraction lines were fairly broad and extra weak lines were observed that indicated incomplete reactions. These preparations should be repeated at a higher temperature. Nevertheless, it is interesting to note that the magnetization for $Zr_5Sb_3Fe_{0.25}$ is almost one-fourth that of $Zr_5Sb_3Fe_{1.0}$, and $Zr_5Sb_3Fe_{0.5}$ is almost half. On the other hand, the magnetization of $Zr_5Sb_3Fe_{0.75}$ is almost equal to that of $Zr_5Sb_3Fe_{1.0}$. Whether these observations are due to intrinsic properties of the compounds or the result of incomplete reaction must be further explored.

There was one other sample measured at 1000 gauss. An as-cast $Zr_5Sb_{3.06}Fe$ composition had a magnetization of 510 gauss. This is in fairly good agreement with the sintered powder sample. All other arc-melted products were measured at different fields so that no quantitative comparisons can be made. The effect of varying iron or antimony content is as yet uncertain. The general features of the magnetization vs temperature curve for all these samples were reproduced.

The data in Figures 22 and 23 confirm that Zr_5Sb_3Fe is magnetically ordered below 550 K. The magnetization as a function of applied field was also investigated and from the hysteresis loop (Figure 24) the saturation magnetization was determined as 700 G at 80 K. The field required to quench the residual magnetization (coercive force) was very small (~50 Oe), and as such Zr_5Sb_3Fe is not suitable as a permanent magnet material. The coercive force is influenced to a great extent by the grain size, but it is unlikely that improved material processing will increase the coercivity to the level required for useful permanent magnets. The compound $SmCo_5$ has a coercivity of 30 – 40 KOe.[82]

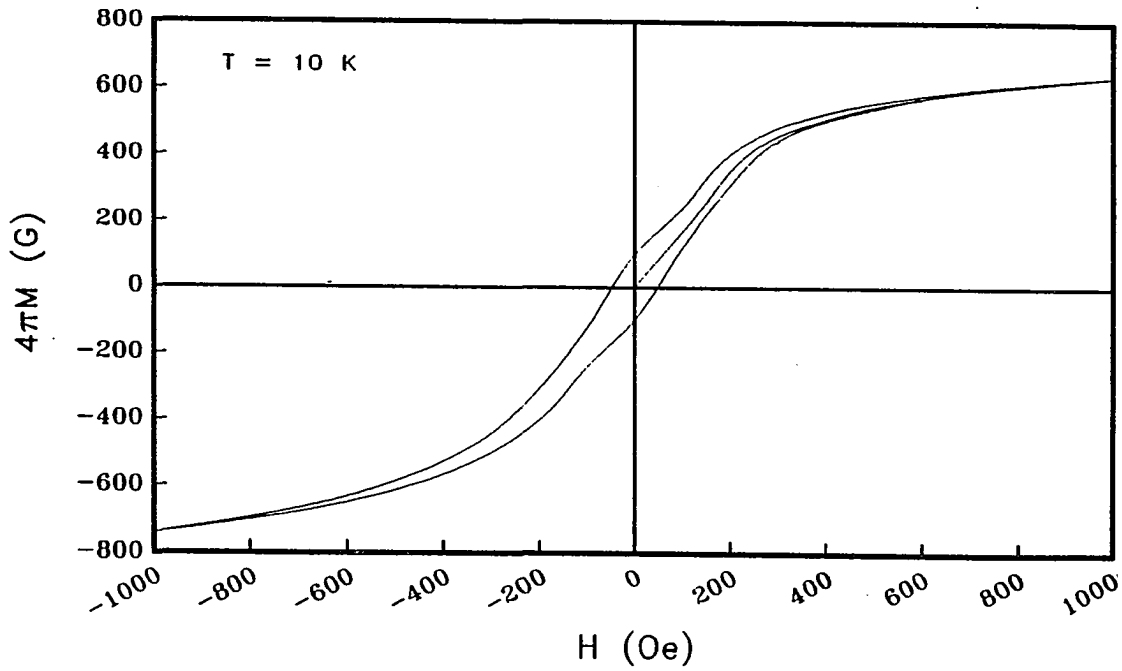

Figure 24. Magnetic hysteresis of Zr_5Sb_3Fe. Note the small reverse magnetic field needed to quench the magnetization ($4\pi M = 0$)

The marked contrast between Zr_5Sb_3Fe and Zr_5Sb_3Z, (Z = Ni, Co), is of theoretical interest. Iron is very dilute in Zr_5Sb_3Fe and the one-dimensional chains of Fe are separated laterally by 8.5 Å. Magnetic ordering would be expected only at low temperature if at all for this compound. The high Curie temperature is remarkable. The magnetic structure and coupling mechanism are of interest, and a neutron powder diffraction experiment is being undertaken elsewhere at the present time, in order to resolve these questions.

Other Zr_5Sb_3Z Compounds

Zr_5Sb_3Ru

Stoichiometric amounts of zirconium, antimony, and ruthenium powders were ground together and sealed in a Ta tube. The container was in turn sealed in a fused silica jacket, and heated in an evacuated furnace at 1350°C for 2 days. A single phase Zr_5Sb_3Z-type product was obtained.

The sharp diffraction lines and quantitative yield led to an identification of the product as Zr_5Sb_3Ru. The lattice parameters are a = 8.634(1), c = 5.855(2), and the a-axis repeat distance is outside the range of the binary phases, Zr_5Sb_{3+x} (see Table 19). No arc-melting experiments were performed, so it is not known whether Zr_5Sb_3Ru exhibits variable lattice parameters as other transition metal interstitial compounds were found to do. Single crystals of the ruthenium compound would be of interest for comparison with Zr_5Sb_3Fe, and may be obtained by arc-melting.

Zr_5Sb_3Ag

In an attempt to synthesize Zr_5Sb_3Ag, zirconium was arc-melted with a quantity of silver and antimony. Because of the low boiling point of silver (2200°C) a 50% excess was used, along with a 20% excess of antimony. Silver was observed to volatilize and emit a green color during arc-melting. The weight of the product at the end of the reaction was 4% greater than calculated for Zr_5Sb_3Ag.

The diffraction lines of the powder pattern were slightly broader than normally observed in most other Zr_5Sb_3Z systems, but a 100% yield of an interstitial compound was indicated. This was encouraging as a preliminary reaction, but a more controlled experiment was needed.

Stoichiometric amounts of zirconium, antimony, and silver powder were ground together, and with a small amount (10 mg) of SbI_3 sealed in a Ta tube. The metal container was protected from oxidation by a fused silica jacket, and heated at 1150°C for 19 days. Diffraction lines of this product were much sharper than the arc-melted sample, and also indicated a single phase Zr_5Sb_3Z-type product. No X-ray size crystals were found. The lattice parameters for this product are assigned to the compound Zr_5Sb_3Ag and listed in Table 19. These lattice parameters are among the largest of any Zr_5Sb_3Z phase, which is not surprising in view of the large Zr-Ag distances of 3.1 Å calculated from the sum of Slater radii.[83]

The preparation of Zr_5Sb_3Ag was repeated, but the transporting agent was omitted. The powders were simply sintered at 1350°C for three days.

Lattice constants for the product obtained by this method were identical to those measured for the vapor transport product.

Zr_5Sb_3 $(Fe_{2/3}In_{1/3})$

Syntheses of Zr_5Sb_3Fe by arc-melting always resulted in one unidentified line in the powder pattern. Attempts to obviate this problem by sintering of powders did not give satisfactory results. A flux reaction such as was used to make the excellent Zr_5Sb_3Zn crystals was, therefore, considered, but because of the likely possibility of a mixed iron-zinc interstitial occupancy, zinc was not used as a solvent. Indium was chosen instead for a number of reasons.

Attempts to make Zr_5Sb_3In by arc-melting and annealing had resulted in unreacted elemental indium in the product. It was, therefore, reasoned that Zr_5Sb_3 and In can coexist at equilibrium, and indium would not compete with iron for the interstitial site. Further impetus was provided by the lack of any Fe-In binary compounds.[84,85] Lastly, indium allows the use of molybdenum as a container material because no Mo-In binary compounds are known, and molybdenum is not significantly soluble in it.[86]

The iron ternary compound, Zr_5Sb_3Fe, was first obtained by arc-melting stoichiometric amounts of zirconium and iron with a slight excess of antimony. The final composition estimated from the weight loss was $Zr_5Sb_{3.05}Fe$. The solidified ingot was then placed in a Mo boat with a large excess of indium (Zr_5Sb_3Fe:In = 1:58). The boat and its contents were sealed in an evacuated fused silica jacket. Evaporation of the solvent, as with zinc, cannot be used to induce supersaturation since

indium is much less volatile. A gradient transport method was employed to induce crystal growth.

The ingot of Zr_5Sb_3Fe was placed at one end of the molybdenum boat where the temperature was maintained at 1100°C. The opposite end of the horizontal container was held at 1000°C. This temperature gradient was maintained for three days, then the reaction was quenched. Approximately one-third of the arc-melted button still remained at the hot end. The molybdenum was brittle, but the solidified indium was easily removed from it indicating that the molten metal had not wet the molybdenum.

The two halves of the indium were separated and the end that had been kept at 1000°C was placed in a hydrochloric acid solution. The indium was allowed to dissolve overnight, the solution filtered, and the reaction product washed with distilled water. Hexagonal prismatic crystals (~0.2 x 0.2 x 1.5 mm) were obtained. These crystals were not magnetic at room temperature. A powder pattern confirmed that they were a Zr_5Sb_3 Z-type compound, but the lattice parameters, a = 8.642(1) and c = 5.872(1), were significantly larger than previously observed for any Zr_5Sb_3Fe preparation.

A crystal was selected for a structural investigation, and experimental details are listed in Table 17. Systematic extinctions in the data were consistent with the space group $P6_3/mcm$. Initial refinement was based on approximate positional parameters of Mn_5Si_3, but an iron atom was included at the origin. Refinement proceeded smoothly, but in the later stages the multiplier of the iron atom indicated an occupancy greater than unity. The assumption was made that the extra electron

density was due to substitution of some iron by indium, despite the hope that this would not happen.

It was decided to refine the amount of the two elements in the structure. The initial proportion of iron and indium in the interstitial site was estimated from the height of the electron density peak. The assumption was also made that the interstitial site was fully occupied and that iron and indium multipliers should sum to unit occupancy. A patch program was written to allow the multipliers to be varied with this constraint. The iron atom multiplier was chosen as the free variable, the indium multiplier being adjusted automatically to comply with the constraint. The thermal parameters of the two atoms were also constrained, and in this case they were set to be equal.

The refinement of the multipliers began with the thermal parameters fixed at an isotropic B = 1.0. All other free parameters were allowed to vary. The thermal parameters of indium was then refined isotropically, and the iron multiplier also varied with the constraints discussed above. Finally, the anisotropic thermal parameters were varied. The final residuals are R = 0.015 and R_w = 0.016. The resulting refined parameters and calculated interatomic distances are listed in Table 27.

With reference to Table 27 it can be seen that the zirconium and antimony positions are fully occupied and constitute a $Zr_{5\cdot01(1)}Sb_{3\cdot01(1)}$ stoichiometry, but despite expectations to the contrary some of the iron has been replaced by indium. Apparently, previous attempts to produce Zr_5Sb_3In had produced $Zr_5Sb_3In_x$ ($x < 1$), and not Zr_5Sb_{3+x} as was assumed. The possibility of superstructure

Table 27. Parameters and interatomic distances for $Zr_5Sb_3(Fe_{2/3}In_{1/3})$[a]

Atom	Site[b]	Occupancy	x	B_{11}	B_{22}	B_{33}
Sb	6(g)	1.000(4)	0.61208(6)	1.02(2)	0.68(2)	0.86(2)
Zr(1)	4(d)	1	1/3	0.67(3)	B_{11}	0.58(4)
Zr(2)	6(g)	0.004(4)	0.2696(9)	1.07(3)	0.76(3)	1.81(4)
Fe	2(b)	0.661(8)[c]	0	0.58(8)[d]	B_{11}	0.6(1)
In	2(b)	0.339[c]	0	0.58(8)	B_{11}	0.6(1)

Interatomic Distances[e] (Å)

Sb - 1Zr(2)	2.960(1)	Zr(2) - 2Fe,In	2.754(1)
Sb - 2Zr(2)	2.976(1)	Zr(2) - 1Sb	2.960(1)
Sb - 4Zr(1)	3.052(1)	Zr(2) - 2Sb	2.976(1)
Sb - 2Zr(2)	3.109(1)	Zr(2) - 2Sb	
Sb - 2Sb	3.518(1)	Zr(2) - 4Zr(1)	3.513(1)
Sb - Fe,In	3.660(1)	Zr(2) - 4Zr(2)	3.748(1)
Zr(1) - 2Zr(1)	2.936(1)	Fe - 6Zr(2)	2.754(1)
Zr(1) - 6Sb	3.052(1)	Fe - 2Fe,In	2.936(1)
Zr(1) - 6Zr(2)	3.513(1)	Fe - 6Sb	3.660(1)

[a]Refined formula = $Zr_{5.01(1)}Sb_{3.00}Fe_{0.661(8)}In_{0.339}$.
[b]Space group $P6_3/mcm$.
[c]Fe and In occupancy constrained to add up to one.
[d]Thermal parameters for iron and indium constrained to be equal.
[e]Distances less than 4.0 Å.

formation was considered. The crystal used for data collection was examined by oscillation and Weissenberg photographs but no evidence of superstructure was observed.

Other Attempted Zr_5Sb_3Z Syntheses

Several other elements were investigated for the possibility of forming Zr_5Sb_3Z interstitial compounds. The results of these synthetic attempts were either inconclusive or negative and are outlined in Table 28. The reactions are more fully discussed below.

Alkali and alkaline earth metal interstitial compounds

Reactions designed to produce Zr_5Sb_3Na and Zr_5Sb_3K were loaded in a tantalum tube. These involved a stoichiometric mixture of Zr_5Sb_3 and the appropriate alkali metal. The binary compound was obtained by arc-melting, and the as-cast powder pattern showed it to be a mixture of the Y_5Bi_3 and Mn_5Si_3 types. The tantalum container was sealed in an evacuated fused silica jacket, and heated at 1150°C for one week. The powder patterns of both products were identical to that of the as-cast binary Zr_5Sb_3. No reaction apparently took place, and the small amount of the alkali metal that must have coated the powder was not detected by powder diffraction.

A second reaction designed to produce Zr_5Sb_3K was carried out. The failure of the first reaction could have been attributable to kinetic barriers preventing the conversion of the Y_5Bi_3 into the Mn_5Si_3 structure, and limited, mobility of antimony in the Zr_5Sb_{3+x} portion of the starting material. (A discussion of these kinetic barriers is presented

Table 28. Failed or uncertain Zr_5Sb_3Z reactions

Z	Product composition (atomic)	Synthesis method[a]	Synthesis conditions temp(°C)	Synthesis conditions time (d)	Products
Na	Na + Zr_5Sb_3	S	1150	7	Zr_5Sb_3
K	K + Zr_5Sb_3	S	1150	7	Zr_5Sb_3
K	K + Zr_5Sb_3	S	1000	10	ZrO_2, Zr_5Sb_{3+x}, $Zr_5Sb_3O_x$?
Ca	Ca + Zr_5Sb_3	S	1000	10	Zr_5Sb_3
Ca	Ca + 5Zr + 3Sb	S	1350	3	Zr_5Sb_{3+x}, $Zr_5Sb_3O_x$?
Mg	Mg + Zr_5Sb_3	S	1000	10	Zr_5Sb_3
Mg	Mg + 5Zr + 3Sb	S	1350	3	ZrO_2, Zr_5Sb_{3+x}, $Zr_5Sb_3O_x$?
Mn	Mn + 5Zr + 3Sb	S	1000	5	unknown cubic phase
Cr	Cr + 5Zr + 3Sb	AM	as-cast		unknown cubic phase
Cr	Cr + Zr_5Sb_3	S	1100	2	Cr, Zr_5Sb_3
Cd	Cd + 5Zr + 3Sb	VT	1150	19	Cd, Zr_5Sb_3

[a]Abbreviations: S - sintered powder; AM - arc-melted; VT - vapor transport.

in part I of this work.) In order to avoid this problem, $Zr_5Sb_{3.0}$ was prepared from powders and the material was repeatedly ground and fired until only a Mn_5Si_3-type diffraction pattern was observed (a = 8.4038(6), c = 5.7669(8) Å). This powder was loaded with a stoichiometric amount of potassium metal in a Ta tube, sealed in fused silica, and allowed to react at 1000°C for ten days. Second thoughts on the possibility that these conditions might not have yielded equilibrium products led to further reaction at 1300°C for three days. The metal container was very bulged upon removal from the furnace, indicating an appreciable potassium pressure which has a boiling point of 760°C, in the container at 1300°C.

A small amount of ZrO_2 (~10%) was detected in the powder pattern. The remaining diffraction lines were very sharp, and could be indexed on the basis of two Zr_5Sb_3 Z-type unit cells. The two were present in about equal amounts, and the lattice parameters were refined as a = 8.543(1), c = 5.860(1) Å, and a = 8.346(1), c = 5.737(1) Å. The large cell is almost certainly that of Zr_5Sb_{3+x}. Application of the lattice parameters versus composition results discussed in part I, yields a composition of $Zr_5Sb_{3.36}$ on the basis of the a-axis parameter, and $Zr_5Sb_{3.35}$ from the c-axis length. The Zr_5Sb_{3+x} phase is probably due to loss of zirconium to form ZrO_2 bringing about an increased antimony to zirconium ratio. The smaller unit cell is not as easily accounted for. The lattice parameters are significantly larger than those of Zr_5Sb_3O (see Table 19), but arc-melted preparations have shown that $Zr_5Sb_3O_x$ ($x < 1$) compositions have lattice constants comparable to the ones observed here.

It is entirely possible that oxygen was introduced to the reaction via the potassium. When the metal was cut in the dry box, a purple tarnish developed on the surface within 10 seconds. The large surface area with respect to the bulk total of the potassium (7 mg) could lead to significant amounts of oxygen contamination. On the other hand, the formulation of the compound as Zr_5Sb_3K cannot be ruled out. Very short zirconium-potassium distances have been observed in a potassium-centered zirconium cluster.[87] Further work is needed to clarify the situation.

The same sintered $Zr_5Sb_{3.0}$ starting material was used with a stoichiometric amount of calcium in an attempt to synthesize Zr_5Sb_3Ca. The reaction was loaded into a tantalum tube, sealed in a fused silica jacket, and maintained at 1000°C for ten days. The powder pattern was identical to that of the starting material. A second reaction was carried out in a sealed Ta tube with a stoichiometric mixture of the elements. The container was placed in an evacuated (10^{-6} torr) recrystallized alumina muffle tube and heated at 1350°C for three days.

The powder pattern from this reaction did not exhibit diffraction lines of any binary oxide, but as with Zr_5Sb_3K, there were once again two Zr_5Sb_3Z-type phases in equal amounts. The larger cell was almost identical in size to the $Zr_5Sb_{3.35}$ observed in the potassium reaction, but the smaller cell was even closer in size to that of Zr_5Sb_3O. The results are once again ambiguous, and Zr_5Sb_3Ca can neither be confirmed nor ruled out.

Magnesium reactions were run at the same time as the calcium ones, and with identical conditions. The attempt at 1000°C apparently resulted

in no reaction. The sample produced at 1350°C yielded a powder pattern that was more similar to that obtained with potassium at 1300°C, than to the calcium product. The two Zr_5Sb_3Z-type cells were of the same size as the two observed in the potassium reaction, and 10% ZrO_2 is also observed. This is surprising since magnesium oxide, unlike potassium oxide, is very stable at high temperature.

The alkali and alkaline-earth metal reactions should be repeated with rigorous attempts to exclude oxygen. Since this work was performed, a dry box with an oxygen scavenged atmosphere has become available. Potassium and sodium can be cut in this dry box with much less oxygen contamination. Freshly distilled calcium should be obtained. Magnesium may also be distilled in a tantalum tube liner at much lower temperature.

Transition metal interstitial compounds

Repeated attempts to synthesize Zr_5Sb_3Mn by arc-melting were inconclusive. Manganese has a substantial vapor pressure at elevated temperatures ($T > 1000°C$), and vaporization was a problem. The volatilized manganese condensed as a fine powder on the copper hearth, and was pyrophoric. To compensate for loss through vaporization, a three-fold excess of manganese was used in one reaction. Along with many other unidentified lines, a Zr_5Sb_3Z-type pattern was observed, but the lattice parameters were consistent with a Zr_5Sb_{3+x} phase.

A sintering reaction was carried out by using a stoichiometric mixture of zirconium, antimony, and manganese powders ground together thoroughly and pressed into a pellet. This pellet was placed in a tantalum crucible, and sealed in a silica jacket under an atmosphere of

argon. The sample was heated at 1000°C for five days. Only a 10% yield of a Zr_5Sb_3 Z-type phase, giving just the three strongest lines at very weak intensity, was observed in the powder pattern. The rest of the diffraction lines could be indexed[16] on the basis of a primitive cubic unit cell a = 11.0975(6) A. This phase was not identified but must have a formula near the Zr_5Sb_3Mn overall composition.

The formation of a cubic phase by sintering powders implies that a hexagonal Zr_5Sb_3Mn-type phase is not stable. Since this cubic phase is not seen in arc-melted products it is apparently unstable at high temperature (~T > 1400°C). One cannot, therefore, rule out a stable hexagonal Zr_5Sb_3Mn phase in the temperature region 1000 to 1400°C. A sintered powder reaction at 1300°C should resolve this question.

Results of the attempted preparation of Zr_5Sb_3Cr by arc-melting were very similar to manganese preparations. Extensive volatilization of chromium and antimony made final composition uncertain. The powder pattern contained only a few lines of Zr_5Sb_3 Z-type phase (10% yield). Most of the diffraction lines matched the pattern of the cubic cell found above for the sintered preparation of Zr_5Sb_3Mn.

A pellet made by pressing a mixture of Zr_5Sb_3 and Cr powder was heated at 1100°C for two days. This was an attempt to obtain the cubic-phase under more controlled conditions, and to rule out Zr_5Sb_3Cr as a stable "filled" Mn_5Si_3-type compound. No reaction took place. The $Zr_5Sb_{3.0}$ starting material had been obtained from an arc-melted preparation, and such starting material has been observed in other systems to be much less reactive than elemental powders. Kinetic barriers evidently

prevented a reaction from taking place. Nevertheless, it is more certain for chromium than manganese, that a hexagonal Zr_5Sb_3Z compound cannot be made. Only the cubic phase was found for chromium, and it would be interesting to see if vanadium, titanium, or scandium also produce this cubic compound.

One other Zr_5Sb_3Z phase can be described with confidence as being unstable. An attempt was made to synthesize Zr_5Sb_3Cd by sealing an appropriate mixture of zirconium, antimony and cadmium in a Ta tube and heating at 1150°C for 19 days. A small quantity of SbI_3 was also included to act as a transporting agent. In order to remove the iodide upon completion of the reaction, the tantalum container was cut open and heated under a vacuum. A metallic film formed on the glass tube outside the furnace at 300°C that was assumed to be cadmium. The powder pattern of the remaining material indicated it was the binary Zr_5Sb_3 phase.

Other M_5X_3Z Compounds

No binary Mn_5Si_3-type phase is known in the zirconium-arsenic system, the compounds closest in composition are Zr_3As and Zr_8As_5.[87,88] In order to confirm this, an attempt was made to synthesize Zr_5As_3. Zirconium and arsenic powder in a molar ratio of 5:3 were ground together, and sealed in an evacuated silica tube. The powders were heated at 750°C for three days to prereact the sample; no evidence of reaction with the silica container was observed. The product was reground, pressed into a pellet, and arc-melted. The prereaction was effective since only a very small amount of volatilization (~4% weight

loss) occurred. The product was composed mainly (90%) of Zr_8As_5 with a small amount of Zr_3As in accordance with published reports.[87,88]

A portion of the same prereacted zirconium and arsenic powder was ground with a stoichiometric amount of silicon in a reaction designed to produce Zr_5As_3Si. The powder was pressed into a pellet and arc-melted. Final composition of the sample was estimated as $Zr_5As_{2.8}Si$, assuming only arsenic loss. The product was annealed for one day at 1050°C, and the powder pattern indicated a 20% yield of ZrAs and $ZrAs_2$. The remaining diffraction lines could be indexed with a hexagonal cell a = 7.9315(7), c = 5.5740(8) and the intensity distribution matched that calculated for the interstitial Mn_5Si_3-type compound, Zr_5As_3Si.

The presence of ZrAs and $ZrAs_2$, along with Zr_5As_3Si, in the product indicates that the reaction was not at equilibrium. Arc-melted preparations for Zr_5Sb_3Z compounds have shown that lattice parameters, and presumably compositions obtained through use of this technique can vary over quite a range. The lattice parameters described above for Zr_5As_3Si must be regarded as only tentative, since the actual composition of the ternary phase is not certain. Despite problems endemic to arc-melting, it is used to advantage in cases such as this, where a quick preliminary investigation can produce promising results. The occurrence of a Mn_5Si_3-type phase in the zirconium-arsenic system only when silicon is present, is very encouraging, and is worthy of further investigation.

A substitution of silicon with aluminum produced similar results. A reaction designed to yield Zr_5As_3Al was carried out by sealing stoichiometric amounts of Zr_5As_3 (see above) and aluminum in a tantalum tube

with ZrI_4 as a transporting agent. This was allowed to react for eleven days at 1000°C. The powder pattern showed a 50:50 mixture of ZrAs and a Zr_5As_3Z-type cell. The diffraction lines of the presumably Zr_5As_3Al phase were broad, implying that the solid solution behavior observed for Zr_5Sb_3Al also occurs here. The lattice constants were not measured because of the broad nature of the diffraction lines, but the unit cell of this Zr_5As_3Al phase is larger than that of Zr_5As_3Si.

An attempt to produce Zr_5As_3Fe, in the same manner as the silicide phase, failed. The powder pattern contained only the diffraction lines of Zr_8As_5. The fate of the iron is unknown, but Zr_8As_5 has a very complicated diffraction pattern that could easily mask any high symmetry, small unit cell.

Extended-Hückel Calculations

The remarkable array of interstitial Zr_5Sb_3Z compounds prompted some theoretical calculations in an attempt to rationalize this unprecedented behavior. The calculations were carried out by extended-Hückel method for three representative compounds. The phases Zr_5Sb_3Fe and Zr_5Sb_3S were chosen because of the pronounced chemical differences between iron and sulfur, and because quantitative structural data were available. A calculation was also performed for Zr_5Sb_3 since the extended-Hückel method is best applied for comparative purposes, rather than in an absolute sense. See Appendix A for the orbital parameters.

The density-of-states (DOS) curve for Zr_5Sb_3 is shown in Figure 25 with the shaded areas under the curve representing the orbital contribution from the three crystallographically independent atoms to the total.

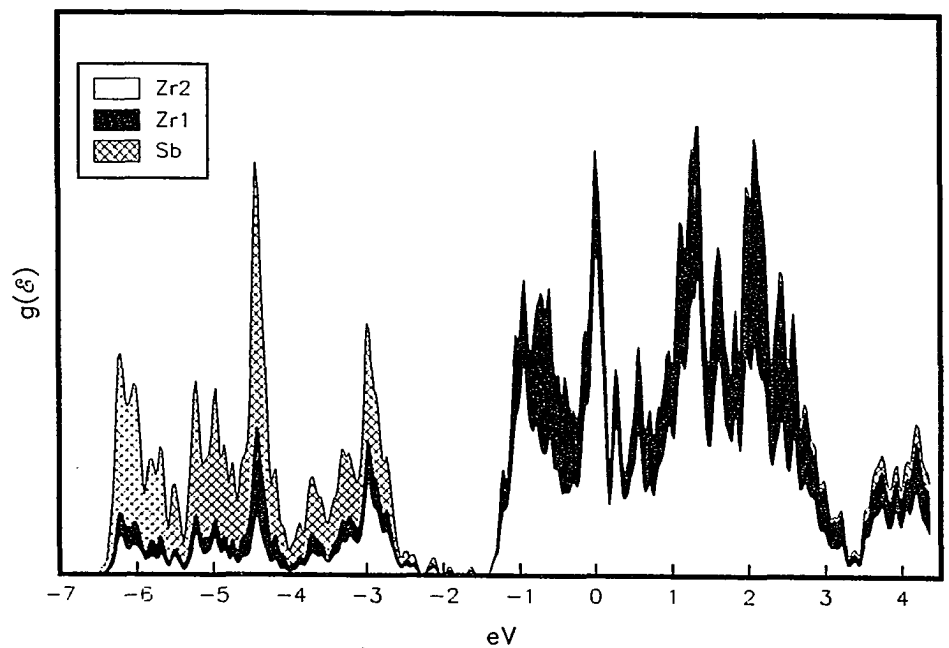

Figure 25. DOS curve for Zr_5Sb_3. The shaded areas under the curve represent the atomic orbital projections as indicated in the legend. The Fermi energy has been set at E = 0.

The curve was calculated using 24 evenly spaced, symmetry weighted k points in the three-dimensional Brillioun zone. The Fermi energy has been set equal to zero. A broad band can be seen from -6.5 to -2.5 eV. This band is mainly antimony in character but a significant amount of Zr(1) (linear chain) and Zr(2) orbitals are also admixed. The conduction band, which starts at -1.5 eV, is almost entirely zirconium in character. The width of these bands indicates a large degree of covalent overlap, since they would be much narrower and the valence band would have much less mixing of the atomic orbitals in any ionic description.

More insight into the bonding in Zr_5Sb_3 can be gained with reference to Figure 26, where the DOS curve has been overlap-weighted for various pairs of atoms, such that a bonding interaction is positive and an antibonding one is negative. These crystal orbital overlap population (COOP) curves give a good representation of the bonding or antibonding effects for various atom pair interactions.[89] Thus, the Zr(1)-Sb and Zr(2)-Sb interactions can be seen to be strongly bonding, these interactions occurring in the valence band. There is no antimony orbital contribution to the DOS near the Fermi energy.

The interzirconium bonding is mainly limited to the conduction band. The transition metal orbitals in the valence band are apparently committed to heteratomic bonding. The Zr(1)-Zr(1), linear chain, interactions are strongly bonding as would have been surmised from the short interatomic spacing. The other Zr-Zr interactions are much weaker, but still quite significantly bonding, and to a greater extent than implied by the interatomic distances. The Zr(1)-Zr(2) distance is 3.5 Å,

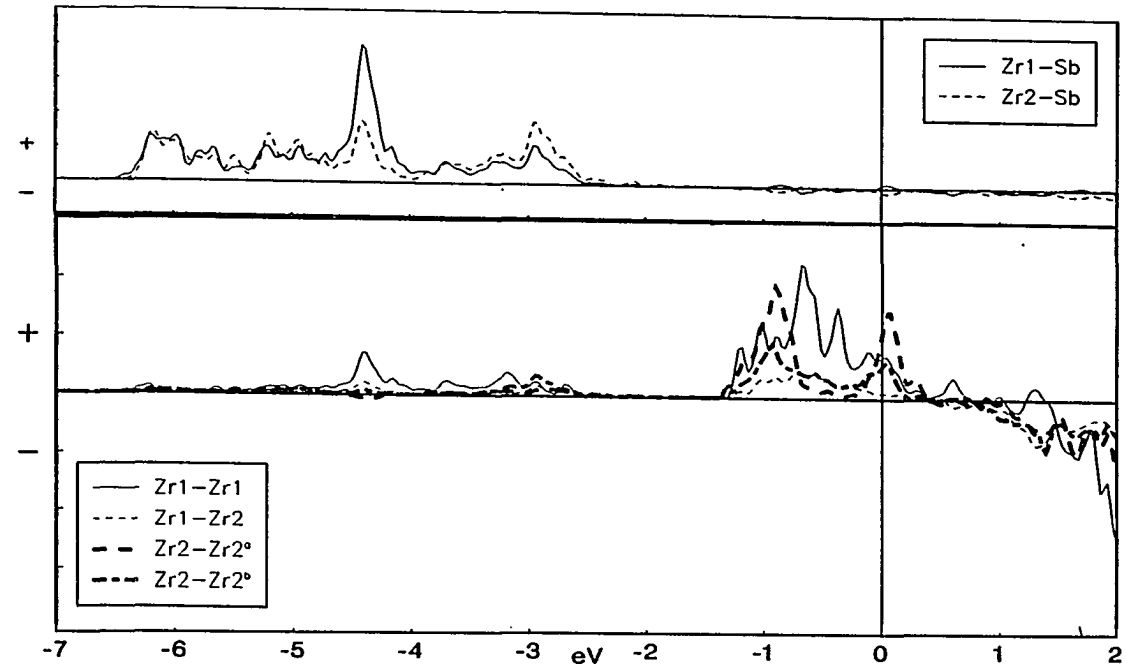

Figure 26. COOP curves for Zr_5Sb_3. The positive values on the curves represent bonding interactions while negative values denote an antibonding character for the atom pairs as indicated. The coplanar Zr(2) - Zr(2) overlap is denoted by the superscript a, and the interplanar Zr(2) - Zr(2) interactions by superscript b in the legend.

coplanar Zr(2)-Zr(2), 3.6 Å, and interplanar Zr(2)-Zr(2) 3.6Å. These can be compared with the Zr(1)-Zr(1) distance of 2.9 Å.

The average overlap population is obtained by intergrating the COOP curves up to E_F. The average overlap populations for all significant pairwise interactions are listed in Table 29. It should be noted that the numbers are only qualitative indicators when comparing different types of interactions, such as Zr-Sb and Zr-Zr. A better comparison of the values is made for the same kind of pairwise overlap, viz., Zr(1)-Sb and Zr(2)-Sb.

These results can be compared with those for Zr_5Sb_3Fe. The DOS curve of the iron compound is drawn in Figure 27. Atomic projections are shown in the same manner as the binary compound. The general features of the two DOS curves are similar. There are still two wide bands for the interstitial compound, but a new narrow band is located in the band gap between them. The valence band seems unperturbed by the interstitial iron. It consists of antimony, zirconium(1), and zirconium(2) atomic orbital contributions, with a negligible contribution from the iron. The conduction band has been more affected by the insertion of the iron atom. The density-of-states below the Fermi energy in the conduction band is now much higher, as most of the iron atomic contribution is located in this energy region. The narrow feature just below the conduction band is almost entirely iron and zirconium(2) in character. The primary coordination sphere of iron, if the reader will recall, is composed of six Zr(2) atoms. The iron atomic orbitals in this narrow feature, are

Table 29. Average overlap population

Overlap Type	Zr_5Sb_3	Zr_5Sb_3Fe	Zr_5Sb_3S
Zr(1)-6Sb	0.28	0.29	0.30
Zr(2)-5Sb	0.25	0.25	0.23
Zr(1)-2Zr(1)	0.35	0.33	0.31
Zr(1)-6Zr(2)	0.10	0.09	0.11
Zr(2)-2Zr(2)[a]	0.17	0.06	0.02
Zr(2)-4Z(2)[b]	0.15	0.08	0.04
Z-6Zr(2)		0.28	0.31
Z- Z		0.05	-0.07

predominately (90%) s in character, while the Fe d-orbitals can be found in the conduction band.

The COOP curves for Zr_5Sb_3Fe are drawn in Figure 28. Only the Zr(1) - Zr(1) curve is plotted for zirconium interactions in the interest of clarity. The Zr-Sb overlap curves are not noticeably different to those of Zr_5Sb_3, a fact that is reflected in the average overlap population (see Table 29). The Zr(1)-Zr(1) and Zr(1)-Zr(2) overlaps also have not

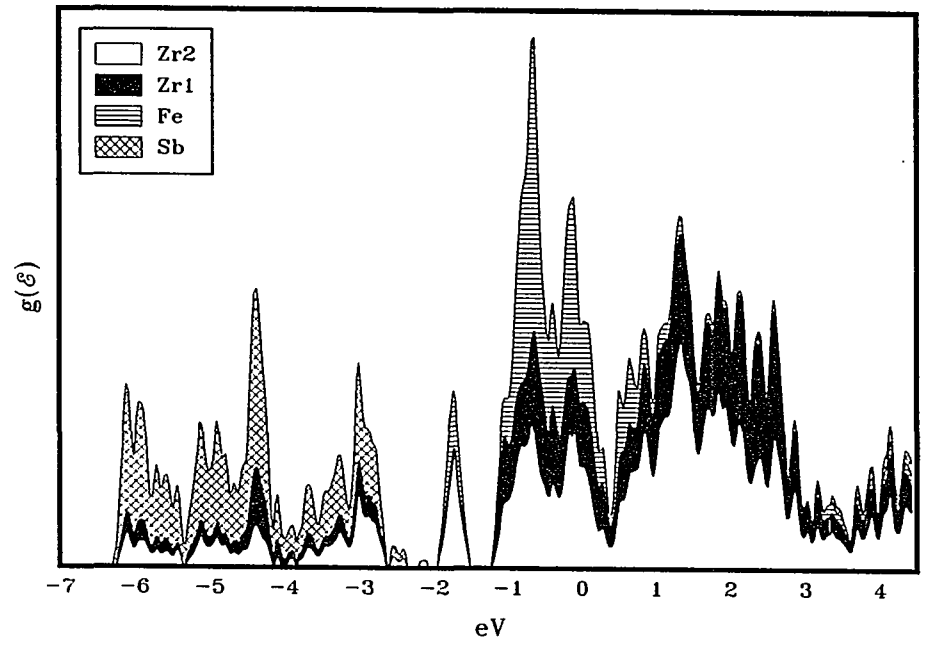

Figure 27. DOS curve for Zr_5Sb_3Fe. The shaded areas under the curve represent the atomic orbital projections as indicated in the legend. The Fermi energy has been set at E = 0

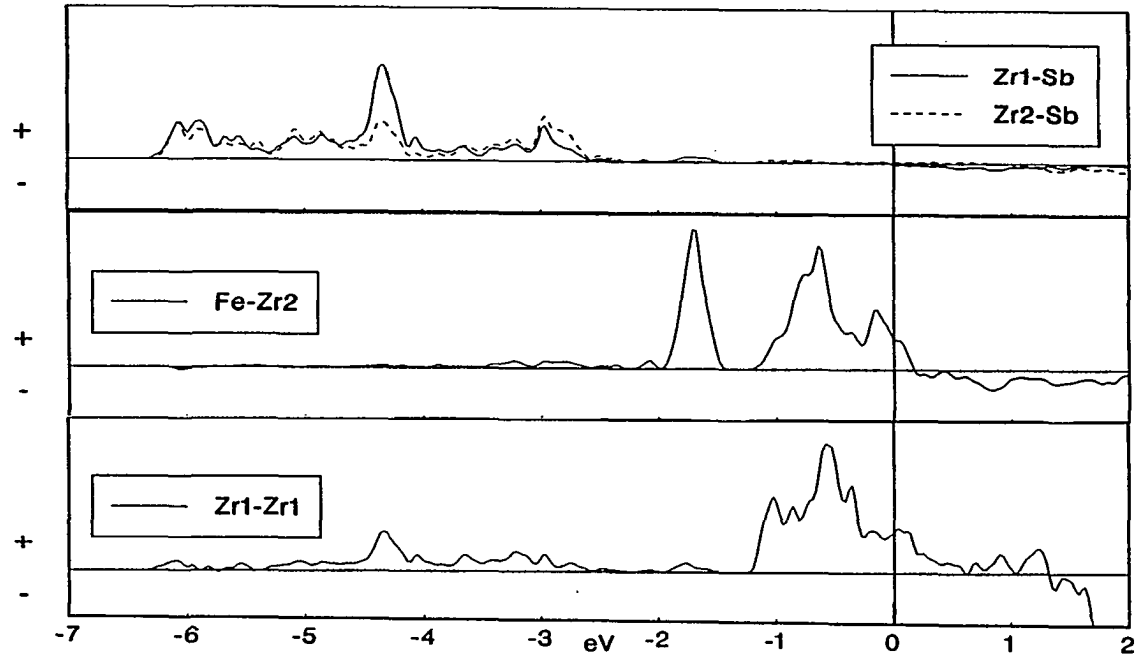

Figure 28. COOP curves for Zr_5Sb_3Fe. The positive values on the curves represent bonding interactions while negative values denote an antibonding character for the atom pairs as indicated. Only the Zr(1) - Zr(1) curve is drawn for zirconium overlaps in the interest of clarity

been affected by the iron interstitial (see Table 29). On the other hand, both types of Zr(2)-Zr(2) overlap interactions have been very much reduced, even though the zirconium-zirconium distances have only increased 0.1-0.2 Å.

The Zr(2)-Fe interactions, which were, of course, absent in the binary compound, can be seen to be strongly bonding. The narrow band in the DOS curve at -2 eV is reproduced in the COOP curve, and the increased height relative to that of the conduction band is attributable to the better overlap of the iron s-orbital with Zr(2). The average overlap population for all significant interactions are also listed in Table 29.

The results for Zr_5Sb_3S can be compared in a similar manner. The DOS and COOP curves are drawn in Figures 29 and 30, respectively. With a sulfur interstitial, it is now the conduction band that remains virtually unchanged. The atomic projections show it to be composed almost entirely of zirconium orbital contributions. The narrow band seen for the iron compound at -2 eV is not reproduced, and a substantial band gap is once again present. The interstitial orbitals are located much lower in energy, reflecting the increased electronegative character of sulfur with respect to iron.

Despite the similar energies of sulfur and antimony orbitals in the valence band, Figure 30 shows that the zirconium-antimony bonding remains unchanged compared with that in Zr_5Sb_3 or Zr_5Sb_3Fe. Only the Zr(1)-Zr(1) curve is plotted in the interest of clarity, but Zr(1)-Zr(2) overlap remains unperturbed, and the Zr(2)-Zr(2) curves are very flat, like those in the iron compound. The Zr(2)-S curve indicates a strong bonding

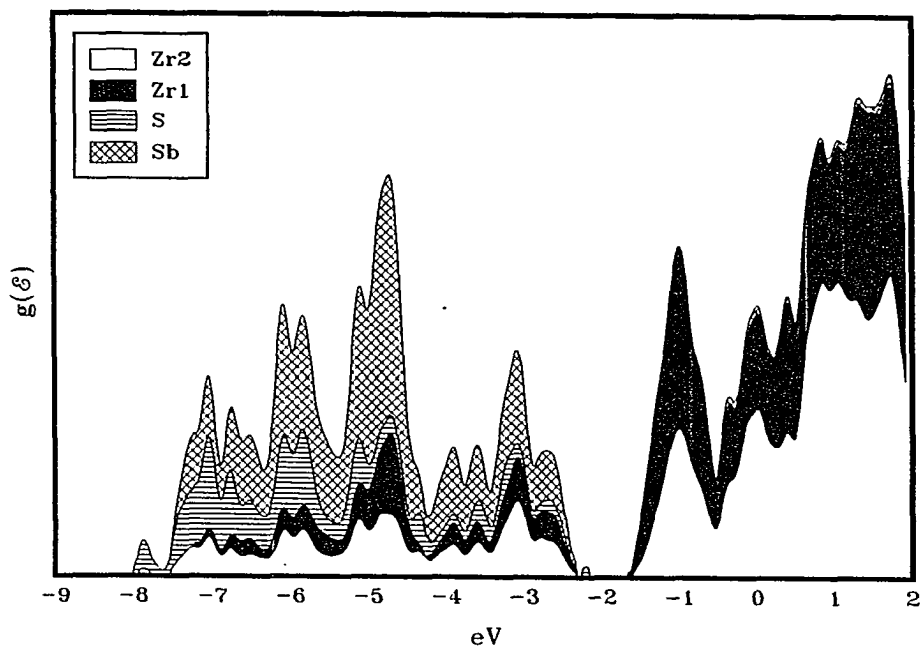

Figure 29. DOS curve for Zr_5Sb_3S. The shaded areas under the curve represent the atomic orbital projections as indicated in the legend. The Fermi energy has been set at E = 0

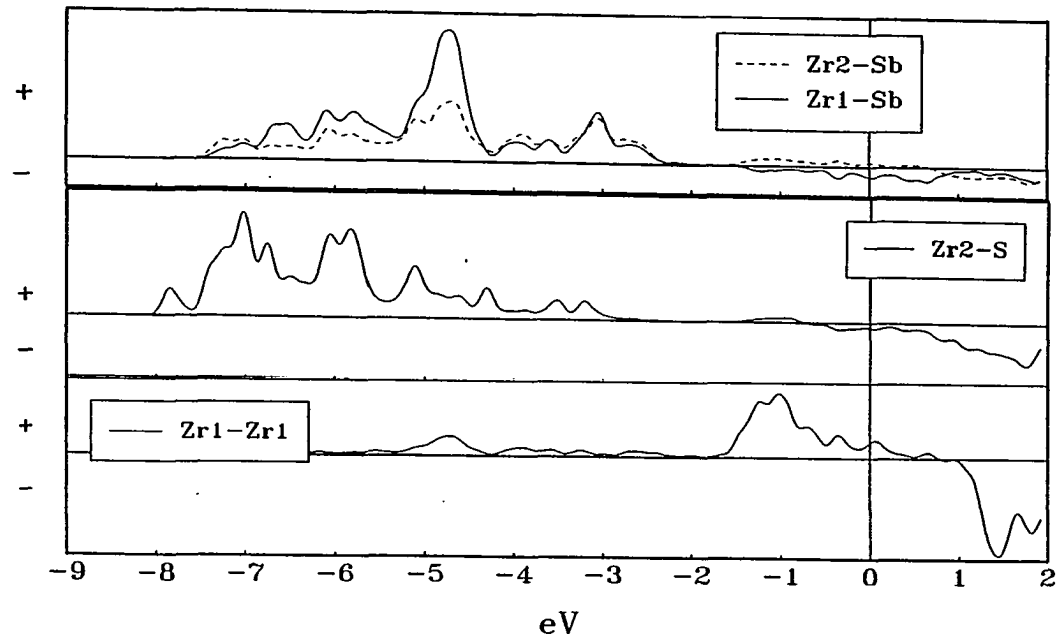

Figure 30. COOP curves for Zr_5Sb_3S. The positive values on the curves represent bonding interactions while negative values denote an antibonding character for the atom pairs as indicated. Only the Zr(1) - Zr(1) curve is drawn for zirconium overlaps in the interest of clarity

interaction. In essence, when the iron interstitial is replaced by sulfur, the interstitial-zirconium bonding shifts to lower energy without affecting Zr-Sb bonding.

A measure of the extent of charge transfer in these compounds can be obtained by integrating under the atomic projections in the DOS, up to the Fermi level. This gives a rough indication of the amount of electrons "owned" by each element, although the method often overestimates the polarity developed. These numbers are listed in Table 30. The antimony is unchanged in all three compounds, but a large difference in the zirconium oxidation state occurs when iron is substituted by sulfur as an interstitial.

The Zr(2) orbitals interact with sulfur, which causes some zirconium orbitals to shift to lower energy, but these interactions are polar and mostly sulfur in character. Most of the Zr(2) orbitals that interact with sulfur are pushed to higher energy. As a result of this fewer Zr(2) orbitals are filled, leaving more Zr(1) sates near the Fermi energy to be occupied, and producing the calculated oxidation states. The average zirconium oxidation state is +0.23, the same as in Zr_5Sb_3 and Zr_5Sb_3Fe. The iron is calculated to be essentially neutral, and the sulfur has a slight negative charge.

Experimental evidence to corroborate the extended-Hückel results was sought by use of photoelectron spectroscopy. Ultraviolet photoelectron spectroscopy (UPS) can be employed to examine the density-of-states near the Fermi level. A sample of Zr_5Sb_3S was prepared by sintering $Zr_5Sb_{3.0}$ and sulfur at 1300°C for three days. This resulted in a

Table 30. Electron transfer as estimated by extended-Huckel

	Atom	e/atom	oxidation state
Zr_5Sb_3	Zr(1)	3.80	+0.20
	Zr(2)	3.75	+0.25
	Sb	5.38	-0.38
Zr_5Sb_3Fe	Zr(1)	3.64	+0.36
	Zr(2)	3.79	+0.21
	Sb	5.44	-0.44
	Fe	8.05	-0.05
Zr_5Sb_3S	Zr(1)	4.07	-0.07
	Zr(2)	3.46	+0.54
	Sb	5.40	-0.40
	S	6.27	-0.27

single phase product. The reaction has been previously discussed (see Synthesis section), and the lattice parameters are listed in Table 19. The sample was ground in a dry box directly attached to the spectrometer, and argon ion etched prior to collection of the spectrum in order to insure a clean surface. Plots of the experimental and calculated data are given in Figure 31.

The resolution of the UPS spectrometer was not sufficient to distinguish the band gap seen in the calculated curve, but a dip in the experimental data can be seen at the same energy. The large Fermi edge leaves no doubt as to the metallic character of the compound, and is also in agreement with the calculation. The broad valence band is reproduced in the experimental results as well. The UPS experiment cannot confirm the details of the extended-Hückel calculation, but the general features can clearly be seen.

A sample of Zr_5Sb_3Fe was also examined with UPS. It was prepared by arc-melting, and the as-cast product was used. The sample was again ground in the dry box, and argon-ion-etched prior to data collection. The experimental and calculated density-of-states for Zr_5Sb_3Fe are shown in Figure 32.

A pronounced Fermi edge is visible, confirming a metallic character. The calculated band curve contains a much higher density-of-states in the conduction compared with the valence band, and this is reflected in the experimental results. Coverage of the indium probe by the sample was not as good with Zr_5Sb_3Fe as with Zr_5Sb_3S, so indium states which are located below -5 eV, prevent the expected drop-off at -6.5 eV. Nevertheless, the

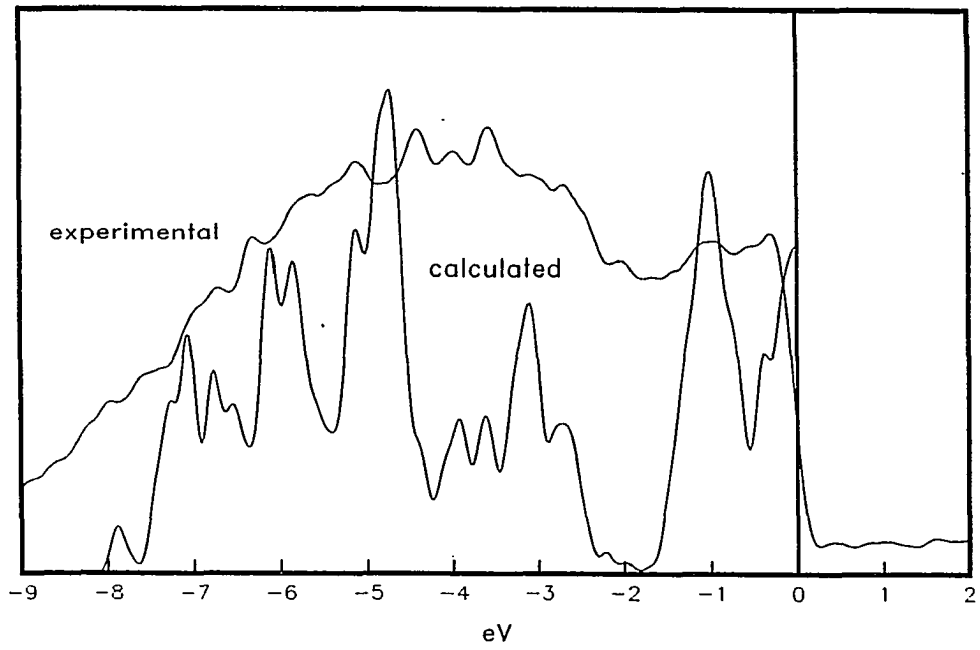

Figure 31. Comparison of experimental (UPS) and calculated (extended-Hückel) valence region of Zr_5Sb_3S.

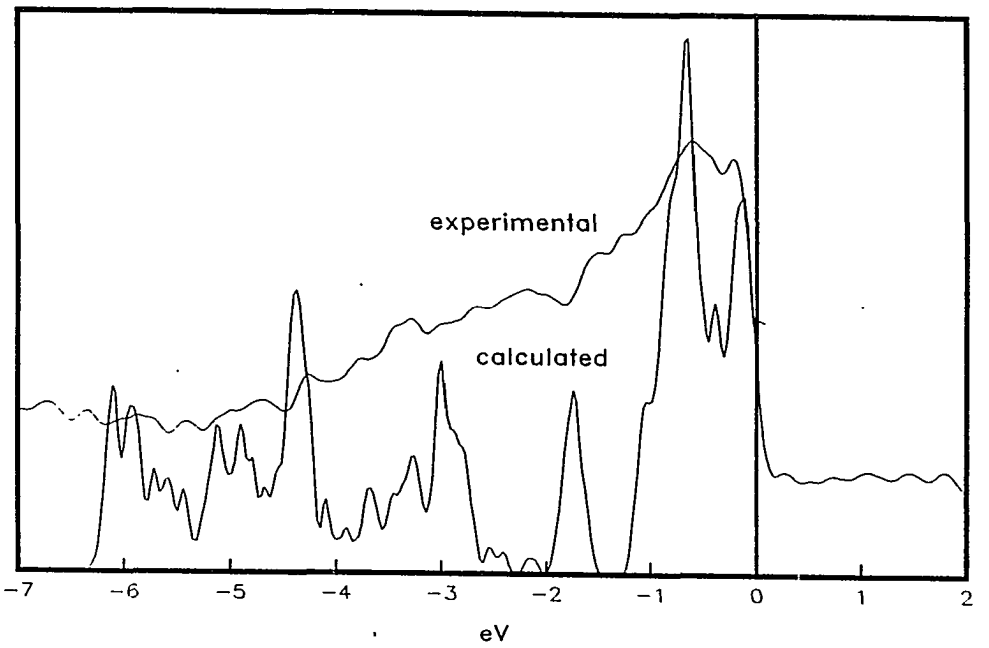

Figure 32. Comparison of experimental (UPS) and calculated (extended-Hückel) valence region of Zr_5Sb_3Fe.

increased density-of-states in the conduction band that results from insertion of an iron atom can be clearly seen.

X-ray photoelecton spectroscopy was used to ascertain the binding energy of core levels for the various elements in Zr_5Sb_3S and Zr_5Sb_3Fe. The binding energy of these levels can give a qualitative measure of oxidation state, and can be compared with the extended-Hückel results.

The binding energies listed in Table 31 were obtained from the same samples used for the UPS experiments. Adventitious carbon, 1s core level (285 eV) was used as an internal standard. Only one type of zirconium peak was observed, and this was the case for the other elements as well. The binding energies are in qualitative agreement with the oxidation states calculated by extended-Hückel. Zirconium in the ternary compounds has a binding energy for the $3d_{5/2}$ level slightly greater (small positive charge) than elemental zirconium. The antimony has a slightly smaller binding energy, in the ternary compound compared to the element (small negative charge). The same can be said of the sulfur in Zr_5Sb_3S (compare binding energy for S and Na_2S). The binding energy for the iron $2p_{3/2}$ level is almost equal to that in elemental iron as predicted by the calculations.

Table 31. XPS data for core level binding energies

core level	Binding energy (eV)						
	Zr_5Sb_3Fe	Zr_5Sb_3S	S	Na_2S[a]	Fe[b]	Zr[c]	Sb[d]
Zr $3d_{5/2}$	179.5	179.5				178.5	
Sb $3d_{5/2}$	527.8	527.6					528.1
Fe $2p_{3/2}$	707.0				706.7		
S 2p		162.5	163.8	161.6			

[a]Reference 90.
[b]Reference 91.
[c]Reference 92.
[d]Reference 93.

DISCUSSION

Comparison of Structural Data

The single crystal structural refinements of various Zr_5Sb_3Z compounds, allow the determination of the effect of various interstitial elements on the structure. The most important distances, certainly in terms of lattice energy, are the zirconium-antimony separations. These are the most numerous, and of course the backbone of the structural framework in the binary Zr_5Sb_3 compound. The other interatomic distances that are of interest, are zirconium to zirconium, and zirconium to interstitial. All these distances from the single crystal refinements are listed in Table 32.

The zirconium-antimony distances in all the Zr_5Sb_3Z compounds are ~3.0 Å. This distance is very typical of Zr-Sb spacings in the binary compounds (see Zr_5Sb_3-Y, ZrSb, $ZrSb_2$ in part I). The notable observation drawn from the list of zirconium-antimony contacts in Table 32, is the lack of a significant variation. The Zr(1)-Sb separations vary by less than 0.1 Å, even when compared with those in the binary compound. The Zr(2) - Sb contacts are even more consistent. The interstitial element seems to have very little effect on the zirconium-antimony distance.

The short interzirconium, interatomic distance (Zr(1) - Zr(1)) also does not change to any great extent (<0.05 Å). This zirconium-zirconium distance is extremely short compared with the element[13] and is comparable to the single bond distance of 2.918 Å.[94] A notable feature of the Mn_5Si_3 structure type, is this linear chain of transition metals. The distance between the zirconium atoms in the linear chain, just as the

Table 32. Interatomic distances in Zr_5Sb_3Z compounds

Compounds	Zr(1)-Sb	Zr(2)-Sb[a]	Zr(1)-Zr(1)
$Zr_5Sb_{2.6}Al_{0.4}(Al_{0.7}Sb_{0.3})$	3.016	3.001	2.923
$Zr_5Sb_{2.9}Si_{0.1}(Si_{0.9}Zn_{0.1})$	3.008	3.023	2.897
$Zr_5Sb_3S_{0.7}$	2.976	3.033	2.930
Zr_5Sb_3Fe	3.031	3.030	2.918
Zr_5Sb_3Zn	3.047	3.004	2.918
$Zr_5Sb_3(Fe_{0.66}In_{0.34})$	3.052	3.026	2.936
$Zr_5Sb_3Sb_{0.17}$	2.974	3.022	2.893

[a]Average distance.

Zr(1)-Zr(2)	Zr(2)-Zr(2)[a]	Zr(2)-Z
3.486	3.778	2.700
3.519	3.738	2.671
3.532	3.636	2.578
3.545	3.722	2.653
3.494	3.833	2.747
3.513	3.844	2.754
3.545	3.574	2.532

zirconium-antimony separations, is not changed by the various interstitial elements.

The next shortest Zr-Zr distance is between the zirconium of the linear chain, Zr(1), and the zirconium surrounding the interstitial site, Zr(2). This distance (~3.5 Å) is much larger than the Zr(1) - Zr(1) separations, and 3.5 Å is usually considered a nonbonding zirconium distance. Extended-Hückel results, on the other hand, have shown this to be a weakly bonding interaction, a greater variation is seen in the Zr(1) - Zr(2) distances than observed for Zr(1) - Zr(1), but the largest difference is still less than 0.06 Å. Once again the interstitial has very little impact.

The final zirconium-zirconium distances to be discussed are the Zr(2) - Zr(2) contacts surrounding the interstitial site. In the binary compound this distance is slightly larger than the Zr(1) - Zr(2) distance (see Table 32), but surprisingly the average overlap population as calculated by extended-Hückel, is 50% greater (see Table 29). The Zr(2) - Zr(2) distances are the most affected by insertion of an interstitial atom. No other distance changed by more than 0.06 Å, whereas, the largest variation in the Zr(2) - Zr(2) distance is 0.27 Å. This difference is found by comparison of the binary compound and the mixed iron-indium interstitial phase, but even among the ternary compounds, much larger differences can be seen than in any of the other types of interatomic spacings. The two calculations performed on interstitial compounds indicate that Zr(2) - Zr(2) bonding interactions are in essence nil after interstitial insertion. Within the basic Zr_5Sb_3 framework,

only the Zr(2) - Zr(2) distances are found to vary with different interstitial elements.

A comparison of zirconium-interstitial distances to other known spacings of the same type would also be interest. The sum of Slater[83] radii for zirconium and aluminum is 2.80 Å. The distance from Zr(2) to the interstitial site (72% Al, 28%Sb) in the single crystal refinement is 2.700(1) Å. The mixed atom occupation of the interstitial site makes the Zr-Al distance only approximate, but is not likely to be very different in the ordered Zr_5Sb_3Al compound. Any change would most likely result in a smaller zirconium to interstitial separation since antimony is larger than aluminum.

Another example of an aluminum-centered zirconium octahedron can be found in the compound $Cs_{0.7}Zr_6I_{14}Al$.[95] The Zr-Al distance in this compound is much shorter (2.4 Å). These zirconium-aluminum distances can be compared to the range of 2.84 - 3.03 Å spacings observed in many intermetallic compound, e.g., Zr_2Al,[96] Zr_5Al_3,[65] Zr_4Al_3,[97] ZrAl,[98] and Zr_2Al_3.[99] The Zr-Al distance in Zr_5Sb_3Al is seen to be shorter than the sum of Slater radii or what comparison with binary compounds would predict. The distance is much longer, however, than observed in the zirconium iodide.

A theoretical treatment of the bonding in Zr_2Al has shown that aluminum p orbitals are principally nonbonding in that binary compound.[100] The electron densities on the zirconium atoms (d-type states) are directed so as to avoid the aluminum positions. In $Cs_{0.7}Zr_6I_{14}Al$, the ionic nature of the compound results in a

significant transfer of electrons from zirconium to iodine. This empties the screening d orbitals on zirconium and allows close contact between Zr and Al. In Zr_5Sb_3Al, electron transfer is much reduced, and the Zr-Al distance is only slightly shorter than in the binary compound. The small transfer of electrons from zirconium to antimony is in agreement with extended-Hückel and XPS results for Zr_5Sb_3Fe and Zr_5Sb_3S.

There is less of a solid solution problem in the structural refinement of Zr_5Sb_3Si, but a small amount of Zn (~10%) was found to occupy the interstitial site. A comparison of zirconium-silicon distances reveals that, 2.67 Å in Zr_5Sb_3Si is longer than the 2.5 Å distance of the silicon-interstitial zirconium iodide, $Cs_{0.3}Zr_6I_{14}Si$.[95] The binary zirconium silicides have a range that spans the shorter observed heteroatomic spacings of 2.71 - 2.88 Å (ZrSi,[101] Zr_2Si,[102] $ZrSi_2$ cited in reference 103). The sum of Slater radii for Zr and Si is 2.65 Å, which agrees well with the crystal data results. In contrast, the binary compounds have distances that are somewhat longer. However, the zirconium to silicon distance in Zr_5Sb_3Si is closer to what would be expected from comparison to the binary compounds than the Zr-Al distance in Zr_5Sb_3Al is to the corresponding binary phases. The p orbitals of Si are lower in energy than the aluminum orbitals and probably are more bonding with respect to zirconium.

The sulfide structural refinement did not reveal a mixed atom interstitial, but did indicate a substoichiometric interstitial occupancy. The zirconium-sulfur distance of 2.578 Å would presumably increase slightly with a filled site. Nevertheless, the Zr-S distance is

consistent with the decrease one would expect when changing the interstitial from aluminum, to silicon to sulfur. The sum of Slater radii is 2.55 Å, and the 2.58 - 2.60 Å separations in the binary compounds ZrS_3,[104] and Zr_9S_2[105] are comparable to the experimental value in $Zr_5Sb_3S_{0.7}$.

The iron interstitial, single crystal refinement does not suffer from the solid solution or nonstoichiometry problems of the above refinement. That is not to say that these complications do not occur for Zr_5Sb_3Fe, they most certainly do (see Synthesis section), but the crystal used in the structural investigation was serendipitously free of those problems. The iron-zirconium distance is 2.653 Å, which is quite a bit shorter than the sum of Slater radii (2.90 Å). This sum of Slater radii does not predict well the iron-zirconium distances in the binary intermetallic compounds. The shortest interatomic spacing found in binary compounds are 2.75 Å in Zr_2Fe,[106] and 2.85 Å in $ZrFe_2$.[39] The compound $Cs_{0.63}Zr_6I_{14}Fe$ also has an iron-centered zirconium octahedron. In that compound the average Zr-Zr distance is 2.48 Å.[107] The zirconium-iron distance in Zr_5Sb_3Fe is much closer in length to the binary intermetallic compounds, but slightly smaller. This distance is in qualitative agreement with the extended-Hückel results that assign a slight positive charge to zirconium, and none to iron.

Upon substitution of one-third of the iron atoms by indium, the average interstitial distance increases from 2.653 Å to 2.754 Å. If 67% of this larger distance is attributable to a Zr-Zr distance of 2.653 Å, then the Zr-In distance can be estimated as 2.96 Å. In the binary

intermetallic compound $ZrIn_3$, the closest heteroatomic distance is 3.00 Å.[108] The interstitial distance is once again very similar to that of the binary intermetallic compound.

The last compound in which quantitative data on the zirconium interstitial distance is available is Zr_5Sb_3Zn. The Zr-Zn distance in this compound is 2.747 Å. The sum of Slater radii would predict a separation of 2.90 Å, and distances of 2.89 - 2.97 are found in the binary intermetallic compounds (ZrZn,[71] $ZrZn_2$[109]). The observed zirconium-zinc distance in Zr_5Sb_3Zn is consistent with that in the iron compound in being slightly shorter than the binary compounds.

The effect of interstitial elements on Zr_5Sb_3Z structural parameters can also be examined with cell volumes determined from from powder data. A plot of unit cell volume vs the number of valence electrons for the third and fourth main group periods is drawn in Figure 33. A steady decrease from group three to group five is noted. Based on the single crystal results, this decrease in distance is caused by changes in zirconium to interstitial distances. Such a trend is consistent with the notion that atoms decrease in size across a transition series. A slight increase in size is expected for the heavier atoms of the same family, and this can also be seen in Figure 33. The volume does not continue to decrease for sulfur or selenium. This is most likely caused by repulsions between the chalcogenide atoms

At first glance, the unit cell volume listed for Zr_5Sb_3Ga in Table 19, seems anomalously large, but the size is consistent with the trend observed for Zr_5Sb_3Z, Z = Ga, Ge, As. It is also consistent with the

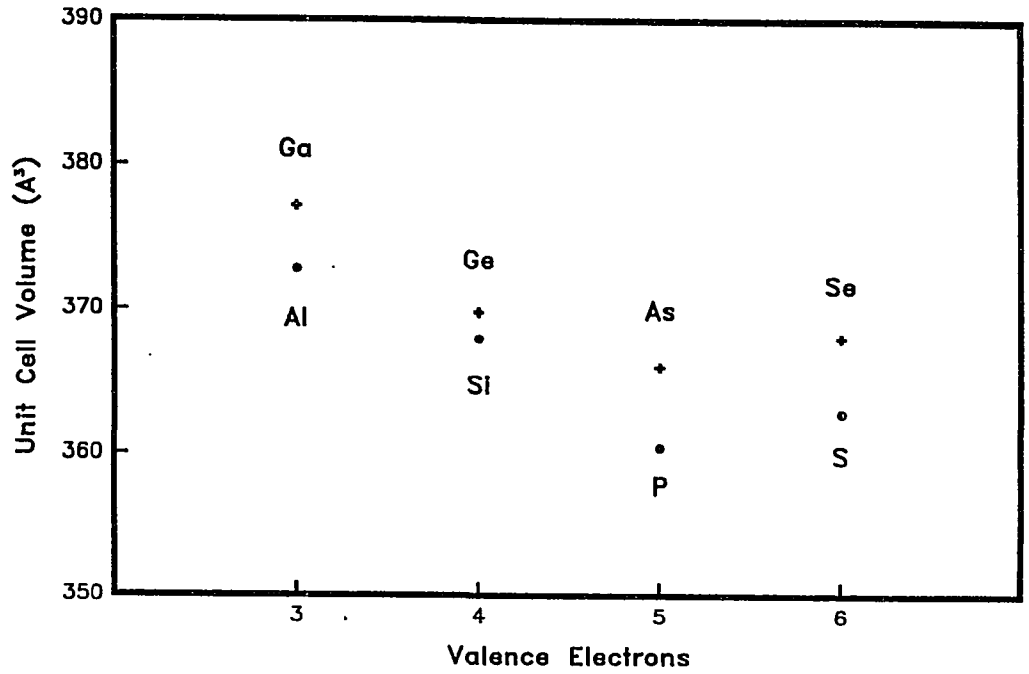

Figure 33. Plot of the unit cell volumes of some Zr_5Sb_3Z compounds as a function of valence electrons. The increase in volume observed as Z is charged from P to S, or As to Se is probably caused by antibonding interactions between the chalcogenide atoms

volume observed for Zr_5Sb_3Al (see Figure 33). A similar plot for transition metal interstitial compounds was not made because of the difficulty in establishing lattice parameters for controlled compositions.

Extended-Hückel

The results of the calculations for Zr_5Sb_3, Zr_5Sb_3Fe, and Zr_5Sb_3S, can be used to rationalize the ability of the binary compound to be interstitially stabilized by such chemically different elements as iron and sulfur. By extension, the rest of the remarkable array of interstitial elements may also be explained.

The compounds all have a large density-of-states at the Fermi energy. A result of this is that a changing election count, i.e., different interstitial elements, will shift the Fermi energy only slightly. Table 33 lists the calculated Fermi energy from the three calculations for a number of different electron counts. If a rigid band approximation is made, then the election counts can be assigned to specific compounds as in Table 33. The rigid band approximation assumes that the bands are not changed, merely filled or emptied by a changing interstitial electron count. Such an approximation is well applied to the 3d transition metals, less so for main groups elements. Nevertheless, it can be said with confidence that the Fermi energy shifts very slightly with a varying electron count.

This fact is not in and of itself very important. The significance of this observation can be derived from the COOP curves. In all the calculations, all the Zr-Sb bonding occurs in the valence band, which is 2.5 eV or more below the Fermi level. Since a changing electron count

Table 33. Fermi energy as a function of electron count

Electron[a] Count	Compound	Fermi Energy (eV)[b]
39	Zr_5Sb_3Si	-8.16
40	Zr_5Sb_3P	-7.97
41	Zr_5Sb_3S	-7.90
42	Zr_5Sb_3Cl	-7.34
42	Zr_5Sb_3Mn	-8.52
43	Zr_5Sb_3Fe	-8.44
44	Zr_5Sb_3Co	-8.36
45	Zr_5Sb_3Ni	-8.24
35	Zr_5Sb_3	-8.37

[a]Total valence electrons.
[b]Based on rigid band approximation using Zr_5Sb_3S or Zr_5Sb_3Fe.

does not shift the Fermi energy to any great extent, no interstitial will cause any of these Zr-Sb states to be emptied of electron density. The greatest part of the lattice energy is derived from zirconium-antimony bonding interactions, and since this is not affected by the interstitial, the compound is well suited to accommodate diverse interstitial elements.

The other type of bonding in the binary compound that can be affected by interstitials, are zirconium-zirconium interactions. Unlike Zr-Sb bonding, these interactions are located in states much nearer the Fermi level. Still, Zr(1) - Zr(1) bonding is mainly located in states 1 eV below the Fermi level in both Zr_5Sb_3Fe and Zr_5Sb_3S (see Figures 27 and 29), and as such is not drastically affected by a changing electron count (see Table 33).

The most dramatically affected interactions are those of Zr(2) - Zr(2). In the binary compound, the Zr(2) - Zr(2) distances are very long at ~3.6 Å, but the positive overlap is surprisingly substantial, though weak compared with Zr(1) - Zr(1) (see Table 29). In the ternary compounds, these weak Zr(2) - Zr(2) interactions have all but disappeared even though the Zr(2) - Zr(2) distance has increased only slightly (~0.1 Å). It is interesting to note that the weak Zr(1) - Zr(2) interactions are not affected by the insertion of an interstitial. Apparently, only Zr(2) orbitals that are directed inward towards the trigonal antiprismatic hole interact with the interstitial atom. When this site is empty the Zr(2) atoms make the best of a bad situation and form weak Zr(2) - Zr(2) bonds. With an interstitial, strong Zr(2) - Z bonds are

formed. This has only been rigorously calculated for sulfur and iron, but the other interstitial elements can be reasonably assumed to behave similarly.

It is the Zr(2) - Zr(2) and Zr(2) - Z interactions that determine the stability of a Zr_5Sb_3Z compound with respect to the binary Zr_5Sb_3. When an interstitial element is introduced into the binary compound, weak Zr(2) - Zr(2) bonding is lost, and strong zirconium(2)-interstitial bonding is gained. Each Zr(2) atom has six Zr(2) neighbors, and two Z close contacts. As long as more energy is gained from two strong Zr(2) - Z bonds than is lost in six weak Zr(2) - Zr(2) interactions, then the ternary phase will be more stable than the binary compound. Since the Fermi energy shifts only slightly with various interstitial valence electron counts, there is no magic electron count rule. The ability to incorporate very chemically diverse elements is derived from the ability of the Zr(2) orbitals to form positive overlaps with those elements. In essence, if an element will form a stable binary compound with zirconium, it can most likely be incorporated as an interstitial in Zr_5Sb_3Z.

One type of overlap that has not yet been discussed is the interstitial-interstitial interaction. The Z-Z distance must, for crystallographic reasons, be the same as Zr(1) - Zr(1). In Zr_5Sb_3Fe, the Fe-Fe average overlap population is 0.03, and negligible. However, in Zr_5Sb_3S, the sulfur to sulfur average overlap population is -0.07. The net interaction is antibonding in character. This can be ascribed to the increased antibonding overlap between the more electronegative sulfur atoms. The result of this repulsion can be seen in the large c/a ratio

for the sulfur compound. The same anomalously large c/a ratio is observed for Zr_5Sb_3Se, and the increased repeat distance along the c-direction serves to separate the interstitial atoms.

The small change in lattice parameters as a function of interstitial element was a point of interest at the outset of this investigation. The small change of unit cell parameters is easily explained by the calculations, indeed this point is central to the results discussed above. If only Zr(2) - Zr(2) bonding is affected by the interstitial atom, then none of the other bond lengths in the compound should change in the various phases. This is borne out by the single crystal structural data, where Zr-Sb bond lengths remain fairly constant. If very few bond lengths are changing, then, of course, the unit cell size will not change.

The results of the extended-Hückel calculations serve in rationalizing the observed Zr_5Sb_3Z systems. The binary compound's ability to incorporate a wide array of interstitial elements is due to a combination of factors. The high density-of-states at the Fermi level, the overwhelming proportion of which are nonbonding zirconium states, and the resulting insulation of zirconium-antimony states from chemical perturbation, allow for this ability. It must be born in mind, however, that these calculations are best in a comparative application rather than in an absolute sense. According to the calculations, Zr_5Sb_3Mn or Zr_5Sb_3Cr should be very similar to Zr_5Sb_3Fe in stability, but the calculations cannot take into account other ternary phases that may be even more stable. This is apparently what happens when Zr_5Sb_3Mn and Zr_5Sb_3Cr form

an unknown cubic phase. Still, the extended-Huckel calculations do provide a good basis for understanding the Zr_5Sb_3Z phases.

FUTURE WORK

The Zr_5Sb_3Z interstitial compounds synthesized during the course of this investigation provide an amazing array of subjects for further study. There are still some synthetic problems which should be addressed. The disagreement between lattice parameters of arc-melted and sintered products, especially for transition metal interstitial compounds, needs to be resolved. The capacity to sinter reactions of controlled composition at temperatures greater than 1100°C which unfortunately was not available until the latter stages of this investigation, should resolve the ambiguity of lattice parameters vs composition.

Preliminary reactions with other Mn_5Si_3-type compounds, such as Zr_5As_3, have indicated that the ability to incorporate a wide array of interstitial elements may not be limited to Zr_5Sb_3. Problems were encountered when attempts were made to synthesize Zr_5Sb_3Z compounds, where the interstitial element was of comparable size to antimony. Cadmium could not be incorporated into the interstitial site, and indium only partially. Such problems with Zr_5As_3 or Zr_5Ge_3 would result in a much more limited interstitial chemistry. Vapor phase transport of Zr_5Ge_3Z or Zr_5As_3Z compounds may be easier to accomplish than with the antimony compounds. The valence atomic orbitals of the lighter main group elements are at a lower energy than antimony, resulting in an increased ionic character, and a greater heat of formation. The higher heat of formation of the solid compound will reduce the temperature at which it will form from the volatile iodides. On the other hand, the iodides themselves will have a greater heat of formation. The two

effects will partially cancel each other, but it may be possible to obtain crystals from vapor transport at a lower temperature than was possible with the antimony compounds.

Another compound that has the potential to exhibit an extensive interstitial chemistry, is Zr_5Bi_3. Binary zirconium-bismuth compounds are pyrophoric; so no arc-melting experiments were performed in this system. Some initial attempts were made to produce Zr_5Bi_3 and Zr_5Bi_3Z compounds by sintering elemental powders. These experiments were conducted before a high temperature furnace (>1100°C) became available, and invariably resulted in incomplete reactions. Sintering reactions at higher temperature should produce fruitful results analogous to be Zr_5Sb_3Z compounds.

The magnetic properties of Zr_5Sb_3Fe need to be re-examined in a systematic manner. A series of controlled compositions achieved with high temperature sintering reactions can be systematically probed to determine the influence of a varying iron content or magnetic properties. There are also many rare earth metal compounds with the Mn_5Si_3 structure,[39] and the magnetic properties of these phases, with and without magnetic interstitial atoms, should prove interesting.

Another area that can be investigated is the chemical interaction or ordering between interstitial atoms. The Mn_5Si_3 framework can serve as a template for one-dimensional chemical interactions, if alternate interstitial sites are occupied by different elements. The distance between interstitial sites in Zr_5Sb_3 is fairly large (2.9 Å), but Zr_5As_3 or Zr_5Ge_3 have smaller cells, and allow closer contacts between the sites.

Even better compounds in terms of Z'-Z" distance, would be phase such as Ti_5As_3 or even Mn_5Si_3. One may imagine compounds such as $Mn_5Si_3(Al_{0.5}P_{0.5})$, where a linear chain of aluminum and phosphorus would be formed.

It may also be possible to mix transition metals in a manner that would also allow closer contact between mixed interstitial atoms. This could be accomplished by a $Zr_3Ti_2Sb_3$ or $Zr_3Ti_2As_3$ compound. In these phases titantium atoms would replace the Zr(1) atoms of the linear chain and bring about a smaller repeat distance for the c-axis. In addition to interesting interstitial chemistry that could result from this, the magnetic properties of a compound such as $Zr_3Ti_2Sb_3Fe$ would be interesting to compare with those of Zr_5Sb_3Fe.

There are quite a few options open to the synthetic chemist who wishes to investigate Mn_5Si_3Z-type compounds. The ability to substitute interstitial or framework elements can lead to an almost infinite variety of compounds. This ability to produce a controlled series of compounds can permit a fine tuning of desired physical properties. Systematic variation of chemical composition will provide further insight into the mechanisms of the properties of interest.

REFERENCES

1. Parthé, E.; Rieger, W. Acta Crystallogr. 1968, B24, 456.
2. Parthé, E.; Rieger, W. J. Dentl. Res. 1968, 47, 829.
3. Parthé, E.; Jeitschko, W.; Sadagopan, V. Acta Crystallogr. 1965, 19, 1031.
4. Setz, S.; Nowotny, H.; Benesovsky, F. Mh. Chem. 1968, 99, 2004.
5. Jeitschko, W.; Nowotny, H.; Benesovsky, F. Mh. Chem. 1963, 94, 844.
6. Rieger, W.; Nowotny, H.; Benesovsky, F. Mh. Chem. 1964, 95, 1413.
7. Parthé, E.; Norton, J. T. Mh. Chem. 1960, 91, 1125.
8. Rieger, W.; Nowotny, H.; Benesovsky, F. Mh. Chem. 1965, 96, 232.
9. Schachner, H.; Cerwenka, E.; Nowotny, H. Mh. Chem. 1954, 85, 246.
10. Hwu, S.-J.; Corbett, J. D.; Poeppelmeier, K. R. J. Solid State Chem. 1985, 57, 43.
11. Ziebarth, R. P.; Corbett, J. D. J. Am. Chem. Soc. 1985, 107, 4571.
12. Smith, J. D.; Corbett, J. D. J. Am. Chem. Soc. 1985, 107, 5704.
13. Holmberg, B.; Dagerham, T. Acta Chem. Scand. 1961, 15, 919.
14. Elwell, D.; Scheel, H. J. "Crystal Growth from High-Temperature Solutions"; Academic Press: New York, 1975.
15. Clark, C. M.; Smith, D. K.; Johnson, G. J. "A FORTRAN IV Program for Calculating X-Ray Diffraction Patterns - Version V", Department of Geosciences, The Pennsylvania State University: University Park, PA, 1973.
16. Werner, P. E. "TREOR-4 Trial and Error Program for Indexing of Unknown Powder Patterns", Department of Structural Chemistry, Arrhenius Laboratory, University of Stockholm: S-106 91 Stockholm, Sweden, 1984.
17. Karcher, B., Ph.D. Dissertation, Iowa State University, Ames, IA, 1981.
18. Kasper, J. S.; Lonsdale, K. "International Tables for X-Ray Crystallography, Vol. II", Kynoch Press, Birmingham, England, 1959.

19. Rodgers, J.; Jacobson, R. A., AEC Report IS- 2155, Ames, IA, 1967.

20. Helland, B., Ames Laboratory, Iowa State University, unpublished research.

21. Lapp, R. L.; Jacobson, R. A., United States AEC Report IS-4708, Iowa State University, Ames, IA, 1979.

22. Powell, R. R.; Jacobson, R. A., United States AEC Report IS-4737, Iowa State University, Ames, IA, 1979.

23. Johnson, C. K. "ORTEP: A FORTRAN Thermal-Ellipsoid Plot Program for Crystal Structure Illustrations", ORNL Report 3794, Oak Ridge National Laboratory, Oak Ridge, TN, 1970.

24. Schaffr, A. M.; Gouterman, M.; Davidson, E. R. Theoret. Chim. Acta B (Berl.) 1973, 30, 9.

25. Hoffmann, R. J. Chem. Phys. 1963, 39, 1397.

26. Hinze, J.; Jaffé, H. H. J. Phys. Chem. 1963, 67, 1501.

27. Moore, C. E. "Atomic Energy Levels", Natl. Stand. Ref. Data Ser., Natl. Bur. Stand. (U.S.) 1971, NSRDS-NBS 35.

28. Basch, H.; Gray, H. B. Theoret. Chim. Acta (Berl.) 1966, 4, 367.

29. Clement, E.; Roetti, C. At. Data Nucl. Data Tables 1974, 14, 179.

30. Russi, R. F.; Wilhelm, H. A., U. S. Atomic Energy Commission Publication AECD-3610, 1951.

31. Betterton, J. O.; Spicer, W. M. Trans. AIME 1958, 212, 456.

32. Boller, H.; Parthé, E. Monat. Chem. 1962, 94, 225.

33. Schubert, K.; Meissner, H. G.; Pötzschke, M.; Rossteutscher, W.; Stolz, E. Naturwissenschaften 1962, 49, 57.

34. Schubert, K.; Raman, A.; Rossteutscher, W. Naturwissenschaften 1964, 51, 506.

35. Rossteutscher, W.; Schubert, K. Z. Metallkde. 1965, 56, 813.

36. Eberle, D.; Schubert, K. Z. Metallkde. 1968, 59, 306.

37. Kjekshus, A. Acta Chem. Scand. 1972, 26, 1633.

38. Garcia, E.; Corbett, J. D. J. Solid State Chem., submitted.

39. Villars, P.; Calvert, L. D. "Pearson's Handbook of Crystallographic Data for Intermetallic Phases"; Amer. Soc. Met.: Metals Park, OH, 1985; Vols. 1-3.

40. Eisenmann, B.; Limartha, H.; Schäfer, H.; Graf, H. A. Z. Naturforsh. 1980, 35B, 1518.

41. Wang, Y.; Gabe, E. J.; Calvert, L. D.; Taylor, J. B. Acta Crystallog. 1976, B32, 1440.

42. Brunton, G. D.; Steinfink, H. Inorg. Chem. 1971, 10, 2301.

43. Pötzschke, M.; Schubert, K. Z. Metalkde. 1962, 53, 474.

44. Schubert, K.; Meissner, H. G.; Raman, A.; Rossteutscher, W. Naturwissenschaften 1964, 54, 284.

45. Potel, M.; Chevrel, R.; Sergent, M.; Decroux, M.; Fischer, Ø. C. R. Acad. Sci. Ser. C 1979, 288, 429.

46. Al-Shahery, G. Y. M.; Jones, D. W.; McColm, I. J.; Steadman, R. J. Less-Common Met. 1982, 85, 233.

47. Al-Shahery, G. Y. M.; Jones, D. W.; McColm, I. J.; Steadman, R. J. Less-Common Met. 1983, 87, 99.

48. Al-Shahery, G. Y. M.; Steadman, R.; McColm, I. J. J. Less-Common Met. 1983, 92, 329.

49. Yoshihara, K.; Taylor, J. B.; Calvert, L. D.; Despault, J. G. J. Less-Common Met. 1975, 41, 329.

50. Watanabe, H.; Yamamoto, H.; Ito, K. J. Phys. Soc. Jpn. 1963, 18, 995.

51. Jacobson, R. A., United States AEC Report IS-3469, Iowa State University, Ames, IA, 1974.

52. Main, P.; Fiske, S. J.; Hull, S. E.; Lessinger, L.; Germain, G.; Declerq, J. P; Woolfson, M. M.; "MULTAN 80. A System of Computer Programs for the Automatic Solution of Crystal Structures from X-Ray Diffraction Data", Department of Physics, University of York Printing Unit: York, England, 1980.

53. Barrett, C. S.; Cucka, P.; Haefner, K. Acta Crystallogr. 1963, 16, 451.

54. Snell, P. O. Acta Chem. Scand. 1968, 22, 1942.

55. Trzebiatowski, W.; Weglowski, S.; Lukaszewics, K. Roczniki Chem. 1958, 32, 189.

56. Hughbanks, T.; Hoffmann, R. J. Am. Chem. Soc. 1983, 105, 1150.

57. Miller, G.; Burdett, J., Department of Chemistry, University of Chicago, Chicago, IL, personal communication, 1984.

58. Hughbanks, T.; Hoffmann, R. J. Am. Chem. Soc. 1983, 105, 3531.

59. Hulliger, F. Nature 1964, 204, 991.

60. Schäfer, H.; Eisenmann, B. Rev. Inorg. Chem. 1981, 3, 29.

61. Deller, K.; Eisenmann, B. Z. Anorg. Allg. Chem. 1976, 425, 104.

62. Schob, G.; Parthe, E. Acta Crystallogr. 1964, 17, 452.

63. Eisenmann, B.; Schäfer, H. Z. Naturforsh. 1974, 29B, 13.

64. Rieger, W.; Parthe, E. Acta Crystallogr. 1968, B24, 456.

65. Kim, S. J.; Kematick, R. J.; Yi, S. S.; Franzen, H. F. J. Less-Common Met., submitted.

66. Boller, H.; Parthe, E. Acta Crystallogr. 1963, 16, 830.

67. Brewer, L.; Krikorian, O. J. Electrochem. Soc. 1956, 103, 38.

68. Parthe, E. Powder Met. Bull. 1957, 8, 23.

69. Schob, O.; Nowotny, H.; Benesovsky, F. Mh. Chem. 1961, 92, 1218.

70. Boller, H.; Parthe, E. Mh. Chem. 1963, 94, 225.

71. Hansen, M. "Constitution of Binary Alloys"; McGraw-Hill: New York, 1958.

72. Pötzschke, M.; Schubert, K. Z. Metallkde. 1962, 53, 474.

73. Parthe, E.; Norton, J. T. Acta Crystallogr. 1958, 11, 14.

74. Weill, A. R. Nature, 1943, 152, 413.

75. Friauf, J. B. Am. Chem. Soc. 1927, 49, 3107.

76. Friauf, J. B. Phys. Rev. 1927, 29, 34.

77. Laues, F.; Witte, H. Metallwirtschaft 1935, 14, 645.

78. Laues, F.; Witte, H. Metallwirtschaft 1936, 15, 840.

79. Pouravian, F.; Wallace, W. E. J. Less-Common Met. 1983, 91, 223.

80. Piegger, E.; Craig, R. S. J. Chem. Phys. 1963, 39, 137.

81. Shelton, R. N., Ames Laboratory, Iowa State University, Ames, IA, private communication, 1987.

82. Menth, A.; Nagel, H.; Perkins, R. S. Ann. Rev. Mater. Sci. 1978, 8, 21.

83. Slater, J. C. J. Chem. Phys. 1964, 41, 3199.

84. Stadelmaier, H. H.; Fiedler, M. L. Z. Metalkde. 1967, 58, 633.

85. Dasarathy, C., Trans. of Met. Soc. of AIME 1969, 245, 1938.

86. Brewer, L.; Lamoreaux, R. H.; Ferro, R.; Marazza, R.; Girgis, K., Atomic Energy Review, Special Issue No. 7, Brewer, L., ed.; International Atomic Energy Agency, Vienna, 1980.

87. Lundström, T. Acta Chem. Scand. 1966, 20, 1712.

88. Carlsson, B.; Gölin, M.; Rundqvist, S. Acta Chem. Scand. Ser. A, 1976, 30, 386.

89. Hughbanks, T.; Hoffmann, R. J. Am. Chem. Soc. 1983, 105, 3531.

90. Lindberg, B. J.; Hamrin, K.; Johansson, G.; Gelius, U.; Fahlmann, A.; Nordling, C.; Siegbahn, K. Phys. Scripta 1970, 1, 277.

91. Wagner, C. D.; Riggs, W. M.; Davis, L. E.; Moulder, J. F. "Handbook of X-Ray Photoelectron Spectroscopy"; Mailenberg, G. E., ed.; Perkin-Elmer: Eden Pairier, Minnesota, 1978.

92. Nefedov, V. I.; Salyn, Ya. V.; Chertkov, A. A.; Padurets, L. N. Russ. J. Inorg. Chem., 1974, 19, 1443.

93. Shalvoy, R. B.; Fiusher, G. B.; Stiles, P. J. Phys. Rev. 1977, B15, 1680.

94. Corbett, J. D. J. Solid State Chem. 1981, 37, 335.

95. Smith, J. D.; Corbett, J. D. J. Am. Chem. Soc. 1985, 108, 1927.

96. Wilson, C. G.; Sams, D. Acta Crystallogr. 1961, 14, 71.

97. Wilson, C. G.; Thomas, D. K.; Spooner, F. J. Acta Crystallogr. 1960, 13, 56.

98. Spooner, F. J.; Wilson, C. G. Acta Crystallogr. 1962, 15, 221.

99. Renouf, T. J.; Beevers, C. A. Acta Crystallogr. 1961, 14, 469.

100. Kematick, R. J.; Franzen, H. F. J. Solid State Chem. 1985, 60, 297.

101. Karpinskii, O. G.; Evseev, B. A. Inorg. Mat. 1965, 1, 312.

102. Pietrokowsky, P. Acta Crystallogr. 1954, 7, 35.

103. Struct. Rep. 1955, 19, 285.

104. Furuseth, S.; Brattas, Leif; Kjekshus, Arne Acta Chem. Scand. Ser. A, 1975, 29, 623.

105. Cheng, H.-Y.; Franzen, H. F. Acta Crystallogr. 1972, B28, 1399.

106. Havinga, E. E.; Damsma, H.; Hokkeling, P. J. Less-Common Met. 1972, 27, 169.

107. Hughbanks, T., Department of Chemistry, Iowa State University, Ames, IA, unpublished research, 1986.

108. Raman, A.; Schubert, K. Z. Metallkde. 1965, 56, 44.

109. Dwight, A. B. Trans. Am. Soc. Met. 1961, 53, 479.

ACKNOWLEDGEMENTS

'How curious! How real!'

Walt Whitman

The author wishes to thank Professor John D. Corbett for asking the questions that needed to be asked, and for allowing him the freedom to pursue the answers.

The author is also indebted to Professor R. A. Jacobson and members of his group for assistance with the single crystal diffractometers and crystallographic programs.

He is thankful to Professor R. N. Shelton and to P. Klavins for the magnetic susceptibility measurements, and for assistance in obtaining resistivity data. Gratitude must also be expressed to S. Wijeyesekera and T. Hughbanks for their guidance in performing the extended-Huckel calculations. Thanks are also due to J. Anderegg for the photoelectron spectra.

The discussions with, and advice of many coworkers were invaluable and they are kindly remembered. Special thanks goes to S. Standley for the patience and tireless efforts to produce a legible type written manuscript from the author's illegible handwritten version.

Finally the authors must acknowledge and thank his parents whose sacrifice and support made it all possible.

APPENDIX. VALENCE ORBITAL IONIZATION ENERGIES AND ZETAS OF ATOMS USED IN EXTENDED HÜCKEL CALCULATIONS

EXTENDED HÜCKEL INPUT PARAMETERS

Atoms	Orbital	H_{ii}(eV)	ξ_1	ξ_2	C_1	C_2
Zr	4d	-8.12	3.84	1.505	0.6213	0.5798
	5s	-8.19	1.82			
	5p	-4.63	1.78			
Fe[1]	3d	-8.73	1.90	2.000	0.5505	0.6260
	4s	-7.40	5.35			
	4p	-3.71	1.90			
Sb	5s	-18.80	2.32			
	5p	-11.68	2.00			
S	3s	-20.00	1.82			
	3p	-13.30	1.82			

[1]Fe H_{ii} values obtained from a self-consistent charge calculation with Zr.